UNIVERSIDADE ESTADUAL PAULISTA "Júlio de Mesquita Filho"
FACULDADE DE ENGENHARIA
CAMPUS DE ILHA SOLTEIRA

MAHDI POURAKBARI KASMAEI

DESPACHO ÓTIMO DE POTÊNCIAS ATIVA E REATIVA DE SISTEMA ELÉTRICOS MULTI-ÁREAS CONSIDERANDO RESTRIÇÕES FÍSICAS, ECONÔMICAS E AMBIENTAIS

Ilha Solteira

2015

MAHDI POURAKBARI KASMAEI

ENVRONMENTALLY CONSTRAINED ACTIVE-REACTIVE OPTIMAL POWER FLOW— A COMPROMISING STRATEGY FOR ECONOMIC-EMISSION DISPATCH AND A MULTI-AREA PARADIGM

Tese apresentada ao Programa de Pós-Graduação em Engenharia Elétrica da Universidade Estadual Paulista "Júlio de Mesquita Filho" – UNESP, Campus de Ilha Solteira, para preenchimento dos pré-requisitos parciais para obtenção do título de Doutor em Engenharia Elétrica. Área de Conhecimento: Automação.

José Roberto Sanches Mantovani

Orientador

Ilha Solteira

2015

unesp UNIVERSIDADE ESTADUAL PAULISTA

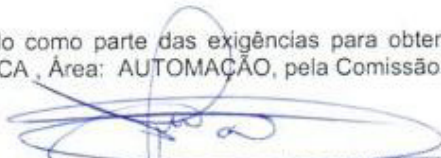CAMPUS DE ILHA SOLTEIRA

FACULDADE DE ENGENHARIA DE ILHA SOLTEIRA

CERTIFICADO DE APROVAÇÃO

TÍTULO: Despacho Ótimo de Potencias Ativa e reativa de Sistemas Elétricos Multiáreas Considerando Restrições Físicas, Economicas e Ambientais.

AUTOR: MAHDI POURAKBARI KASMAEI

ORIENTADOR: Prof. Dr. JOSE ROBERTO SANCHES MANTOVANI

Aprovado como parte das exigências para obtenção do Título de DOUTOR EM ENGENHARIA ELÉTRICA , Área: AUTOMAÇÃO, pela Comissão Examinadora:
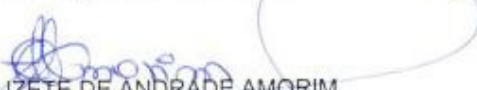
Prof. Dr. JOSE ROBERTO SANCHES MANTOVANI
Departamento de Engenharia Elétrica / Faculdade de Engenharia de Ilha Solteira

Prof. Dr. RUBEN AUGUSTO ROMERO LAZARO
Departamento de Engenharia Elétrica / Faculdade de Engenharia de Ilha Solteira

Prof. Dr. ANTONIO PADILHA FELTRIN
Departamento de Engenharia Elétrica / Faculdade de Engenharia de Ilha Solteira

Profa. Dra. ELIZETE DE ANDRADE AMORIM
Centro de Engenharia e Ciências Exatas Cece / Universidade Estadual do Oeste do Paraná

Prof. Dr. ROBERTO CHOUHY LEBORGNE
Departamento de Engenharia Elétrica / Universidade Federal do Rio Grande do Sul

Data da realização: 21 de fevereiro de 2015.

DEDICATION

To my parents, **Rafat** and **Parviz**, who have always been my greatest inspiration and incredibly supportive.

To my siblings, **Hossein**, **Roghaye**, and **Milad**, who are my closest friends as well.

To memory of my grandpa, who taught me "an academic degree is nothing if you don't respect others".

Acknowledgment

RESUMO

Nos estudos de planejamento da operação de sistemas de energia elétrica a formulação e solução dos problemas de despacho econômico-ambiental e multi-área são considerados dois problemas de otimização desafiadores. Neste trabalho propõem-se dois novos modelos matemáticos que visam contribuir e contornar algumas desvantagens dos modelos existentes na literatura para os problemas de fluxo de potência ótimo ativo-reativo econômico-ambiental (FPOAREA), e uma formulação integrada para problema multi-área (FPOAREA-MA).

No FPOAREA propõe-se uma formulação eficaz para obter um compromisso adequado entre os custos de geração e de emissão, através de um paradigma baseado em normalização inequívoca (PBNI). Ao contrário dos métodos comumente utilizados, que são principalmente aplicáveis a problemas de FPO simples (despacho econômico, despacho econômico com restrições de segurança, etc.), na abordagem PBNI, ao invés de usar um custo do controle da poluição com base na potência máxima (CCPBPM), utiliza-se um custo de controle adaptativo da poluição (CCAP), que representa o custo de controle baseado na topologia atual de operação da rede. A principal contribuição desse paradigma é utiliza a teoria da normalização para o FPO econômico-orientado, o FPO ambiental-orientado, e até mesmo para o fator CCAP.

No modelo proposto para o FPOAREA-MA em vez de usar metodologias de decomposição descritas na literatura que têm várias desvantagens e problemas de coordenação, uma formulação integrada que considera as restrições ambientais é proposta. Esta formulação integrada foi desenvolvida com base nos conceitos de modelos centralizados e descentralizados. Este modelo pode ser facilmente resolvido através de solvers comerciais e a sua resposta é precisa, e os resultados obtidos podem ser usados em mercados de eletricidade, planejamento de linhas de interconexões entre sistemas vizinhos, etc.

Para mostrar a versatilidade e as aplicações do FPOAREA-MA, ele é aplicado em um problema de planejamento da linha de interconexão. Nesta aplicação para obter as linhas de interconexão ideais, o planejamento é realizado sob a condição de ponto de máximo carregamento (PMC). Com base na análise de um sistema de energia no PMC, as barras fracas e fortes para alocar linhas de interconexões são inseridas em um conjunto de barras candidatas para o planejamento da linha de interconexão e, em seguida, através da solução de um problema de programação não linear inteira mista, as linhas de interconexão são alocadas

de forma otimizada. Além disso, para determinar um plano mais apropriado em todos os pontos de funcionamento, as linhas de interconexão são consideradas seccionáveis.

A fim de validar as metodologias propostas e para fins didáticos, são utilizados sistemas testes de pequeno porte. Além disso, a fim de considerar a qualidade das metodologias, vários estudos de caso de sistemas de energia de grande e médio porte são apresentados. Os resultados confirmam a eficácia e a utilidade das metodologias propostas.

Palavras-chave: FPOAR econômico-ambiental. Custo de controle de poluição flexível. Otimização baseada em normalização. FPOAR multi-área. Planejamento de linha de interconexão. Linha de interconexão seccionada.

ABSTRACT

In a power system, the economic and emission dispatch and multi-area-based problems are considered as the two most challenging optimization problems. This work presents two novel mathematical models to address some drawbacks of the existing models in the domain of the aforementioned problems, including an economic and emission active-reactive optimal power flow (AROPF), and an integrated formulation for multi-area environmentally-constrained AROPF.

In order to obtain an effective formulation to make an appropriate compromise between cost and emission, an unequivocal normalization-based paradigm (UNBP) is presented that solves the dynamic economic and emission AROPF problems. Unlike the commonly used methods, which are mostly applicable to simple OPF problems (economic dispatch, security-constrained economic dispatch, etc.), in the UNBP approach, rather than using a maximum output-based pollution control cost (MOPCC), an adaptive pollution control cost (APCC) is employed, which is a topology-based control cost is used. The main contribution of this paradigm is to make use of the normalization theory for the economic-oriented OPF, the environment-oriented OPF, and even for the APCC factor.

In addition, in this work a multi-area active-reactive optimal power flow (MA-AROPF) is proposed. In the MA-AROPF model, instead of using decomposition methodologies that have several disadvantages and shortcomings, an integrated formulation that considers the environmental constraints is proposed. This integrated formulation has been created based on the concepts of centralized and decentralized models. This model can be easily solved via commercial solvers and because of its precise answer, it can be used in electricity markets, tie line planning, etc.

In order to show the easy implementable characteristic of the MA-AROPF, it is applied on a tie line planning problem. In this work, in order to obtain optimal tie lines, the planning is performed under the MLP condition. Based on the analysis of a power system at the MLP, the weak and strong buses are determined and a set of strong and weak buses are selected as candidate buses for tie line planning and then, via a mixed integer nonlinear programming problem, the appropriate tie lines are selected. Moreover, in order to have a more appropriate plan at all the operating points, the switchable tie lines are considered.

In order to validate the proposed methodologies and for didactical purposes, small-scale systems are used. Furthermore, in order to consider the quality of the methodologies, several case studies of medium and large scale power systems are conducted. The results confirm the effectiveness and usefulness of the proposed methodologies.

LIST OF FIGURES

LIST OF TABLES

LIST OF ABBREVIATIONS

AC	Alternating current
ACOPF	AC optimal power flow
AMPL	A mathematical programming language
APCC	Adaptive pollution control cost
AROPF	Active-reactive optimal power flow
CAAA	Clean Air Act Amendments
CODIF	Maximum difference of costs obtained from economic- and emission-oriented dynamic AROPF
DC	Direct current
DEEOPF	Dynamic economic and emission OPF
DOPF	Dynamic optimal power flow
EED	Economic and emission dispatch
ED/ELD	Economic dispatch/ Economic load dispatch
EMA	Area emission limit
EMDIF	Maximum difference of costs obtained from economic- and emission-oriented dynamic AROPF
LP	Linear programming
MOPCC	Maximum output-based pollution control cost
MA-AROPF	Multi-area active-reactive OPF
MW	Megawatt
MVAr	Megavolt ampere reactive
NLP	Nonlinear programming
OPF	Optimal power flow
QP	Quadratic programming
RTO	Regional transmission organization

RDR   Ramp-down rate

RUR   Ramp-up rate

UNBP   Unequivocal normalization-based paradigm

LIST OF SYMBOLS

The main symbols used in this thesis are listed below for quick reference. Other symbols are defined as needed throughout the text.

Sets

Ω_A	Set of areas
$\Omega_b^{A_x}$	Set of buses in area x
Ω_b	Set of buses
Ω_g	Set of generating buses
Ω^s	Set of sub-area (regions in an area).
$\Omega_g^{A_x}$	Set of generators in area x.
Ω_{IA}	Set of interconnected areas.
Ω_L	Set of transmission lines
$\Omega_L^{A_x}$	Set of transmission lines in area x.
Ω_s	Set of generator in sub-area s
$\Omega_s^{A_x}$	Set of sub-areas in area x
$\Omega_s^{A_x^s}$	Set of generators in the sub-area s of area x.
$\Omega_{TL}^{A_{xy}}$	Set of tie lines between areas x and y.
T	Time index set

Variables and Functions

a_{ij}^l	Magnitude of transformer tap in line l, between buses ij.
$a_{ij,t}^l$	Magnitude of transformer tap in line l, between buses ij, at hour t.
$C_i(\cdot)$	Cost function of unit i.
$C_{i,t}(\cdot)$	Cost function of unit i at hour t
$Em_i(\cdot)$	Emission function of unit i.
$Em_{i,t}(\cdot)$	Emission function of unit i at hour t
E_i	Voltage of bus i
E^*	Conjugate of bus voltage.
$EMSA^s$	Emission limits of sub-area (region) s
$F^C(\cdot)$	Cost objective function

$F_C^{MA}(\cdot)$	Total cost of the multi-area system
$F^{Em}(\cdot)$	Cost objective function
$fl_{ij}^l(\cdot)$	Transmission line flow of line l between buses ij
h^f	Adaptive pollution control cost
I_{ij}^l	Current in line l between buses ij
k	Scaling factor
$Nh_{i,t}^f$	Normalized adaptive pollution control cost of unit i at hour t.
$NOx_{i,t}$	Nitrogen oxide emission of unit i at hour t
$P_{g_i}^M(Q_{g_i})$	Capability curve limit for generating bus i.
P_{g_i}	Active power generation (MW) at bus i
P_i	Active power injection (MW) at bus i
p_{ij}, p_{ji}	Direct and reverse active power injections between buses ij.
$p_{ij,t}, p_{ji,t}$	Direct and reverse active power injections between buses ij at hour t
Q_{g_i}	Reactive power generation ($MVAr$)at bus i
Q_i	Reactive power injection ($MVAr$) at bus i
$Q_{g_{i,t}}$	Reactive power generation of bus i at hour t
q_{ij}, q_{ji}	Direct and reverse reactive power injections between buses ij.
$q_{ij,t}, q_{ji,t}$	Direct and reverse reactive power injections between buses ij at hour t
RU_i	Ramp-up rate of unit i
RD_i	Ramp-down rate of unit i
S^{l^*}	Conjugate of complex power
$SOx_{i,t}$	Sulfur oxide emission of unit i at hour t
S_{d_i}	Apparent power demand
tp_{ij}^l	Tap of a transformer in line l between buses ij
v_i	Voltage magnitude of bus i
$v_{i,t}$	Voltage magnitude of bus i at hour t
w_1, w_2	Weighting factors of emission and cost objectives, respectively.
θ_i	Voltage angle of bus i
φ	Phase shifting of the transformer
$\varphi_{ij,t}$	Phase of a transformer tap in line l, between buses ij at hour t.

Parameters

a_i, b_i, c_i	quadratic ($\$/MW^2h$), linear ($\$/MWh$), and constant ($\$$) cost coefficients.
$b_{ij}^{l,ch}$	shunt susceptance , known as charging susceptance, of line l between buses ij
$b_i^{b,sh}$	Shunt susceptance of bus i ($\mho$).
b_{ij}^l	susceptance ($\mho$) of line l between buses ij

$\overline{fl}_{ij}^{l}$	Maximum limit of power flow in line l between buses ij
g_{ij}^{l}	conductance (Ω) of line l between buses ij
$g_{i}^{b,sh}$	Shunt conductance of bus i (Ω)
h	Maximum output-based pollution control cost
P_{d_i}	Active power demand (MW) at bus i.
$P_{d_{i,t}}$	Active power demand of bus i at hour t
$\underline{P}_{g_i}$, $\overline{P}_{g_i}$	Lower and upper bounds of the active power generation at bus i
$Q_{d_{i,t}}$	Reactive demand of bus i at hour t
Q_{d_i}	Reactive power demand ($MVAr$) at bus i
$\underline{Q}_{g_i}$, $\overline{Q}_{g_i}$	Lower and upper bounds of the reactive power generation at bus i
r_{ij}^{l}	resistance (Ω) of line l, between buses ij
$\underline{V}_i$, $\overline{V}_i$	Lower and upper bounds of the voltage magnitude at bus i
x_{ij}^{l}	reactance (Ω) of line l, between buses ij
y_{ij}^{l}	admittance ($\mho$) of line l between buses ij
z_{ij}^{l}	impedance (Ω) of line l between buses ij
α_i , β_i , c_i	quadratic (kg/MW^2h), linear (kg/MWh), and constant (kg) emission coefficients.
ε_i , λ_i	Coefficients of NO_X emissions.
φ	phase shifting of the transformer

CONTENTS

INTRODUCTION

Electric power and energy systems as the infrastructure of each community are an essential ingredient for the development of any country. Electric energy is a serviceable form of energy in several basic considerations such as generation, transmission, and distribution which are the main parts of a basic structure of an electric energy system. Over the years, the electric power industry has faced several significant changes. According to the fast growing power demand associated with the fuel cost increase, the generation planning and construction of complex transmission networks have been taken into account in order to transmit electricity to load centers which are in these days far away from the power plants (SILVA et al., 2005; POURAKBARI-KASMAEI; RASHIDI-NEJAD, 2011). The deregulation of power systems has introduced competitive market, where it yields reducing costs but brings uncertainty to the generation forecasting. Increasing the utilization of renewable sources, such as wind and solar energies, has added more complexity to scheduling of the power flows. On the other hand, one of the most important issues in power systems is to find the operating point of a power system at the minimum cost, whereas all the network and operating constraints are satisfied. The aforementioned considerations demonstrate the necessity of using an appropriate and reliable optimization tool to simultaneously consider both security and economic issues of a power system (TONG et al., 2006). In the early 1920's or even earlier, the economic dispatch (ED) tool was introduced to consider the economic aspect of the committed units (HAPP, 1977). As the ED minimizes the generated power costs, in several studies, it has been considered as the kernel of a power system. Lack of considering all network and operating constraints has forced the researchers and operators to introduce a proper tool in order to consider the aforementioned concerns. An optimal power flow (OPF) tool was introduced by Carpentier in 1962 (ZHU, 2009) aiming to have a proper power system by considering unavoidably essential constraints, such as active and reactive power balance, power flow limit, and power generation limits.

The basic objectives of an OPF are to minimize a given cost function, find the optimal planning of a system, maximize the reliability of a power system from a long-term scheduling horizon to the online adjustment of real and reactive power dispatch (ZHU, 2009) without violating the aforementioned constraints. The general OPF problem is considered as a large-scale, non-linear, and non-convex mathematical programming problem, and depending on its objective, it may contain both discrete and continuous variables. Many different formulations have been developed to solve the OPF-based problems. Most of these developments and

modifications are related to the objective function, control variables, and constraints, while some of them are related to the OPF paradigm. Although in the literature, the researchers have used different names based on the aforementioned developments or modifications, generally in a power system, each optimization problem that considers the power flow equations is considered as an OPF problem.

There are numerous methodologies to find a solution for the OPF problem, where some are analytical, and the rest are heuristic-based search methods. In (AL-MUHAWESH; QAMBER, 2008), in order to consider the effects of power wheeling in a power system, a linear programming-based OPF (LP-based OPF) has been presented. In (ZEHAR; SAYAH, 2008), the authors have presented a fast and efficient successive linear programming method to solve the environmentally constrained OPF. A semi-smooth Newton-type algorithm, which is a useful method for reducing the dual variables, has been proposed in (TONG; LIN, 2005). In (PUDJIANTO et al., 2002), the application of a nonlinear programming-based OPF to allocate VAr support has been presented. In (YAN et al., 2006), a decomposed predictor-corrector interior point method has been provided to solve the reactive OPF. In order to address the infeasibility issues related to the large variations such as wind generation, an exact penalty function-based constraints relaxation method has been presented in (DING et al., 2014b). A convex relaxation method has been presented in (MADANI et al., 2014); via which, finding a global optimal solution is guaranteed. The heuristic-based algorithm has been widely used in the OPF-based problems. Furthermore, a teaching-learning-based optimization (TLBO) technique has been presented in (BOUCHEKARA et al., 2014). The TLBO is a robust method that can provide effective and high-quality solutions. In (CHEN et al., 2014), a multi-hive bee foraging algorithm has been proposed to solve the multi-objectives OPF problem, where in this work, three objectives such as cost, emission, and loss have been considered. In (CAI et al., 2004), in order to find the optimal choice and allocate FACT devices, a genetic-based OPF has been presented, where the rate and type of FACT devices can be optimized simultaneously. In (ONGSAKUL; JIRAPONG, 2005), the authors have applied an evolutionary programming to allocate FACTS devices in order to maximize the total transfer capability (TTC) of power transmission. In this regard, a multi-objective OPF with FACT devices that includes the TTC and penalty functions has been used. A modified shuffle frog leaping algorithm (MSFLA) to solve the multi-objective OPF problem has been proposed in (NIKNAM et al., 2011c), in which two conflicting objectives of cost and emission have been considered. Moreover, some works have considered the combination

of two or more techniques in order to modify the drawbacks of the aforementioned methods. In (XU et al., 2012), a combination of the evolutionary algorithm and the classic deterministic method for solving the transient-constrained OPF has been proposed. A genetic evolving ant direction differential evolution (EADDE) has been presented in (VAISAKH; SRINIVAS, 2010) to solve the OPF problems with non-smooth cost function, while an innovative statistical analysis was considered. In (SIVASUBRAMANI; SWARUP, 2011), a sequential quadratic programming method combined with a differential evolution algorithm, which has the potential to solve the problems with more non-convexity, has been proposed.

After developing some features, concepts, and technologies in a power system such as energy storage systems, smart grid, demand side management, etc., a single-hour dispatch is no longer desirable. Instead, the multi-period or dynamic dispatch has been taken into account. Several methods have been introduced to solve the dynamic OPF (DOPF). A Benders decomposition method, which is a useful method for deregulated power markets to solve the DOPF, has been proposed in (YAMIN et al., 2003). In (NIKNAM et al., 2011a), a modified honey bee mating optimization (HBMO) technique has been proposed, in which the modification on the mutation operator of this technique overcomes the main drawback of the HBMO, related to the probability of trapping in a local minimum. In (NIKNAM et al., 2012), in order to solve the reserve constrained DOPF considering valve-point, prohibited operating zones, and multi-fuel constraints, an enhanced charged system search algorithm has been proposed. In (CHEN et al., 2005), a reduced gradient method, which is a successful method for solving the multi-stage DOPF problems, has been proposed. In (CHUNG et al., 2011), a predictor-corrector interior point has been used to solve the dynamic OPF problems, in which in order to avoid unnecessary computations, an inequality iteration strategy has been introduced.

Furthermore, the harmful environmental impacts of generating electricity are the inseparable part of each technology used in this area. In these days, there is a growing concern on these harmful environmental impacts (BASU et al., 2006; KASMAEI et al., 2013). Along with harming human health, air pollution can cause a variety of environmental consequences such as acid rain, eutrophication, haze, the effects on wildlife, ozone depletion, crop and forest damage, and global climate change. Since 1990, according to the Clean Air Act Amendments (CAAA), the utilities have to modify their design or operational strategies to deplete the pollution and atmospheric emissions (SUDHAKARAN et al., 2004, LAMONT; OBESSIS, 1995). Moreover, usually in power systems, the operating costs and emissions

have conflicted the objectives. In fact, the joint cost and emission consideration is one of the most challengeable problems in power systems. In the literature, there are numerous methods that can be harnessed in order to make a compromise between emissions and costs, such as conventional, heuristic-based, and hybrid methods. In (PALANICHAMY; BABU, 2008), an analytical solution, which has superiority in CPU time than the classical methods, has been applied to the joint economic and emission dispatch problem. In (GONG et al., 2010), a hybrid method of particle swarm optimization (PSO) and evolutionary programming has been proposed, in which the results showed a high-quality performance. A hybrid PSO and gravitational search has been proposed in (JIANG et al., 2014) to solve economic and emission dispatch by considering practical constraints such as ramp-rate, valve-point, and prohibited operating zones. The conventional methods mentioned in the literature mostly use a constant pollution control cost and usually these methods cannot make a good compromise. The metaheuristic methods are time consuming and are not good for such real-time problems (VENKATESH et al., 2003; NIKNAM; DOAGOU-MOJARRAD, 2012a). In this dissertation, we propose an unproblematic method that can find an acceptable compromise via a precise mathematical formulation, where the multi-period and contingency condition considerations make the problem a hardly non-linear, and a very large-scale problem.

To achieve higher efficiency in a power system, the operators of small-scale systems are willing to connect to other systems in order to form an interconnected large-scale system. In a centralized power system, each area transfers the necessary information to a central controller, and this controller optimizes the problem and returns the optimal value of the state variables to each area. After any change in one or more areas, the optimization process will be repeated and bulk of information will be transferred between the central controller and areas. Although such interconnected systems have several benefits, it is quite difficult to determine the optimal operation point in such large systems, and the use of decentralized methods is more practical to determine the optimal solution of such systems on an area-by-area basis (NOGALES et al., 2003; GRANADA et al., 2008), where only a small amount of information must be interchanged among the involved areas (CONEJO; AGUADO, 1998). In other words, in a decentralized power system, each area has its own controller that solves the corresponding optimization problem. In order to have a synchronized power system, each area communicates with the adjacent areas and shares the border information, until a tradeoff is obtained.

The decomposition methods, which are the general approaches for solving a large-scale problem through breaking into smaller problems via a parallel or sequential approach, are used to solve such problems in DC or AC power systems (BOYD et al., 2008). In order to develop the algorithm for multi-area systems, most of the relevant works have focused on DC-OPF. An iterative decentralized DC-OPF that can be implemented on a network workstation was reported in (BISKAS et al., 2005). In (CONEJO et al., 2007), a proper and simple coordination among area operators was proposed. In (CARO et al., 2011), a non-iterative method that does not require a central coordinator was reported. In (BAKIRTZIS; BISKAS, 2003), a decentralized method that is based on a pricing mechanism was offered, with the coordination of the areas being based on the prices of the power exchange between the interconnected areas; however, the main drawback of such methodologies is their iterative nature. In this dissertation, for a multi-area OPF, an integrated formulation that contains the concepts of both centralized and decentralized models is proposed, which makes it an effortless problem to be used for operating or/and planning problems. In a multi-area power system, all activities in each area will affect the prices, reliability, degrees of freedom, etc. of other interconnected areas and in this regard, a tie line can play an important role. From an operational standpoint of a regional transmission organization (RTO), tie lines are used to facilitate the energy exchange between areas under a pre-defined agreement (BALDICK; CHATTERJEE, 2013); moreover, measuring the transmitted power between areas via a tie line is necessary to know whether the area is balancing its active and reactive generation and load. The management of energy flows across the grid and the exchange of power flow information by RTO results in an appropriate power system. In order to verify the effectiveness and usefulness of the proposed method, a tie line planning problem is taken into consideration. In this regard, at first a novel approach for finding the maximum loadability point is presented, and then, a mixed-integer nonlinear programming problem for handling the tie line planning is taken into account.

1.1 OBJECTIVES

The main objectives of this work are as follow:

a) To provide an appropriate (flexible and adjustable) model for finding an acceptable compromise between cost and emission, which should be fast enough in order to be applicable in power markets.

b) To propose an integrated formulation for multi-area environmentally constrained active-reactive optimal power flow.

c) To create a mixed-integer nonlinear programming problem for solving tie line planning problem, where a novel formulation for calculating the maximum loadability point is presented.

1.2   ORGANIZATION

In Chapter 2, the transmission line models, transformer models, as well as the latest models for optimal power flow (OPF) are provided. The economic-oriented OPF, and the environment-oriented OPF are discussed and finally, the mathematical formulation of an active-reactive OPF is presented.

In Chapter 3, an unequivocal paradigm for solving the economic and emission active-reactive OPF is presented. This paradigm is a flexible normalization-based approach, which works based on the concept of traditional compromising methodologies. In this proposed methodology, instead of the maximum output-based pollution control cost (MOPCC), an adaptive pollution control cost (APCC) is used, which has the capability of considering the system topology in dynamic scheduling and under various system conditions including the normal, outage, and critical conditions.

In Chapter 4, a multi-area environmentally constrained active-reactive optimal power flow (MA-AROPF) is presented, where in the current work, rather than applying the commonly used decomposition methods in multi-area power system, which have several drawbacks, an integrated formulation is alternatively proposed. The proposed model works based on the centralized and decentralized concepts and also according to the multi-start feature of the commercial solver (KNITRO 9.1) for solving such problems. In order to show the effectiveness of a multi-area system, several cases are considered.

In Chapter 5, the proposed multi-area, in chapter 4, is applied to a tie line planning problem. The tie lines are planned under maximum possible loading point, where instead of applying the commonly used mathematical formulation to find the maximum loadability of a system, a novel mathematical formulation is proposed. Moreover, in order to have an appropriate system under different loading condition, switchable tie lines are taken into account.

In Chapter 6, case studies and results related to chapters 3-6 are presented.

In Chapter 7, concluding remarks and possible future works are presented.

Chapter 2

STATE-OF-THE-ART MODELS FOR OPTIMAL POWER FLOW

2.1 INTRODUCTION

The economic-oriented tools play a significant role in power systems. Generally, three commonly used tools are considered in this domain including: the economic load dispatch (ELD), power flow, and optimal power flow. The optimal power flow (OPF) is an extension of the conventional ELD, and since the ELD minimizes the generated power cost, it is considered as the kernel of a power system but does not consider all network and operating constraints. On the other hand, in order to have an appropriate power system operation, the consideration of constraints such as active and reactive power balance, power flow limits, and active and reactive power generation limits are unavoidably essential. Therefore, using a reliable and precise model to satisfy these constraints has always been a momentous issue. The idea of using a unified model to consider the aforementioned concerns was introduced by Carpentier in 1962 (ZHU, 2009). Unlike the power flow, which needed to predefine some system parameters based on the bus types, an AC optimal power flow (ACOPF) may need a slack bus for the power flow iterations, but even then, it is unnecessary to fix the voltage magnitude of the slack bus. The basic objectives of the optimal power flow (OPF) are to minimize the total cost of active or reactive generation, to minimize the network loss, and VAr planning along various constraints.

The complexity of this problem can be considered from three standpoints: electrical (it is an alternating current, with a nonlinear perspective), computational (it is non-convex, and in some considerations, it contains both binary and continuous variables), and economic (a multi-part non-linear pricing is in fact an inseparable part of the efficient market equilibrium) (CAIN et al., 2012). It should be mentioned that this complexity has forced the researcher to propose several different formulations considering different assumptions related to functions, control variables, and other constraints, in order to find or accelerate finding the optimal solution of OPF problems.

This chapter is prepared in order to cover the shortage of some formulations of OPF in the reference power systems' books or even in the literature.

2.2   MODELS FOR OPTIMAL POWER FLOW PROBLEMS

In order to obtain a complete AC OPF model, at first the commonly used models for transmission lines and transformers are considered. Thus, the operational and physical constraints will be considered in detail.

2.2.1   Transmission line and the transformer models

2.2.1.1 Transmission line models

A transmission line is modeled by using four important elements of series resistance (r_{ij}^l), series inductance (x_{ij}^l), shunt capacitance and shunt conductance ($b_{ij}^{l,ch}$). The physical composition of a conductor defines the series resistance, which is a temperature-dependent element (ZARCO; GOMEZ-EXPOSITO, 2000). The magnetic and electric fields around the conductors yield series inductance and shunt capacitance. Flowing of leakage currents across the insulators and air produces the shunt conductance. In such systems, compared with the nominal current, the leakage current is considerably small and negligible. Therefore, for simplicity, it is usually neglected and normally not considered in the transmission line modeling. On the other hand, the line resistance and inductive reactance are considered as the most important elements, whereas in some researches, in order to simplify the model, it is possible to omit the shunt capacitance and conductance. The equivalent π model of a transmission line between buses ij has been presented in Figure 1, where E_i and E_j are the voltages at buses i and j, respectively.

The impedance of series elements are as (1).

$$z_{ij}^l = r_{ij}^l + jx_{ij}^l \qquad i \neq j \tag{1}$$

where z_{ij}^l is the impedance (Ω) of line l between buses ij, and r_{ij}^l and x_{ij}^l are the resistance (Ω) and reactance (Ω) of line l, between buses ij, respectively.

Based on the electrical relationship, in order to find the admittance of each line, it is necessary to find the inverse of impedance as (2).

$$y_{ij}^l = (z_{ij}^l)^{-1} = g_{ij}^l + jb_{ij}^l = \frac{r_{ij}^l}{(r_{ij}^l)^2 + (x_{ij}^l)^2} - j\frac{x_{ij}^l}{(r_{ij}^l)^2 + (x_{ij}^l)^2} \qquad i \neq j \tag{2}$$

where y_{ij}^l is the admittance ($\mho$) of line l between buses ij.

Then the conductance (g_{ij}^l) and susceptance (b_{ij}^l) of each line are as (3) and (4).

Figure 1- The π model of a transmission line
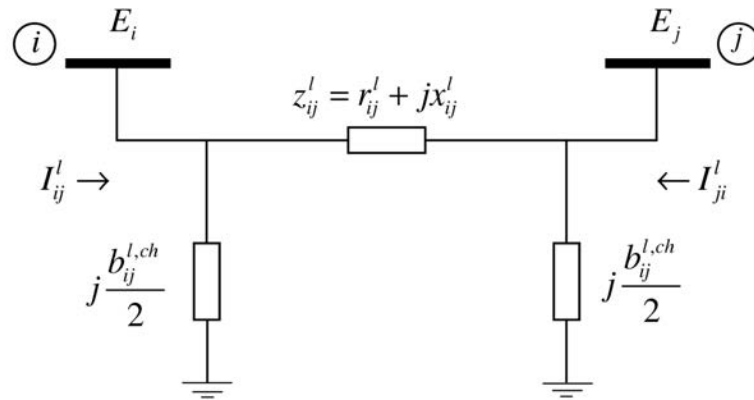
Source: Monticelli (1946).

$$g_{ij}^l = \frac{r_{ij}^l}{(r_{ij}^l)^2 + (x_{ij}^l)^2} \qquad i \neq j \tag{3}$$

$$b_{ij}^l = \frac{-x_{ij}^l}{(r_{ij}^l)^2 + (x_{ij}^l)^2} \qquad i \neq j \tag{4}$$

It is worth mentioning that in the π model with positive resistance and inductance, the conductance is positive and the susceptance is negative (which shows its inductive characteristic). Also, the shunt element is positive, which presents that the shunt element is a capacitive one.

Using Figure 1, the direct and indirect currents of I_{ij}^l and I_{ij}^l are calculated as (5) and (6) respectively.

$$I_{ij}^l = y_{ij}^l (E_i - E_j) + j\frac{b_{ij}^{l,ch}}{2} E_i \tag{5}$$

$$I_{ji}^l = y_{ij}^l (E_j - E_i) + j\frac{b_{ij}^{l,ch}}{2} E_j \tag{6}$$

where $E_i = v_i e^{j\theta_i}$ and $E_j = v_j e^{j\theta_j}$ are the voltages of buses i and j with the magnitude of v_i and v_j and angles of θ_i and θ_j respectively. Additionally, $b_{ij}^{l,ch}$ is the shunt susceptance, known as charging susceptance, of line l between buses ij.

The complex power flow is defined as (7).

$$S_{ij}^{l^*} = E_i^* \left[y_{ij}^l (E_i - E_j) + jE_i \frac{b_{ij}^{l,ch}}{2} \right]$$

$$= y_{ij}^l E_i^2 - y_{ij}^l E_i^* E_j + j \frac{b_{ij}^{l,ch}}{2} E_i^2 \qquad (7)$$

$$= \left[g_{ij}^l + j(b_{ij}^l + j \frac{b_{ij}^{l,sh}}{2}) \right] v_i^2 - (g_{ij}^l + jb_{ij}^l) v_i v_j (\cos\theta_{ij} - j\sin\theta_{ij})$$

where S^{l^*} and E^* are the conjugates of complex power and bus voltage, respectively. g_{ij}^l and b_{ij}^l are the susceptance and series conductance of line l between buses ij respectively, and θ_{ij} is defined as the difference between the angles of two buses ($\theta_{ij} = \theta_i - \theta_j$).

The active and reactive power flows are the real and imaginary parts of the complex power flow as (8) and (9), respectively.

$$p_{ij}^l = \Re\{s_{ij}^{l^*}\} = g_{ij}^l v_i^2 - v_i v_j (g_{ij}^l \cos\theta_{ij} + b_{ij}^l \sin\theta_{ij}) \qquad (8)$$

$$q_{ij}^l = \Im(\iota_{ij}^{l^*}) = -(b_{ij}^l + \frac{b_{ij}^{l,ch}}{2}) v_i^2 - v_i v_j (g_{ij}^l \sin\theta_{ij} - b_{ij}^l \cos\theta_{ij}) \qquad (9)$$

The reverse active and reactive flows from bus i to bus j are obtained in the same way of direct power flows as (10) and (11).

$$p_{ji}^l = g_{ij}^l v_j^2 - v_i v_j (g_{ij}^l \cos\theta_{ij} - B_{ij}^l \sin\theta_{ij}) \qquad (10)$$

$$q_{ji}^l = -(b_{ij}^l + \frac{b_{ij}^{l,ch}}{2}) v_j^2 + v_i v_j (g_{ij}^l \sin\theta_{ij} + b_{ij}^l \cos\theta_{ij}) \qquad (11)$$

2.2.1.2 Transformer model

If using a transformer in the transmission line taken into consideration, some changes will apply to the abovementioned formulation. Usually a phase shifting transformer is modeled as Figure 2. In this figure tp_{ij}^l is the tap of a transformer in line l between buses ij, and I_{ij}^l and I_{ji}^l are the currents from one side to the other side of a circuit.

Figure 2- Transmission line considering the transformer model
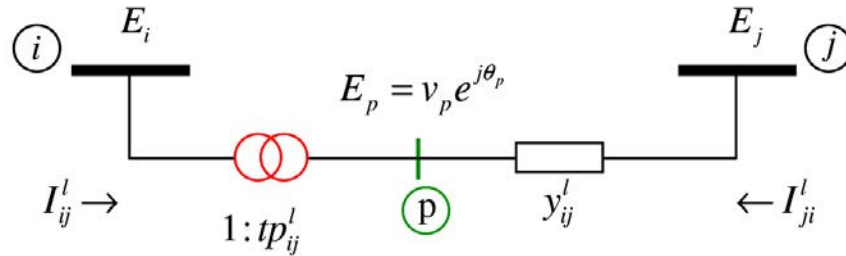
Source: Monticelli (1946).

In Figure 2, the bus p is a fictitious bus. Based on the transformer type, the tap is defied in such a way that for the boosting transformer that does not influence on the phase, $tp_{ij}^{l} = a_{ij}^{l}$; for a phase-shifting transformer the tap is $tp_{ij}^{l} = e^{j\varphi_{ij}^{l}}$; and for a phase shifting transformer and tap changer, $tp_{ij}^{l} = a_{ij}^{l}e^{j\varphi_{ij}^{l}}$.

Note that a_{ij}^{l} is a real number and φ is the phase shifting of the transformer.

a) Boosting transformer

The model for a boosting transformer is presented in Figure 3.

Figure 3- Boosting transformer model in transmission line
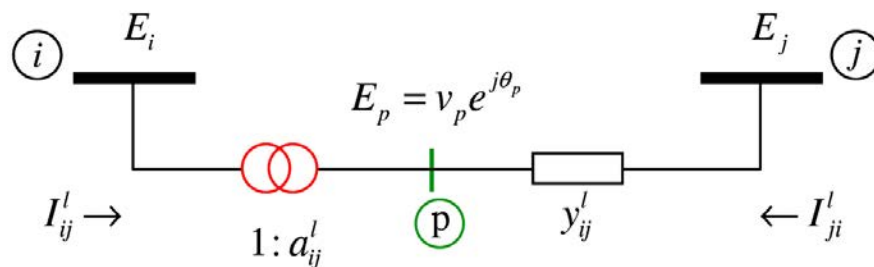
Source: Monticelli (1946).

Based on the model displayed in Figure 3, the following relations are obtained.

$$\frac{E_i}{E_p} = \frac{1}{a_{ij}^{l}} = -\frac{I_{ji}^{l}}{I_{ij}^{l}} = \frac{I_{pj}^{l}}{I_{ij}^{l}} \tag{12}$$

$$
\begin{aligned}
I_{ij}^l &= a_{ij}^l I_{pj}^l = a_{ij}^l(-I_{ji}^l) \\
&= a_{ij}^l[y_{ij}^l(E_p - E_j)] \\
&= a_{ij}^l \, y_{ij}^l(a_{ij}^l E_i - E_j)
\end{aligned}
\tag{13}
$$

And on the other hand, for I_{ji}:

$$
\begin{aligned}
I_{ji}^l &= -I_{pj}^l \\
&= -[y_{ij}^l(E_p - E_j)] \\
&= -y_{ij}^l(a_{ij}^l E_i - E_j)
\end{aligned}
\tag{14}
$$

The complex power flow is defined as (15).

$$
\begin{aligned}
S_{ij}^{l^*} &= E_i^*\left[a_{ij}^l \, y_{ij}^l(a_{ij}^l E_i - E_j)\right] \\
&= (a_{ij}^l)^2 \, y_{ij}^l E_i^2 - a_{ij}^l y_{ij}^l E_i^* E_j \\
&= (a_{ij}^l)^2 (g_{ij}^l + jb_{ij}^l)v_i^2 - a_{ij}^l(g_{ij}^l + jb_{ij}^l)v_i v_j(\cos\theta_{ij} - j\sin\theta_{ij})
\end{aligned}
\tag{15}
$$

Then the active and reactive power flows are as follow.

$$
p_{ij}^l = (a_{ij}^l \, v_i)^2 g_{ij}^l - (a_{ij}^l \, v_i)v_j(g_{ij}^l \cos\theta_{ij} + b_{ij}^l \sin\theta_{ij})
\tag{16}
$$

$$
q_{ij}^l = -(a_{ij}^l \, v_i)^2 b_{ij}^l - (a_{ij}^l \, v_i)v_j(g_{ij}^l \sin\theta_{ij} - b_{ij}^l \cos\theta_{ij})
\tag{17}
$$

$$
p_{ji}^l = g_{ij}^l v_j^2 - (a_{ij}^l v_i)v_j(g_{ij}^l \cos\theta_{ij} - B_{ij}^l \sin\theta_{ij})
\tag{18}
$$

$$
q_{ji}^l = -b_{ij}^l v_j^2 + (a_{ij}^l v_i)v_j(g_{ij}^l \sin\theta_{ij} + b_{ij}^l \cos\theta_{ij})
\tag{19}
$$

By considering the charging susceptance, $b_{ij}^{l,ch}$, in the model the formulations of (16)-(19) are modified as (20)-(23). A detailed consideration of $b_{ij}^{l,ch}$ is presented in the boosting and phase-shifting transformer section.

$$
p_{ij}^l = (a_{ij}^l \, v_i)^2 g_{ij}^l - (a_{ij}^l \, v_i)v_j(g_{ij}^l \cos\theta_{ij} + b_{ij}^l \sin\theta_{ij})
\tag{20}
$$

$$
q_{ij}^l = -(a_{ij}^l \, v_i)^2(b_{ij}^l + \frac{b_{ij}^{l,sh}}{2}) - (a_{ij}^l \, v_i)v_j(g_{ij}^l \sin\theta_{ij} - b_{ij}^l \cos\theta_{ij})
\tag{21}
$$

$$
p_{ji}^l = g_{ij}^l v_j^2 - (a_{ij}^l v_i)v_j(g_{ij}^l \cos\theta_{ij} - B_{ij}^l \sin\theta_{ij})
\tag{22}
$$

$$
q_{ji}^l = -(b_{ij}^l + \frac{b_{ij}^{l,ch}}{2})v_j^2 + (a_{ij}^l v_i)v_j(g_{ij}^l \sin\theta_{ij} + b_{ij}^l \cos\theta_{ij})
\tag{23}
$$

b) Phase-shifting transformer

The model of a phase-shifting transformer, which has a little influence on the power flows ($a_{ij} \simeq 1$) has been modeled as Figure 4, where in this model, it has been considered that $a_{ij} = 1$.

Figure 4- Phase-shifting transformer model in the transmission line
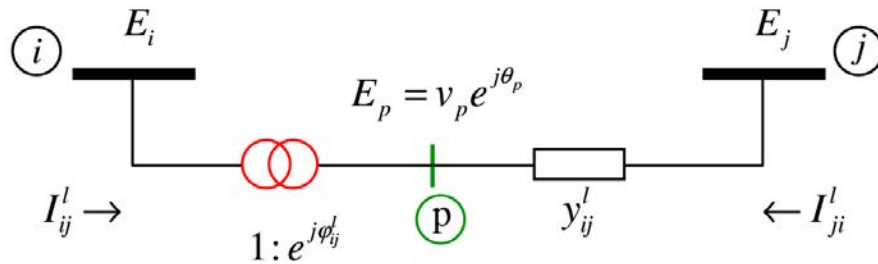
Source: Monticelli (1946).

Based on the model, the relationship of (24) is at hand.

$$\frac{E_i}{E_p} = \frac{1}{e^{j\phi_{ij}^l}} \implies E_p = E_i e^{j\phi_{ij}^l}$$

$$\implies v_p e^{j\theta_p} = v_i e^{j(\theta_i + \phi_{ij}^l)} \tag{24}$$

As the voltage magnitudes are equal ($v_p = v_i$) then:

$$\theta_p = \theta_i + \varphi_{ij} \tag{25}$$

On the other hand the relationship between direct and indirect power flows considering an ideal transformer is as (26).

$$\begin{aligned}
E_i I_{ij}^{l*} + E_p I_{ji}^{l*} &= 0 \\
E_i I_{ij}^{l*} + E_i e^{j\phi_{ij}^l} I_{ji}^{l*} &= 0 \\
I_{ij}^{l*} + I_{ji}^{l*} e^{j\phi_{ij}^l} &= 0
\end{aligned} \tag{26}$$

Then,

$$\frac{I_{ij}^l}{I_{ji}^l} = -e^{-j\phi_{ij}^l} = -tp^* \tag{27}$$

where, the current I_{ji}^l is calculated as (28).

$$I_{nm}^l = y_{mn}^l (E_n - E_p)$$
$$= y_{mn}^l (E_n - tp_{mn}^l E_m)$$
$$= (-tp_{mn}^l y_{mn}^l) E_m + y_{mn}^l E_n) \tag{28}$$

Therefore the direct current from bus m to bus n is calculated as (29).

$$I_{ij}^l = -tp_{ij}^{l\,*} I_{ji}$$
$$= -tp_{ij}^{l\,*} [(-tp_{ij}^l y_{ij}^l) E_i + (y_{ij}^l) E_j]$$
$$= (|tp_{ij}^l|^2 y_{ij}^l) E_i + (-tp_{ij}^{l\,*} y_{ij}^l) E_j, \text{ and in this model } |tp_{ij}^l| = |e^{j\varphi_{ij}^l}| = 1 \tag{29}$$
$$= (y_{ij}^l) E_i + (-tp_{ij}^{l\,*} y_{ij}^l) E_j$$

The complex power is calculated as (30).

$$S_{ij}^* = E_i^* [I_{ij}]$$
$$= y_{ij} v_i e^{-j(\theta_i + \varphi_{ij})} (v_i e^{j(\theta_i + \varphi_{ij})} - v_j e^{j\theta_j}) \tag{30}$$

According to (30) and by separating its real and imaginary parts, the active and reactive power flows are obtained.

$$p_{ij} = v_i^2 g_{ij}^l - v_i v_j [g_{ij}^l \cos(\theta_{ij} + \varphi_{ij}) + b_{ij}^l \sin(\theta_{ij} + \varphi_{ij})] \tag{31}$$

$$q_{ij} = -v_i^2 b_{ij}^l - v_i v_j [g_{ij}^l \sin(\theta_{ij} + \varphi_{ij}) - b_{ij}^l \cos(\theta_{ij} + \varphi_{ij})] \tag{32}$$

$$p_{ji} = g_{ij}^l v_j^2 - v_i v_j [g_{ij}^l \cos(\theta_{ij} + \varphi_{ij}) - B_{ij}^l \sin(\theta_{ij} + \varphi_{ij})] \tag{33}$$

$$q_{ji} = -b_{ij}^l v_j^2 + v_i v_j [g_{ij}^l \sin(\theta_{ij} + \varphi_{ij}) + b_{ij}^l \cos(\theta_{ij} + \varphi_{ij})] \tag{34}$$

In the aforementioned formulation, if the charging susceptance, $b_{ij}^{l,ch}$, is taken into account, some modifications will be applied as (35)-(38). The details about considering $b_{ij}^{l,ch}$ has been stated in the boosting and phase-shifting transformer section.

$$p_{ij} = v_i^2 g_{ij}^l - v_i v_j [g_{ij}^l \cos(\theta_{ij} + \varphi_{ij}) + b_{ij}^l \sin(\theta_{ij} + \varphi_{ij})] \tag{35}$$

$$q_{ij} = -v_i^2 (b_{ij}^l + \frac{b_{ij}^{l,ch}}{2}) - v_i v_j [g_{ij}^l \sin(\theta_{ij} + \varphi_{ij}) - b_{ij}^l \cos(\theta_{ij} + \varphi_{ij})] \tag{36}$$

$$p_{ji} = g_{ij}^l v_j^2 - v_i v_j [g_{ij}^l \cos(\theta_{ij} + \varphi_{ij}) - b_{ij}^l \sin(\theta_{ij} + \varphi_{ij})] \tag{37}$$

$$q_{ji} = -(b_{ij}^l + \frac{b_{ij}^{l,ch}}{2}) v_j^2 + v_i v_j [g_{ij}^l \sin(\theta_{ij} + \varphi_{ij}) + b_{ij}^l \cos(\theta_{ij} + \varphi_{ij})] \tag{38}$$

c) Boosting and phase-shifting transformer

This is a complete model that considers both the boosting and phase-shifter characteristics of a transformer as shown in Figure 5. In practice, it may be necessary to use two separate transformers, a magnetizing transformer and a boosting transformer.

Figure 5- Boosting and phase-shifting transformer model in transmission line
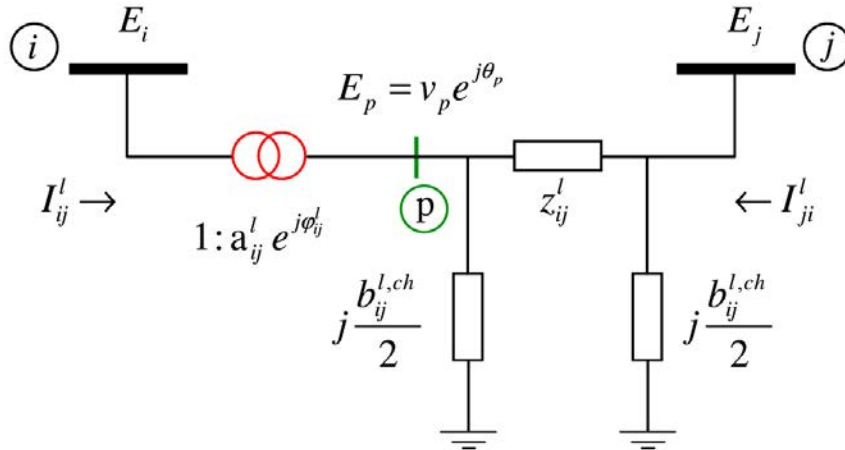
Source: Monticelli (1946).

The direct and reverse currents of this model are defined as (39) and (40).

$$I_{ij}^l = \left(\left|tp_{ij}^l\right|^2 y_{ij}^l + j\frac{b_{ij}^{l,ch}}{2}\right)E_i + \left(-tp_{ij}^{l\,*} y_{ij}^l\right)E_j \tag{39}$$

$$I_{ij}^l = \left(-tp_{ij}^l y_{ij}^l\right)E_i + \left(y_{ij}^l + j\frac{b_{ij}^{l,ch}}{2}\right)E_j \tag{40}$$

where, in this model $tp_{ij}^l = a_{ij}^l\, e^{j\varphi_{ij}^l}$.

By separating the real and imaginary part of the complex powers of (41), the active and reactive power flows are as (42)-(45).

$$S_{ij}^{l\,*} = E_i^* I_{ij}^l$$
$$S_{ji}^{l\,*} = E_j^* I_{ji}^l \tag{41}$$

$$p_{ij} = (a_{ij}^l v_i)^2 g_{ij}^l - (a_{ij}^l v_i)v_j[g_{ij}^l \cos(\theta_{ij} + \varphi_{ij}) + b_{ij}^l \sin(\theta_{ij} + \varphi_{ij})] \tag{42}$$

$$q_{ij} = -(a_{ij}^l v_i)^2\left(b_{ij}^l + \frac{b_{ij}^{l,ch}}{2}\right) - (a_{ij}^l v_i)v_j[g_{ij}^l \sin(\theta_{ij} + \varphi_{ij}) - b_{ij}^l \cos(\theta_{ij} + \varphi_{ij})] \tag{43}$$

$$p_{ji} = g_{ij}^l v_j^2 - (a_{ij}^l v_i)v_j[g_{ij}^l \cos(\theta_{ij} + \varphi_{ij}) - b_{ij}^l \sin(\theta_{ij} + \varphi_{ij})] \tag{44}$$

$$q_{ji} = -(b_{ij}^l + \frac{b_{ij}^{l,ch}}{2})v_j^2 + (a_{ij}^l v_i)v_j[g_{ij}^l \sin(\theta_{ij} + \varphi_{ij}) + b_{ij}^l \cos(\theta_{ij} + \varphi_{ij})] \qquad (45)$$

2.2.2 Optimal power flow model

In this work, the formulations of (42)-(45) are used to obtain a general OPF model. Upon the request, this general formulation may be used to optimize various single objective functions as well as multi-objective problems (MOMOH, 2000). There are numerous methodologies that can be employed in order to find a solution for an OPF problem, where some are classical optimization methods and the others are heuristic search based methods such as what are used in linear programming (LP) (LIMA et al., 2003), Newton-Raphson (NR) (LO; MENG, 2004), nonlinear programming (NLP) (PUDJIANTO et al., 2002), quadratic programming (QP) (BERIZZI et al., 2005), interior point (IP) and decomposed predictor-corrector interior point (DPCIP) (YAN et al., 2006; CHUNG; YAN; LIU, 2011), genetic algorithm (GA) (CAI et al., 2004), miscellaneous artificial intelligent (MAI) (MORI; GOTO, 2000), evolutionary programming (EP) (ONGSAKUL; JIRAPONG, 2005), ant colony optimization (ACO) (SHI et al., 2004), particle swarm optimization (PSO) (VLACHOGIANNIS; LEE, 2005), fuzzy logic (FL) (PADHY, 2004), etc. Moreover, some works have considered the combination of classical methods and a metaheuristic algorithm in order to modify the drawbacks of these methods (ALRASHIDI; EL-HAWARY, 2007; SIVASUBRAMANI; SWARUP, 2011; XU et al., 2012).

The general mathematical formulation of an OPF is presented in (46)-(48).

Min or Max $f(x,u)$ \qquad (46)

subject to:

$\mathbf{G}(x,u) = 0$ \qquad (47)

$\underline{\mathbf{H}} \leq \mathbf{H}(x,u) \leq \overline{\mathbf{H}}$ \qquad (48)

where $f(x,u)$ in (46) as the objective function can be minimized or maximized depending on the controller center policy. $\mathbf{G}(x,u)$ in (47) is related to quality constraints, and $\mathbf{H}(x,u)$ in (48) presents the inequality constraints between the lower bound, $\underline{\mathbf{H}}$, and the upper bound, $\overline{\mathbf{H}}$. The commonly used objectives are as follow.

> ➢ Active power-related objectives: Economic dispatch objectives (related to minimization of the generation costs and transmission losses), emission dispatch, maximum allowable transfer of the active power.

> ➢ Reactive power-related objectives (minimization of active and/or reactive power losses, minimizing the investment cost of VAr planning).

> ➢ Minimizing the number of controls' shift to alleviate the violation.

> ➢ Minimizing the deviations from a target schedule.

where, a variety of constrains are taken into consideration such as:

> ➢ The constraints on control variables such as: active and reactive generation limits, transformer tap limit, shunt capacitor range limit.

> ➢ The operating constraints such as: flow limits of line and transformer (apparent power limit, current limit, active power flow limit, and reactive power flow limit), interchange limit (active and/or reactive limit), fixed/dynamic reserve margins (active and/or reactive), voltage and angle limits.

Other constraints can be defined based on the main objective of the OPF such as: using some engineering rules to handle the violations, some preferable operating limits, or changing the control rates may be applied as control parameters. In some problems based on localization several controls may be applied.

2.2.2.1 Economic-oriented OPF

One of the most important issues in power systems is their economic considerations and in these days, the tools related to this issue have received more attention in a way that the power system operators consider such tools as the kernel of a power system.

The economic-oriented OPF considers the cost objective function. Several approximations may be used as an objective function such as: piecewise linear, quadratic, cubic, and piecewise quadratic. A linear approximation is usually used in power market models. In this work, the commonly used model, which is a quadratic approximation, is taken into account. The statement of the formulation of this problem is presented as (49).

$$\min F^C(P_g)$$

$$\textit{subject to}: \textit{system and operational constraints} \tag{49}$$

where the objective function of $F^C(P_g)$ is defined as (50).

$$F^C(P_g) = \sum_{i=1}^{N_g} C_i(P_{g_i}) \tag{50}$$

In general the fuel cost function in (50) is defined as the quadratic function of (51) (MITTAL, 2011).

$$C_i(P_{g_i}) = \sum_{j=1}^{PL} a_{ji}(P_{g_i})^j + a_{0i} + r_i, \qquad i \in \Omega_g \tag{51}$$

where $C_i(\cdot)$ is the cost function of bus i; P_{g_i} is the active power generation (MW) at bus i; Ω_g is the set of generating buses; a_{0i} and a_{ji} are the cost coefficients, r_i is the corresponding error of the ith equation; and PL defines the order of the objective function.

In this work, the commonly used model, which is a quadratic approximation, (52), is taken into account.

$$C_i(P_{g_i}) = a_i(P_{g_i})^2 + b_i P_{g_i} + c_i, \qquad i \in \Omega_g \tag{52}$$

where $a_i\,(\$/MW^2h)$, $b_i\,(\$/MWh)$, $c_i\,(\$)$ are the quadratic, linear, and constant cost coefficients.

The constraints for such problems are considered in detail in below.

➢ Active and reactive equality constraints: the active equality constraint is as (53) and the reactive equality constraint is as (54).

$$P_{g_i} - P_{d_i} - P_i(V, \delta, tp) = 0, \qquad i \in \Omega_b \tag{53}$$

$$Q_{g_i} - Q_{d_i} - Q_i(V, \delta, tp) = 0, \qquad i \in \Omega_b \tag{54}$$

where, P_{g_i}, P_{d_i}, and P_i are the active power generation (MW), active power demand (MW), and active power injection (MW) at bus i respectively; Q_{g_i}, Q_{d_i}, and Q_i are the reactive

power generation ($MVAr$), rective power demand ($MVAr$), and rective power injection ($MVAr$) at bus i, respectively; and Ω_g is the set of all buses, containing generating buses.

➢ Transmission line flow limit: in power systems, each line has a power flow limit based on the surge impedance loading limit, voltage drop limit, and thermal limits. This limit, $fl_{ij}^l(\cdot)$, is formulated as (55).

$$\left| fl_{ij}^l(V,\delta,tp) \right| \le \overline{fl}_{ij}^l, \qquad ij \in \Omega_L \tag{55}$$

where, $\overline{fl}_{ij}^l$ is the maximum limit of power flow in line l between buses ij; Ω_L is the set of transmission lines.

➢ Voltage magnitude limit: the voltage magnitude of each bus has a lower and upper bound as (56).

$$\underline{V}_i \le V_i \le \overline{V}_i, \quad i \in \Omega_b \tag{56}$$

➢ Active and reactive power limit: each generator can generate within its limit for active and reactive power as (57) and (58) respectively.

$$\underline{P}_{g_i} \le P_{g_i} \le \overline{P}_{g_i}, \quad i \in \Omega_g \tag{57}$$

$$\underline{Q}_{g_i} \le Q_{g_i} \le \overline{Q}_{g_i}, \quad i \in \Omega_g \tag{58}$$

where, $\underline{P}_{g_i}$ and $\overline{P}_{g_i}$ are the lower and upper bounds of the active power generation, respectively. $\underline{Q}_{g_i}$ and $\overline{Q}_{g_i}$ are the lower and upper bounds of the reactive power generation, respectively.

➢ Transformer tap: along a transformer winding, there is a connection point that prepares a certain number of turns to be selected for regulation of the output voltage. Each tap changing generator has an upper and lower limit as (59).

$$\underline{tp}_{ij}^l \le tp_{ij}^l \le \overline{tp}_{ij}^l, \quad ij \in \Omega_L \tag{59}$$

where, $\underline{tp}_{ij}^l$ and $\overline{tp}_{ij}^l$ are lower and upper bounds of a transformer tap in line l between bus ij.

Then, the overall formulation for an OPF problem can be shown as (60).

$$\min F^C(P_g)$$

subject to:

$$P_{g_i} - P_{d_i} - P_i(V, \delta, tp) = 0, \qquad i \in \Omega_b$$

$$Q_{g_i} - Q_{d_i} - Q_i(V, \delta, tp) = 0, \qquad i \in \Omega_b$$

$$\left| fl_{ij}^l(V, \delta, tp) \right| \le \overline{fl_{ij}^l}, \qquad ij = \Omega_L \tag{60}$$

$$\underline{V_i} \le V_i \le \overline{V_i}, \qquad i \in \Omega_b$$

$$\underline{P_{g_i}} \le P_{g_i} \le \overline{P_{g_i}}, \qquad i \in \Omega_g$$

$$\underline{Q_{g_i}} \le Q_{g_i} \le \overline{Q_{g_i}}, \qquad i \in \Omega_g$$

$$\underline{tp_{ij}^l} \le \left| tp_{ij}^l \right| \le \overline{tp_{ij}^l}, \qquad ij = \Omega_L$$

By taking into consideration the active and reactive equality constraints of (53) and (54) in detail, the equality constraints of (61)-(66) are achieved.

$$P_{g_i} - P_{d_i} - g_i^{b,sh} v_i^2 - \sum_{ij \in \Omega_L} p_{ij} - \sum_{ji \in \Omega_L} p_{ji} = 0, \qquad i \in \Omega_b \tag{61}$$

where $g_i^{b,sh}$ is the shunt conductance of bus i (Ω), p_{ij} and p_{ji} are the direct and reverse active power injections.

$$p_{ij} = (a_{ij}^l v_i)^2 g_{ij}^l - (a_{ij}^l v_i) v_j [g_{ij}^l \cos(\theta_{ij} + \varphi_{ij}) + b_{ij}^l \sin(\theta_{ij} + \varphi_{ij})] \tag{62}$$

$$p_{ji} = g_{ij}^l v_j^2 - (a_{ij}^l v_i) v_j [g_{ij}^l \cos(\theta_{ij} + \varphi_{ij}) - B_{ij}^l \sin(\theta_{ij} + \varphi_{ij})] \tag{63}$$

also for the reactive power flow:

$$Q_{g_i} - Q_{d_i} + b_i^{b,sh} v_i^2 - \sum_{ij \in \Omega_L} q_{ij} - \sum_{ji \in \Omega_L} q_{ji} = 0, \qquad i \in \Omega_b \tag{64}$$

where $b_i^{b,sh}$ is the shunt susceptance of bus i ($\mho$), q_{ij} and q_{ji} are the direct and reverse reactive power injections.

$$q_{ij} = -(a_{ij}^l v_i)^2 (b_{ij}^l + \frac{b_{ij}^{l,ch}}{2}) - (a_{ij}^l v_i) v_j [g_{ij}^l \sin(\theta_{ij} + \varphi_{ij}) - b_{ij}^l \cos(\theta_{ij} + \varphi_{ij})] \tag{65}$$

$$q_{ji} = -(b_{ij}^l + \frac{b_{ij}^{l,ch}}{2}) v_j^2 + (a_{ij}^l v_i) v_j [g_{ij}^l \sin(\theta_{ij} + \varphi_{ij}) + b_{ij}^l \cos(\theta_{ij} + \varphi_{ij})] \tag{66}$$

2.2.2.2 Environment-oriented OPF

Harmful environmental impacts of generating electricity are the inseparable parts of

each technology used in this field. These days, there is a growing concern for harmful environmental impacts (BASU et al., 2006; KASMAEI et al., 2013), which can extensively affect human health. Air pollution, in particular, can cause a variety of environmental effects such as acid rain, eutrophication, haze, effects on wildlife, ozone depletion, crop, forest damage, and global climate change. Since 1990, the Clean Air Act Amendments (CAAA) state that utilities have to modify their design or operational strategies in order to decrease atmospheric pollution emissions (SUDHAKARAN et al., 2004; LAMONT; OBESSIS, 1995).

An environment-oriented OPF considers the environmental effects of generating electric power. The mathematical model of such a problem is the same as the model for an economic-oriented OPF, but with a different objective function. The objective function minimizes the total amount of emissions of a power system. The mathematical model for such a problem has been presented in .

$$\min F^E(P_g)$$

$$subject\ to:$$

$$
\begin{aligned}
P_{g_i} - P_{d_i} - P_i(V, \delta, tp) &= 0, &\quad i &\in \Omega_b \\
Q_{g_i} - Q_{d_i} - Q_i(V, \delta, tp) &= 0, &\quad i &\in \Omega_b \\
\left| fl_{ij}^l(V, \delta, tp) \right| &\le \overline{fl_{ij}^l}, &\quad ij &= \Omega_L \\
\underline{V_i} \le V_i &\le \overline{V_i}, &\quad i &\in \Omega_b \\
\underline{P_{g_i}} \le P_{g_i} &\le \overline{P_{g_i}}, &\quad i &\in \Omega_g \\
\underline{Q_{g_i}} \le Q_{g_i} &\le \overline{Q_{g_i}}, &\quad i &\in \Omega_g \\
\underline{tp_{ij}^l} \le tp_{ij} &\le \overline{tp_{ij}^l}, &\quad ij &= \Omega_L
\end{aligned}
$$

(67)

where the objective function of can be considered as (68), which is a commonly used function, or as (69), which usually refers to NO_x emission model.

$$
\begin{aligned}
F^{Em}(P_g) &= \sum_{i=1}^{\Omega_g} Em_i(P_{g_i}) \\
&= \sum_{i=1}^{\Omega_g} \alpha_i(P_{g_i})^2 + \beta_i P_{g_i} + \gamma_i
\end{aligned}
$$

(68)

where, $\alpha_i \left(\frac{kg}{MW^2 h}\right)$, $\beta_i \left(\frac{kg}{MWh}\right)$, c_i (kg) are the quadratic, linear, and constant emission coefficients.

$$F^{Em}(P_g) = \sum_{i=1}^{\Omega_g} Em_i(P_{g_i})$$

$$= \sum_{i=1}^{\Omega_g} \alpha_i (P_{g_i})^2 + \beta_i P_{g_i} + \gamma_i + \xi_i \exp(\kappa_i P_{g_i})$$

(69)

The constraints of this problem are completely the same as (60).

2.2.3 Active-reactive optimal power flow model

On the other hand, the reactive power has a key role in power systems, where it affects the voltage profile. Additionally, it has a close relationship with the active power generation as the generation and transfer of the reactive power yields an active power loss and therefore, consumes energy. In order to consider this profound effect, application of an active-reactive optimal power flow (AROPF) is taken into account and as a result, the capability curve, as a nonlinear constraint, is considered (XIA; CHAN, 2006; ALMEIDA; SENNA, 2011; GABASH; LI, 2012). For a synchronous generator, operating at the rated voltage, the capability curves give the maximum active and reactive power loadings, which can be supplied without an armature heating limit or with the field heating limit (ALMEIDA; SALGADO, 2000). In this work, the active-reactive OPF is formulated as (70), where only the effects of reactive power flow on active power flow is taken into consideration.

$$\min F^E(P_g)$$
$$subject\,to:$$
$$P_{g_i} - P_{d_i} - P_i(V, \delta, t) = 0, \qquad i \in \Omega_b$$
$$Q_{g_i} - Q_{d_i} - Q_i(V, \delta, t) = 0, \qquad i \in \Omega_b$$
$$\left| fl_{ij}^l(V, \delta, t) \right| \le \overline{fl_{ij}^l}, \qquad ij = \Omega_L$$
$$\underline{V_i} \le V_i \le \overline{V_i}, \qquad i \in \Omega_b$$
$$\underline{P_{g_i}} \le P_{g_i} \le P_{g_i}^M(Q_{g_i}), \qquad i \in \Omega_g$$
$$\underline{Q_{g_i}} \le Q_{g_i} \le \overline{Q_{g_i}}, \qquad i \in \Omega_g$$
$$\underline{t_{ij}^l} \le t_{ij}^l \le \overline{t_{ij}^l}, \qquad ij = \Omega_L$$

(70)

The difference between this formulation and (60) is the consideration of $P_{g_i}^M(Q_{g_i})$ instead of $\overline{P_{g_i}}$. Since the capability curve, $P_{g_i}^M(Q_{g_i})$, is a highly nonlinear function, finding an optimal solution for problem (70) is a complicated task.

$P_{g_i}^M(Q_{g_i})$ limit is imposed by the capability curve and turbine. The capability curve has three different portions, as can be seen in Figure 6. The constant and maximum armature current is defined as the central portion. The constant and maximum excitation is modeled as the right-hand portion, where the output power of an overexcited machine is limited by the imposed limit of this curve. The left-hand portion is defined for an under-excited machine related to the theoretical stability limit or the maximum allowable heating of the armature windings and is usually approximated by a straight line. The details of this curve are considered as follow (RUEDA; ALMEIDA, 2001).

Figure 6- Capability curve
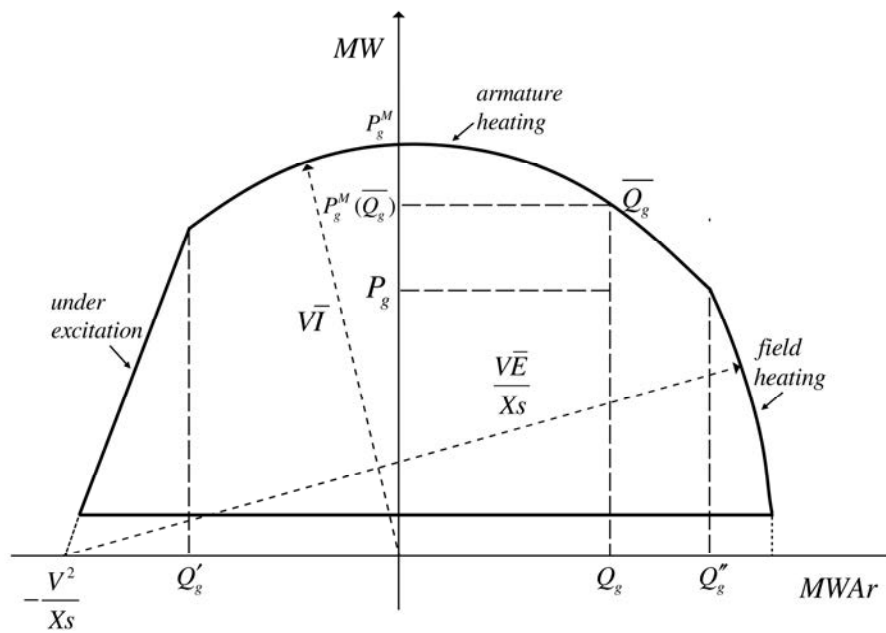
Source: The author

In order to get the mathematical formulation to calculate $P_{g_i}^M(Q_{g_i})$, the model and the phase diagram depicted in Figure 7 is used. In this figure, Xs_i is the synchronous reactance of the machine, E_i is the excitation voltage, v_i is the bus voltage magnitude and is usually assumed as $1(p.u)$, I_i the injected current, Φ_i is the power factor angle, and θ_i is the load angle.

The active and reactive powers injected by the machine are defined as (71), which are shown in the phase diagram of Figure 7 (B).

Figure 7- Model of a machine and the phase diagram
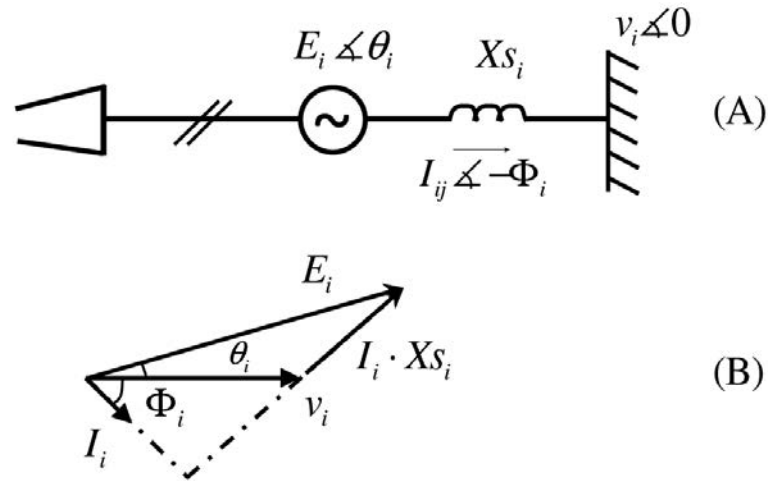
Source: The author

$$P_{g_i} = V_i I_i \cos \Phi_i = \frac{V_i E_i}{Xs_i} \sin \theta_i, \qquad i \in \Omega_b$$

$$Q_{g_i} = V_i I_i \sin \Phi_i = \frac{V_i E_i \cos \theta_i - V_i^2}{Xs_i}, \qquad i \in \Omega_b$$

(71)

The central region is related to the limits imposed by the machine's armature current and its power factor. In this region, the following relation of (72) is at hand.

$$P_{g_i}^M (Q_{g_i}) = \sqrt{S_{g_i}^2 - Q_{g_i}^2}, \qquad i \in \Omega_b$$

(72)

where S_{g_i} is the rated VA of the machine.

Then the values of the central part of the capability curve are defined as (73)-(76).

$$Q'_{g_i} = S_{g_i} \sin(-\Phi), \qquad i \in \Omega_b$$ (73)

$$Q''_{g_i} = S_{g_i} \sin(\Phi), \qquad i \in \Omega_b$$ (74)

$$P'_{g_i} = S_{g_i} \cos(-\Phi), \qquad i \in \Omega_b$$ (75)

$$P''_{g_i} = S_{g_i} \cos(\Phi), \qquad i \in \Omega_b$$ (76)

The intersection of the central and the right regions occurs in (P''_{g_i}, Q''_{g_i}). Thus, the maximum excitation voltage $\overline{E_i}$ is calculated using (77).

$$\overline{E_i} = \sqrt{\frac{(Xs_i P''_{g_i})^2 + (Xs_i P''_{g_i} + V_i^2)^2}{V_i^2}}, \qquad i \in \Omega_b \tag{77}$$

For $Q_{g_i} \geq Q''_{g_i}$, the machine's power output is calculated as (78).

$$\begin{aligned} P_{g_i}^M &= \frac{V_i \overline{E_i}}{Xs_i} \sin\theta_i, & i \in \Omega_b \\ Q_{g_i} &= \frac{V_i \overline{E_i} \cos\theta_i - V_i^2}{Xs_i}, & i \in \Omega_b \end{aligned} \tag{78}$$

In order to obtain the maximum value of Q_{g_i}, the load angle is considered to be zero ($\theta_i = 0$). The maximum reactive power, $\overline{Q_{g_i}}$, is as (79).

$$\overline{Q_{g_i}} = \frac{V_i \overline{E_i} - V_i^2}{Xs_i}, \qquad i \in \Omega_b \tag{79}$$

Thus, for $Q''_{g_i} \leq Q_{g_i} \leq \overline{Q_{g_i}}$, we are in the right-hand region of Figure 6 which is defined as (80) using (78).

$$P_{g_i}^M(Q_{g_i}) = \frac{\sqrt{V_i^2 (\overline{E_i})^2 - (Q_{g_i} Xs_i + V_i^2)^2}}{Xs_i}, \qquad i \in \Omega_b \tag{80}$$

The minimum value of reactive generating capacity is obtained when $\theta = 90$ as (81).

$$\underline{Q_{g_i}} = -\frac{V_i^2}{Xs_i}, \quad i \in \Omega_b \tag{81}$$

Finally for the straight line of the left-hand region in Figure 6, the maximum output power is defined as (82).

$$P_{g_i}^M(Q_{g_i}) = \left(\frac{P'_{g_i}}{Q'_{g_i} - \underline{Q_{g_i}}} \right)(Q_{g_i} - \underline{Q_{g_i}}), \quad i \in \Omega_b \tag{82}$$

It should be noted that, if the turbine limit is taken into consideration for $Q'_{g_i} \leq Q_{g_i} \leq Q''_{g_i}$, (83) is used to define the maximum output power.

$$P_{g_i}^M(Q_{g_i}) = P_{g_i}', \qquad i \in \Omega_b \tag{83}$$

And finally the nonlinear equation related to the capability curve is as (84).

$$P_{g_m}^M(Q_{g_m}) = \begin{cases} \left(\dfrac{P_{g_i}'}{Q_{g_i}' - \underline{P_{g_i}}} \right)(Q_{g_i} - \underline{Q_{g_i}}), & \underline{Q_{g_i}} \leq Q_{g_i} \leq Q_{g_i}', & i \in \Omega_b \\[3mm] \sqrt{S_{g_i}^2 - Q_{g_i}^2}, & Q_{g_i}' \leq Q_{g_i} \leq Q_{g_i}'', & i \in \Omega_b \\[3mm] \dfrac{\sqrt{V_i^2(E_i^{\max})^2 - (Q_{g_i} Xs_i + V_i^2)^2}}{Xs_i}, & Q_{g_i}'' \leq Q_{g_i} \leq \overline{Q_{g_i}}, & i \in \Omega_b \end{cases} \tag{84}$$

The conventional OPF problem is a very large and non-linear mathematical programming problem. Consequently, the AROPF is considered as a highly nonlinear problem in the power systems.

Chapter 3

DYNAMIC ECONOMIC AND EMISSION ACTIVE-REACTIVE OPTIMAL POWER FLOW

3.1   INTRODUCTION

The conventional economic dispatch (ED) (HESLIN; HOBBS, 1989) as a simple OPF plays a crucial role in the optimal operation of power systems and refers to minimizing the total operating costs with considering the equality and inequality constraints. This problem is considered as a large non-linear constrained optimization problem. However, in order to satisfy the demand, a large number of thermal units are committed and according to the fast-growing power demand, the quantity of coal burnt has been also increasing, which yields increasing the released emissions to the atmosphere including SO_2, NO_x, mercury, and other pollutants. Based on the clean air policies and regulations, the electric utilities and power producers have been forced to consider the harmful environmental impacts of the technology that they use for generating electricity under the normal operating condition of power systems. Therefore, in these days, the power plants not only need to consider the economic dispatch problem, but also must consider the emission dispatch problem simultaneously, and such a problem is considered as an economic and emission dispatch (EED) problem. In power systems, the operating costs and emissions have conflicted objectives. In fact, the joint cost and emission considerations are one of the most challenging problems for power systems. In the literature, there are numerous methods that can be harnessed in order to make a compromise between emissions and costs, such as the conventional, heuristic, and hybrid methods (PALANICHAMY; BABU, 2008; GONG et al., 2010). An economic and emission OPF is the extension of an EED, where it is a very large, highly non-linear, and non-convex optimization problem.

In order to find an acceptable compromise between costs and emissions, two type of methodologies have been presented in the literature as follow:

1)   The conventional methodologies, which have been applied to find a compromise point of the EED problems, such as interior-point method, linear programming (LP), non-linear programming (NLP), and quadratic programming (QP) (SONI; BHURIA, 2012). For systems with low non-linearity or for small-scale systems, these methods can find a good compromise solution, while for large-scale or highly non-linear systems, finding an

acceptable or optimal solution is a complicated or very time-consuming task and sometimes they are trapped into a local minimum.

2) The heuristic-based methods, which are the widely-used methodologies in the compromise approach, or the multi-objective problems, such as particle swarm optimization (PSO) (SWARNKAR et al., 2009), artificial bee colony optimization (ABCO) (DIXIT et al., 2011), fuzzy mutated evolutionary programming (FMEP) (PRASANNA; SOMASUNDARAM, 2008), non-dominated sorting differential evolution (NSDE) algorithm (SINHA et al., 2007), artificial immune system (AIS) (GEETHA et al., 2008), intelligent water drops-continuous optimization (IWD-CO) (NAGALAKSHMI et al., 2011), hybrid genetic algorithm (HGA) (KUMARAPPAN; MOHAN, 2004), hybrid cultural approach (HCA) (BHATTACHARYA et al., 2011), and hybrid differential evolution algorithm (HDEA) (GUNDA et al., 2011). Heuristic-based methods were introduced to overcome the drawbacks of conventional methods, but these methods have their own weaknesses and even hybrid methods are the time-consuming approaches (VENKATESH et al., 2003; NIKNAM; DOAGOU-MOJARRAD, 2012b). In these methods and for a single objective function, using a pollution control cost as a compromising factor is undeniable in finding a compromise point, since the compromise point is highly dependent on the compromising factor. In fact, if using a heuristic pollution control cost is taken into account, these methods will become very time consuming and consequently inapplicable for the online-based problems, such as market-based subjects.

In this work, a straight-forward compromise methodology of the dynamic economic and emission active-reactive optimal power flow (AROPF) is proposed. Considering the environmental effects, the AROPF is a highly non-linear problem, and the dynamic consideration of such a problem makes it an even more complicated and extra-high nonlinear problem. Finding an appropriate compromise solution for such problems is regarded as an intricate task. In one hand, the traditional compromise methodologies cannot find an acceptable compromise point for large-scale systems, and on the other hand, the metaheuristic methods are time consuming. In this proposed methodology, some of the drawbacks of the aforementioned methodologies have been oppressed. In this proposed unequivocal normalization-based paradigm (UNBP), instead of maximum output-based pollution control cost (MOPCC), an adaptive pollution control cost (APCC) is used to consider the system

topology in dynamic scheduling and under various system conditions, such as normal, outage, and critical conditions. By using a normalization process and an adaptive pollution control cost, a uniform compromise procedure is obtained.

The above-mentioned contribution will be applied to a dynamic model. A dynamic optimal power flow (DOPF) problem is formulated with the consideration of dynamic constraints. For the DOPF, the ramping constraints couple the scheduling hour. A traditional approach for OPF with N units and T scheduling hours requires solving an optimization problem of size N×T, which is considerably a more complex problem than solving the OPF of an *N*-units system for *T* times (CHUNG et al., 2011; NIKNAM et al., 2011b). Moreover, the dynamic economic and emission OPF (DEEOPF) handles two conflicting objective functions (which are the minimization of total costs and total emissions), in order to acquire a compromise between costs and emissions. This, as a result, makes the problem an even more difficult one. In this chapter, the dynamic economic and emission compromise via an AROPF is taken into consideration. The main contributions of this chapter are as follow: 1) Proposing a paradigm based on a normalization theory in order to find a compromise between costs and emissions via a dynamic active-reactive optimal power flow and 2) Proposing an adaptive pollution control cost (APCC) for the compromise problem with respect to (KASMAEI et al., 2013).

3.2   DYNAMIC ECONOMIC AND EMISSION ACTIVE-REACTIVE OPF

The objective of a dynamic economic and emission AROPF problem is to derive the optimal output of generators. This involves assessing the operating costs and evaluating that how much the corresponding emissions would be produced, in order to be able to provide an acceptable compromise during the scheduling time horizon while satisfying the network and operating constraints and in this regard, the role of a good compromise strategy is incontrovertible.

3.2.1   The compromise strategy

From an engineering standpoint, compromise is an agreement between two different objectives. While each objective accepts less than what it wants, the situations are slightly altered in such a way that they can co-exist together. In addition, it should be stated that in power systems, finding an acceptable compromise between costs and emissions has always

been a challenging issue.

A general formulation for the economic and emission AROPF can be seen in problem (85).

$$\min_{x} F^{C}(x) + h \cdot F^{Em}(x)$$
$$\text{subject to}$$
$$x \in X$$
$$G^{e}(x) = 0$$
$$G^{i}(x) \geq 0$$

(85)

where $F^{C}(\cdot)$ and $F^{Em}(\cdot)$ are the cost and emission objective functions respectively; x and X are respectively the optimization variable and the feasibility set for the power flow variables; $G^{e}(\cdot)$ is the constrained function associated with the equality constrains, and $G^{i}(\cdot)$ is the constrained function associated with the inequality constrains.

In the literature, h is the maximum output-based pollution control cost (MOPCC), which is a ratio of $F^{C}(\cdot)$ and $F^{E}(\cdot)$ at the upper bound output limit ($\overline{x}$) as (86) (VENKATESH et al., 2003).

$$h = \frac{F^{C}(\overline{x})}{F^{Em}(\overline{x})}$$

(86)

In problem (85), both cost and emission objectives are jointly considered where the optimal solution of each objective is not considered in the formulation. Therefore, it may yield a compromise solution that is far from the optimal solution, which means that the compromise methodology is an inappropriate method. For small-scale systems, finding an appropriate compromise point is not a complex task, but for medium- and large-scale systems, where finding an acceptable compromise is considered a highly compound task, the drawback of this formulation will be exposed. In order to alleviate this drawback, it has been proposed in this work to minimize the distance between these objective functions and their optimal solutions.

The drawbacks of this controlling factor are that: 1) the systems usually do not work at their maximum output limits, and 2) with a change in the system topology, they stay at a constant value where these drawbacks may yield an inappropriate compromise under outage

and load fluctuation conditions during the scheduling time horizon. In order to modify this drawback considering (POURAKBAR-KASMAEI et al., 2013), an adaptive pollution control cost (APCC), which is a topology-based factor as (87), is proposed.

$$h^f = \frac{F^C(x^{Em^*})}{F^{Em}(x^{C^*})}$$

(87)

where x^{C^*} is the optimal solution of a cost minimization problem ($F^C(\cdot)$), and x^{Em^*} represents an optimal solution for the emission minimization problem ($F^{Em}(\cdot)$); the numerator represents the operating cost when the emission rate has been minimized. The denominator is the emission rate when the operating cost minimization has been taken into account.

A conflict exists between the cost and emission functions that when the system emissions are minimized, the generation costs are high, and also, when the generation costs are minimized, the amount of system emissions for each generator is high. This adaptive control cost is then regarded as a worthy controlling factor, which is necessary for making a good compromise.

The modified formulation (88) works based on the distances and the adaptive control factor.

Figure 8- The compromise arc between the two optimal points
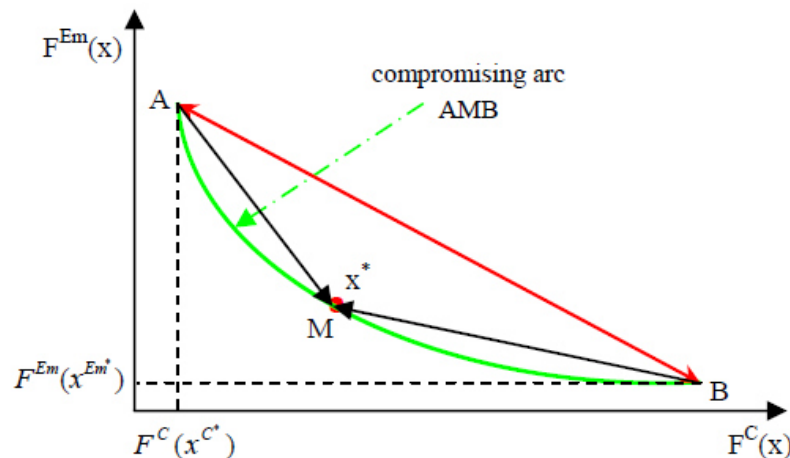
Source: The author

$$\min_{X}[F^{C}(x) - F^{C}(x^{C^{*}})] + h^{f} \cdot [F^{Em}(x) - F^{Em}(x^{Em^{*}})]$$

subject to

$$x \in X \tag{88}$$

$$\mathbf{G}^{e}(x) = 0$$

$$\mathbf{G}^{i}(x) \geq 0$$

In problem (88) and based on Figure 8, the optimal points are $x^{Em^{*}} = B$ and $x^{C^{*}} = A$. Vectors AM and BM are respectively the distances of cost and emission functions from their optimal points, and vectors AB and BA respectively show the maximum distance from the optimal solution of each objective function (the red line). The arc AMB has depicted based on the intersection of two objective functions as $h^{f} \cdot F^{Em}(x) = F^{C}(x)$ (the green arc).

In Figure 8, in the interest of simplicity, $h^{f} \cdot F^{Em}(x)$ has been considered as the unique function of $F^{Em}(x)$. The compromise point (x^{*}) is located on this arc (the red point). It is worth mentioning that this method can be used via a metaheuristic technique, which randomly searches the region between A and B, or via an enumeration technique, which starts from one of the optimal solutions of A or B and moves toward another point. For both metaheuristic and enumeration techniques, it is necessary to solve many AROPFs, which wastes a great amount of time.

Additionally, it is worth stating that, Figure 8 has been portrayed by considering two conflicting quadratic objective functions, and for other multi-objective problems, this figure may have a different appearance.

During the present compromise study, it has been realized that even with these modifications, finding a good compromise is sometimes still a difficult task. This might happen specifically when compromising between two functions with a large gap is taken into account and under the respective operational conditions, the controlling factor would be unable to compensate that. For example, in (88), if $F^{C} >> F^{Em}$, then finding an acceptable compromise point for medium- and large-scale systems is difficult or even impossible. In order to modify this drawback, the normalization application is proposed (89). While in one hand, it removes the large gap between two objectives, on the other hand, it lessens the compromise area. As a consequence, a smooth compromise is resulted and the execution time will decrease.

$$\min_{X} \left\{ \left[\frac{F^C(x) - F^C(x^{C^*})}{\max[F^C(x^{Em^*}) - F^C(x^{C^*})]} \right] \right.$$

$$\left. + Nh^f \cdot k \cdot \left[\frac{F^{Em}(x) - F^{Em}(x^{Em^*})}{\max[F^{Em}(x^{C^*}) - F^{Em}(x^{Em^*})]} \right] \right\} \qquad (89)$$

subject to

$$x \in X$$

$$\mathbf{G}^e(x) = 0$$

$$\mathbf{G}^i(x) \geq 0$$

Moreover, as the formulation is based on a normalization approach, the controlling factor (h^f) must be normalized as well. In general, such a controlling factor can be normalized as (90), but this normalization will map the factor into interval [0 1] and sometimes for a small value of h^f, it may yield a negative compromise.

$$Nh^f = \frac{h^f - \min(h^f)}{\max(h^f) - \min(h^f)} \qquad (90)$$

In (89), parameter k acts as a scaling factor and can be defined based on the weighting factor of each function as (91).

$$k = \frac{w_1}{w_2}, \qquad 0 \leq w_1 \leq 1, 0 \leq w_2 \leq 1 \qquad (91)$$

where w_1 and w_2 are the weighting factors of emission and cost objectives, respectively and $w_1 + w_2 = 1$.

The main reason is that in the denominator of (89), the maximum difference has been used to weight the distances from an optimal solution, in a way that if the distance is great, it will need more attention. For instance, if the distance is at its greatest, its weight will be equal to 1 and by decreasing the distance, the weight will decrease slightly.

3.2.2 Application of the compromise strategy to dynamic economic and emission active-reactive OPF

In order to apply the compromise methodology to dynamic economic and emission active-reactive OPF, three scenarios must be considered. The first scenario is an economic-

oriented dynamic AROPF, which finds the least amount of cost for the system. The second is an emission-oriented dynamic AROPF, which finds the least amount of emissions for the system. The final scenario is a compromise-oriented dynamic AROPF that will make a compromise via the UNBP.

3.2.2.1 Scenario I: Economic-oriented dynamic AROPF

The objective function of this scenario focuses on the cost minimization of a steady state operational condition, which is the most important issue in power systems.

$$\min F^C = \sum_{t \in T} \sum_{i \in \Omega_g} [C_{i,t}(P_{g_{i,t}})] \tag{92}$$

subject to :

$$P_{g_{i,t}} - P_{d_{i,t}} - P_{i,t}(V, \theta, tp) = 0, \quad i \in \Omega_b, t \in T \tag{93}$$

$$Q_{g_{i,t}} - Q_{d_{i,t}} - Q_{i,t}(V, \theta, tp) = 0, \quad i \in \Omega_b, t \in T \tag{94}$$

$$\left| fl^l_{ij,t}(V, \theta, tp) \right| \le \overline{fl^l_{ij}}, \qquad ij = \Omega_L, t \in T \tag{95}$$

$$\underline{V_i} \le V_{i,t} \le \overline{V_i}, \qquad i \in \Omega_b, t \in T \tag{96}$$

$$\underline{P_{g_i}} \le P_{g_{i,t}} \le P^M_{g_{i,t}}(Q_{g_{i,t}}), \qquad i \in \Omega_g, t \in T \tag{97}$$

$$\underline{Q_{g_i}} \le Q_{g_{i,t}} \le \overline{Q_{g_i}}, \qquad i \in \Omega_g, t \in T \tag{98}$$

$$\underline{tp^l_{ij}} \le tp^l_{ij,t} \le \overline{tp^l_{ij}}, \qquad ij = \Omega_L, t \in T \tag{99}$$

$$P_{g_{i,t}} - P_{g_{i,t-1}} \le RU_i, \qquad i \in \Omega_g, t \in T \tag{100}$$

$$P_{g_{i,t-1}} - P_{g_{i,t}} \le RD_i, \qquad i \in \Omega_g, t \in T \tag{101}$$

$$\sum_{i \in \Omega_g^s} Em_{i,t}(P_{g_{i,t}}) \le EMSA^s, \qquad s \in \Omega_s, \ t \in T \tag{102}$$

$$\sum_{i \in \Omega_g} Em_{i,t}(P_{g_{i,t}}) \le EMS, \qquad t \in T \tag{103}$$

$$\sum_{i \in \Omega_g} NOx_{i,t}(P_{g_{i,t}}) \le \overline{NOx}, \qquad t \in T \tag{104}$$

$$\sum_{i \in \Omega_g} SOx_{i,t}(P_{g_{i,t}}) \le \overline{SOx}, \qquad t \in T \tag{105}$$

where i and j are the bus indices; t is the time index; T is the time index set; Ω_b, and Ω_g are the index sets of buses, and generating units, respectively; Ω_s and Ω_g^s are the sets of sub-

area (regions in an area) and sets of generator in sub-area s., respectively; Ω_L is the index set of branches..

In this formulation, $C_{i,t}(\cdot)$ is the fuel cost of unit i at hour t, which is approximated by a quadratic function such as (106) (VAHIDINASAB; JADID, 2010).

$$C_{i,t}(P_{g_{i,t}}) = a_i(P_{g_{i,t}})^2 + b_i P_{g_{i,t}} + c_i \qquad (106)$$

where a_i, b_i, and c_i are the quadratic, linear, and constant coefficients of the cost function, respectively.

The extended formulations for the equality constrains (93) and (94) as the active and reactive power balance equations, can be presented as (107) and (108), respectively.

$$P_{g_{i,t}} - P_{d_{i,t}} - g_i^{sh} v_{i,t}^2 - \sum_{ij \in \Omega_L} p_{ij,t} - \sum_{ji \in \Omega_L} p_{ji,t} = 0, \qquad i \in \Omega_b, t \in T \quad (107)$$

$$Q_{g_{i,t}} - Q_{d_{i,t}} + b_i^{sh} v_{i,t}^2 - \sum_{ij \in \Omega_L} q_{ij,t} - \sum_{ji \in \Omega_L} q_{ji,t} = 0, \qquad i \in \Omega_b, t \in T \quad (108)$$

where $P_{d_{i,t}}$ is the active power demand of bus i at hour t; $Q_{g_{i,t}}$ and $Q_{d_{i,t}}$ are the reactive power generation and reactive demand of bus i at hour t, respectively; g_i^{sh} and b_i^{sh} are the shunt conductance and susceptance of bus i, respectively; $v_{i,t}$ is the voltage of bus i at hour t; $p_{ij,t}$ and $p_{ji,t}$ are the direct and reverse active power injections at hour t as (109) and (110), respectively; $q_{ij,t}$ and $q_{ji,t}$ are the direct and reverse reactive power injections at hour t as (111) and (112), respectively.

$$p_{ij,t} = (a_{ij,t}^l v_{i,t})^2 g_{ij}^l - (a_{ij,t}^l v_{i,t})v_{j,t}[g_{ij}^l \cos(\theta_{ij,t} + \varphi_{ij,t}) + b_{ij}^l \sin(\theta_{ij,t} + \varphi_{ij,t})] \qquad (109)$$

$$p_{ji,t} = g_{ij}^l v_{j,t}^2 - (a_{ij,t}^l v_{i,t})v_{j,t}[g_{ij}^l \cos(\theta_{ij,t} + \varphi_{ij,t}) - b_{ij}^l \sin(\theta_{ij,t} + \varphi_{ij,t})] \qquad (110)$$

$$q_{ij} = -(a_{ij,t}^l v_{i,t})^2 (b_{ij}^l + \frac{b_{ij}^{l,ch}}{2}) - (a_{ij,t}^l v_{i,t})v_{j,t}[g_{ij}^l \sin(\theta_{ij,t} + \varphi_{ij,t}) - b_{ij}^l \cos(\theta_{ij,t} + \varphi_{ij,t})] \qquad (111)$$

$$q_{ji} = -(b_{ij}^l + \frac{b_{ij}^{l,ch}}{2})v_{j,t}^2 + (a_{ij,t}^l v_{i,t})v_{j,t}[g_{ij}^l \sin(\theta_{ij,t} + \varphi_{ij,t}) + b_{ij}^l \cos(\theta_{ij,t} + \varphi_{ij,t})] \qquad (112)$$

where $a_{ij,t}^l$ and $\varphi_{ij,t}$ are the magnitude and phase of a transformer tap in line l, between buses i and j, at hour t, respectively; $\theta_{ij,t}$ is the angle differences of bus i and j, along with line l at hour t; and b_{ij}^l and $b_{ij}^{l,ch}$ are the susceptance and charging susceptance of line l, respectively.

Constraint (95) is related to the line flow limit, where $fl_{ij,t}^l(\cdot)$ is the line flow of transmission line l in corridor ij at hour t, and $\overline{fl_{ij}^l}$ is the maximum allowed power flow of transmission line l in corridor ij. Constraints (96)-(99) are related to the limitations of voltage, active power generation, reactive power generation, and transformer tap between their lower bound ($\underline{V_i}, \underline{P_{g_i}}, \underline{Q_{g_i}}, \underline{tp_{ij}^l}$) and upper bound ($\overline{V_i}, P_{g_{i,t}}^M(Q_{g_{i,t}}), \overline{Q_{g_i}}, \overline{tp_{ij}^l}$), respectively.

All of the lower and upper bounds are considered as constants, except the upper bound for active power generation ($P_{g_{i,t}}^M(\cdot)$), which is a highly nonlinear function of reactive power generation. This limit is imposed by the capability curve and turbine, and then, instead of $\overline{P_{g_i}}$ that is constant and used under ideal conditions, the upper bound of generators' output is defined by $P_{g_{i,t}}^M(\cdot)$, which has three different portions, as can be seen in (113) (RUEDA; ALMEIDA, 2001).

$$
P_{g_{i,t}}^M(Q_{g_{i,t}}) = \begin{cases} \left(\dfrac{P_{g_i}'}{Q_{g_i}' - \underline{Q_{g_i}}}\right)(Q_{g_{i,t}} - \underline{Q_{g_i}}), & \underline{Q_{g_i}} \le Q_{g_{i,t}} \le Q_{g_i}',\ i \in \Omega_g, t \in T \\[2ex] \sqrt{S_{g_i}^2 - Q_{g_{i,t}}^2}, & Q_{g_i}' \le Q_{g_{i,t}} \le Q_{g_i}'',\ i \in \Omega_g, t \in T \\[2ex] \dfrac{\sqrt{V_{i,t}^2(\overline{E_{i,t}})^2 - (Q_{g_{i,t}}Xs_i + V_{i,t}^2)^2}}{Xs_i}, & Q_{g_i}'' \le Q_{g_{i,t}} \le \overline{Q_{g_i}},\ i \in \Omega_g, t \in T \end{cases} \quad (113)
$$

where S_{g_i} is the rated VA of the machine; Xs_i is the synchronous reactance of the machine; and $\overline{E_{i,t}}$ is the maximum excitation voltage of unit i at hour t and is calculated by (114).

$$
\overline{E_{i,t}} = \sqrt{\frac{(Xs_i P_{g_i}'')^2 + (Xs_i Q_{g_i}'' + V_{i,t}^2)^2}{V_{i,t}^2}}, \quad i \in \Omega_g, t \in T \qquad (114)
$$

and Q_{g_i}', Q_{g_i}'', P_{g_i}', and P_{g_i}'' are calculated by (115), (116), (117), and (118), respectively.

$$Q'_{g_i} = S_{g_i} \sin(-\Phi), \qquad i \in \Omega_g \tag{115}$$

$$Q''_{g_i} = S_{g_i} \sin(\Phi), \qquad i \in \Omega_g \tag{116}$$

$$P'_{g_i} = S_{g_i} \cos(-\Phi), \qquad i \in \Omega_g \tag{117}$$

$$P''_{g_i} = S_{g_i} \cos(\Phi), \qquad i \in \Omega_g \tag{118}$$

It should be noted that the bus voltage magnitude ($V_{i,t}$) is usually supposed to be $1(p.u)$, but in this work, in order to have a more precise model, the actual voltage magnitude is taken into consideration.

The real power generation limit may change due to the generators' ramp-rate limits. When the generation of a unit is increased, the ramp-up rate (RUR) is taken into account, and in contrast, by decreasing the generation of a unit, the ramp-down rate (RDR) is considered. Therefore, the detailed consideration of ramp-rate limits (100) and (101) have been presented in (119) and (120), respectively.

$$P_{g_{i,t}} \leq \min(P_{g_{i,t}}^M(Q_{g_{i,t}}), P_{g_{i,t-1}} + RU_i), \qquad i \in \Omega_g, \ t \in T \tag{119}$$

$$\max(\underline{P_{g_i}}, P_{g_{i,t-1}} - RD_i) \leq P_{g_{i,t}}, \qquad i \in \Omega_g, \ t \in T \tag{120}$$

where RU_i and RD_i are the ramp-up and ramp-down rates of unit i; and $P_{g_{i,t-1}}$ is the generated power of unit i at the previous hour ($t-1$).

In addition, each power system may consider several emission limits and these limitations may vary during the scheduling time horizon. The area and system emission limits are considered as (102) and (103), respectively. In these constraints, $EMSA^s$ represents the emission limits of sub-area (region) s, and EMS denotes the system emission limit; $NOx_{i,t}$ and $\overline{NOx}$ are the nitrogen oxide emission and its maximum limit, respectively; $SOx_{i,t}$ and $\overline{SOx}$ are the sulfur oxide emission and its maximum limit, respectively. The mathematical formulation of emissions is considered in scenario II (3.2.2.2).

3.2.2.2 Scenario II: Emission-oriented dynamic AROPF

In considering the harmful environmental impacts of generating electricity, the concerns about the emissions resulted from fossil fuel burning are the highly serious ones. Among the resultant emissions, Sulfur Oxides (SO_X) and Nitrogen Oxides (NO_X) are the

most important ones. In this scenario, in order to minimize the amount of emissions via the AROPF tool during the scheduling horizon, the following formulation is used.

$$\min F^{Em} = \sum_{t \in T} \sum_{i \in \Omega_g} [Em_{i,t}(P_{g_{i,t}})]$$

$$subject\ to:$$ (121)

$$Constrains\ (93) - (105)$$

In this work, a combination of polynomial and exponential terms for representing the mathematical formulation of SO_X and NO_X emissions is used (VAHIDINASAB; JADID, 2010).

The amount of emission is calculated by a quadratic function as (122).

$$Em_{i,t}(P_{g_{i,t}}) = SOx_{i,t}(P_{g_{i,t}}) + NOx_{i,t}(P_{g_{i,t}})$$ (122)

where $Em_{i,t}(\cdot)$ is the emissions resulted from unit i at hour t; and in this formulation, SO_X and NO_X are defined as (123) and (124), respectively.

$$SOx_{i,t}(P_{g_{i,t}}) = \alpha_i(P_{g_{i,t}})^2 + \beta_i P_{g_{i,t}} + \gamma_i$$ (123)

$$NOx_{i,t}(P_{g_{i,t}}) = \varepsilon_i \exp(\lambda_i P_{g_{i,t}})$$ (124)

where α_i, β_i, and γ_i are the quadratic, linear and constant coefficients of SO_X emissions; and ε_i and λ_i are the coefficients of NO_X emissions.

3.2.2.3 Scenario III: Compromise-oriented dynamic AROPF

After finding the optimal solutions for the first and second scenarios, the answers will be applied to the compromise-oriented dynamic AROPF via the UNBP methodology in order to find an acceptable compromise.

$$\min UNBP = \sum_{t \in T} \sum_{i \in \Omega_g} \left\{ \frac{C_{i,t}(P_{g_{i,t}}) - C_{i,t}^{BC}}{CODIF_{i,t}} \right.$$

$$\left. + Nh_{i,t}^f \cdot k \cdot \frac{Em_{i,t}(P_{g_{i,t}}) - Em_{i,t}^{BE}}{EMDIF_{i,t}} \right\}$$ (125)

$$subject\ to:$$

$$Constrains\ (93) - (105)$$

$$CODIF_{i,t} = \max_{i \in \Omega_g} \left| C_{i,t}^{BC} - C_{i,t}^{BE} \right|, \qquad t \in T \tag{126}$$

$$EMDIF_{i,t} = \max_{i \in \Omega_g} \left| Em_{i,t}^{BC} - Em_{i,t}^{BE} \right|, \qquad t \in T \tag{127}$$

$$Nh_{i,t}^{f} = 0.1 + \frac{h_{i,t}^{f} - \min_i (h_{i,t}^{f})}{\max_i (h_{i,t}^{f}) - \min_i (h_{i,t}^{f})}, \qquad i \in \Omega_g, t \in T \tag{128}$$

$$h_{i,t}^{f} = \frac{C_{i,t}^{BE}}{Em_{i,t}^{BC}}, \qquad i \in \Omega_g, t \in T \tag{129}$$

where $C_{i,t}^{BC}$ and $C_{i,t}^{BE}$ are the generation costs of unit i at hour t obtained from scenarios I and II, respectively; $Em_{i,t}^{BC}$ and $Em_{i,t}^{BE}$ are the resultant emissions of unit i at hour t obtained from scenarios I and II, respectively; $CODIF_{i,t}$ in (126) is the maximum difference of costs obtained from scenarios I ($C_{i,t}^{BC}$) and II ($C_{i,t}^{BE}$) among all generating units at hour t; and $EMDIF_{i,t}$ in (127) is the maximum difference of emissions resulted from scenarios I ($Em_{i,t}^{BC}$) and II ($Em_{i,t}^{BE}$) among all generating units at hour t. It is worth mentioning that, $CODIF_{i,t}$ and $EMDIF_{i,t}$ are defined based on this fact that cost and emission have conflicting objectives. $Nh_{i,t}^{f}$ is the normalized adaptive pollution control cost of unit i at hour t;

In (128), the normalized adaptive pollution control cost of unit i at hour t ($Nh_{i,t}^{f}$) have been mapped out with an interval of [0.1, 1.1]. If the normalization of an APCC maps out as [0, 1], it means that it is neglecting to compromise those generators, which have the smallest APCC.

As the APCC ($h_{m,t}^{f}$), in (129), is a topology-based factor and consequently it is a dispatch dependent factor, it will be a flexible factor and for contingency conditions and hourly demand fluctuations, it will be adjusted in order to make an acceptable compromise. The normalization of this factor as the (128), makes it an even more effectible element during the compromising process.

Chapter 4

MULTI-AREA ENVIRONMENTALLY-CONSTRAINED ACTIVE-REACTIVE OPF

4.1   INTRODUCTION

To achieve higher efficiency in a power system, the operators of small-scale systems prefer and tend to connect to other systems to form an interconnected large-scale system. In a centralized power system, each area transfers the necessary information to the central controller, and then, optimizes the problem and returns the optimal value of the state variables to the area. After any change in one or more areas, the optimization process will be repeated and the bulk of information will be transferred between the central controller and areas. Although such interconnected systems have several benefits, it is quite difficult to determine the optimal operation point of such large-scale systems, and the use of decentralized methods is more practical in determining the optimal solution of such systems on an area-by-area basis (NOGALES et al., 2003; GRANADA et al., 2008), where only a small amount of information must be interchanged among the involved areas (CONEJO; AGUADO, 1998). In other words, in a decentralized power system, each area has its own controller that solves the corresponding optimization problem. To have a synchronized power system, each area communicates with the adjacent areas and shares the border data until a tradeoff is obtained. Decomposition methods, which are the general approaches for solving the large-scale problems, through breaking the problem into smaller problems via a parallel or sequential approach, try to solve such problems in DC or AC power systems (BOYD et al.,). In order to develop the algorithm for multi-area systems, most of the relevant works have focused on DC-OPF. An iterative decentralized DC-OPF that can be implemented on a network workstation was reported in (BISKAS et al., 2005). In (CONEJO et al., 2007), a proper and simple coordination among area operators was proposed. In (CARO et al., 2011), a non-iterative method that does not require a central coordinator was reported. In (BAKIRTZIS; BISKAS, 2003), a decentralized method that is based on a pricing mechanism was reported with coordination of areas, based on the prices of the power exchange between the interconnected areas. However, the main drawback of such methodologies is their iterative manner. In this work, for a multi-area OPF, an integrated formulation containing the concepts of both centralized and decentralized models is proposed, which makes it an effortless problem to be used for the operating or/and planning problems.

In a multi-area power system, all the activities in each area will affect the prices, stability, degrees of freedom, etc., of other interconnected areas. In this regard, a tie line can play an important role. From an operational standpoint of a regional transmission organization (RTO), tie lines are used to facilitate the energy exchange between areas based on a pre-defined agreement (BALDICK; CHATTERJEE, 2013). Moreover, measuring the transmitted power among areas through a tie line requires the knowledge that whether the area is balancing its active and reactive generation and load or not. Similar to an independent system operator (ISO), the RTO coordinates, controls, and monitors the operation of a large power system, such as a multi-area power system (SHAHIDEHPOUR et al., 2002). While safety and stability are the two most important issues in an RTO, providing the security of a power system is considered as the main role of an RTO in a power system market to ensure that the supply and demand are in balance and the frequency fluctuations and interruptions, which may result in a shedding of power or a blackout, are avoided. Thus, both ISO and RTO are responsible for managing every single-area power system, and also the interconnections of these areas in an online consideration via a multi-area active-reactive OPF (MA-AROPF). The management of energy flows across the grid and the exchange of power flow information via the RTO will result in a properly functioning power system. One of the functions of the RTO is expansion planning, and more specifically, tie line planning ("Regional Transmission Organizations, Available: http://www.ferc.gov/legal/maj-ord-reg/land-docs/2000A.pdf", 2000). The coordination between the generation and transmission expansion planning is a critical issue in a power system, since it can enhance the stability of each area, thereby resulting in the entire power system's stability (KHODAEI et al., 2012).

Traditionally, tie line planning is performed by considering the location, the capacity of tie lines, as well as the rate of return, in order to obtain the optimal economic operation of the system. In the literature, the candidate buses for tie line planning are pre-defined, and therefore, the problem is mostly a transmission expansion planning in which the stability of interconnected systems, the tie line investment costs, the multi-area security, etc. are taken into consideration. In order to determine an appropriate tie line, four types of methods can be used: metaheuristic, enumeration, sensitivity index (DA SILVA et al., 2001), and the proposed methodology in this work, which is based on determining the weak and strong buses. In the real world, determining the appropriate transmission tie lines that yield an improvement on the voltage stability and decrease the system's total operating costs and even the regional or total system emissions while enhancing the degrees of freedom, is highly

dependent on finding the critical buses/segments of each area in a power system. In this work, in order to find proper buses, the system operation at its maximum loadability point (MLP) has been taken into account. Although metaheuristic and enumeration methods may determine the appropriate tie lines that result in a lower cost than the sensitivity index method, these methods have some drawbacks. For instance, they are time consuming, and also inefficient in finding an appropriate tie line that satisfies several objectives. For example, in enumeration methods, it is quite difficult to find a compromise between several objectives via a classic approach, while for metaheuristics, adjusting the compromise coefficients of the objectives is a complicated task (KASMAEI et al., 2013). In the sensitivity index method, if the load changes, the MA-AROPF solution will change, and consequently, the Lagrangian multipliers, which determine the sensibilities, will change and an inappropriate tie line plan may be resulted.

The optimal tie line is considered as the tie line that under the MLP condition, most effectively enhances the multi-area stability as well as its degree of freedom (easily reschedulable), while reducing the total operating costs and/or emissions. In this dissertation, based on the analysis of a power system at the MLP, the weak and strong buses are determined and a set of strong and weak buses is selected as candidate buses for tie line planning and then, via a mixed integer nonlinear programming problem, the appropriate tie lines are selected. Moreover, in order to have a more appropriate plan at the entire operating points, switchable tie lines are considered.

In this chapter, at first, two well-known decomposition techniques are considered and afterwards, an integrated formulation for the multi-area active-reactive OPF (MA-AROPF) is presented in order to modify some drawbacks of the commonly used decentralized methods, whereas in the proposed model, the system emission limit (EMS), the regional emission limit (EMA), and the sub-area emission limit (EMSA) as the emission control constraints are taken into account.

4.2   CENTRALIZED AND DECENTRALIZED POWER SYSTEMS

4.2.1   The centralized model

The word "centralized" in an electric power system may refer to a centralized power generation or a centralized controller. In the centralized model of a power system, the multiple areas are controlled by a centralized controller (Figure 9). In this regard and in order

to synchronize the areas, all areas send their data to the central controller and this controller solves one optimization problem only. In this model, after obtaining the optimal solution, the controller sends the optimal data back to each area. In a centralized power system, all the actions such as energy management, congestion management, planning and scheduling, etc. are performed through a centralized controller. The system utilizes a computer program that optimizes the objective function. Although a centralized model consists of several single and/or interconnected areas, a single objective function is defined by the central controller for all the areas.

Figure 9- The centralized model
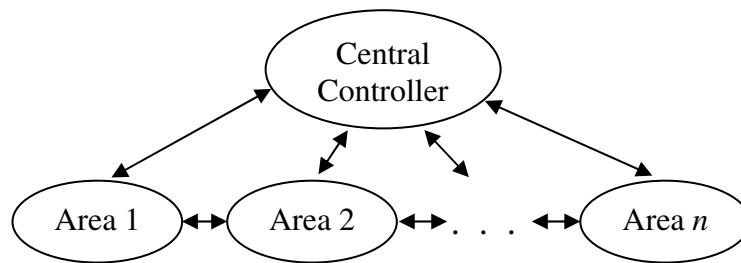
Source: The author

A mathematical model for the centralized model of a power system can be defined as (130).

$$\min_{\substack{x_1 \in A_1, x_2 \in A_2 \\ \ldots, x_n \in A_n}} F(x_1, x_2, \ldots, x_n)$$

subject to : (130)

Operating Constraints

where $x_1, x_2, \ldots, x_n$ are the variables, corresponding to areas $A_1, A_2, \ldots, A_n$, respectively, and $F(\cdot)$ is the defined unique objective of the central controller.

After sending the necessary information to the central controller, it optimizes the problem and returns the optimal value of the aforementioned variables to the areas. After any change in one or more areas, the optimization process will be repeated and a bulk of information will be transferred between the central controller and all the areas. Some of the advantages and disadvantages of centralized systems are as follow.

➢ Advantages of centralized systems

✓ Once the master is installed on the system, all the functions and facilities of the system can be used.

✓ The expansion costs are lower than the decentralized systems, since the input and output modules contain less intelligence and hence, fewer components.

➢ Disadvantages of centralized systems

✓ Lack of robustness: if the central supervisor fails to perform as expected, the whole areas of the integrated system will lose control.

✓ Exchanging a large amount of data between the areas and the central controller is required.

✓ A long computational time is necessary for solving the optimization problem and by expanding the system, the computational time will increase exponentially.

✓ The capital costs are higher than the decentralized systems because it is necessary to invest in the master controller, which is generally the most expensive component of the installation.

4.2.2   The decentralized model

A decentralized power system consists of several interconnected areas. Unlike a centralized model, each area has its own controller and solves its related sub-problem. In order to have a synchronized power system, the sub-problems share their data with the adjacent areas (Figure 10).

Figure 10- The decentralized model
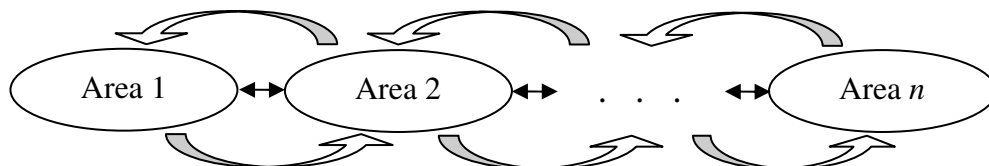
Source: The author

In section 4.3, the problem formulation and the decomposition techniques that are used in the decentralized model will be taken into consideration.

Some of the advantages and disadvantages of centralized systems are as follow.

➢ Advantages of decentralized systems

✓ Only the information of dedicated variables in border regions are exchanged among the neighboring areas.

✓ If a failure occurs in one area, it does not result in a failure in the whole system.

✓ Each area can handle its own arbitrary objective function.

✓ By increasing the size of the system, the optimization problem is linearly expanded.

➢ Disadvantages of decentralized systems

✓ A lack of coordination or a bad coordination results in an improper system performance and consequently, in an unsatisfactory sub-optimality for the whole system, or otherwise, the constraints might be violated.

✓ In decompositions of such systems, defining a criterion largely effects on the preciseness of the solution.

4.3   DECOMPOSITION TECHNIQUES

In a multi-area power system, the centralized system is re-defined within several areas as a decentralized model, which enables modifying the drawbacks of the centralized model. Until now, in order to obtain the optimal solution of a decentralized model, decomposition techniques have been usually used. Two of the commonly used decomposition methods are, the decompositions based on the adjustment of the common border variables (Figure 11), and the decompositions based on information exchange between the border areas (Figure 12).

4.3.1   Decomposition based on the adjustment of the shared border variables

In this technique, an adjustment procedure for the shared border is used in order to decompose the optimization problem. In the literature, two methods for the adjustment procedure have been introduced (KIM; BALDICK, 1997; WANG et al., 2001). The aforementioned decomposition method is illustrated in Figure 11, in which a system consisting of two overlapping areas has been employed. Furthermore, both areas share the

variables of their border demonstrated by y (in the yellow area). In this regard, there are two objective functions as $F_{A_1}(x)$ and $F_{A_2}(z)$, which are related to areas A_1 and A_2, respectively. The overall objective function is as (131).

$$
\begin{aligned}
&\min_{(x,y)\in A_1,(y,z)\in A_2} F_{A_1}(x)+F_{A_2}(z) \\
&\quad \text{subject to}: \\
&\qquad G_{A_1}(x, y_{A_1})=0 \\
&\qquad G_{A_2}(y_{A_2}, z)=0 \\
&\qquad H_{A_1}(x, y_{A_1})\le 0 \\
&\qquad H_{A_2}(y_{A_2}, z)\le 0
\end{aligned}
\tag{131}
$$

Figure 11- Decomposition based on the adjustment of border variables
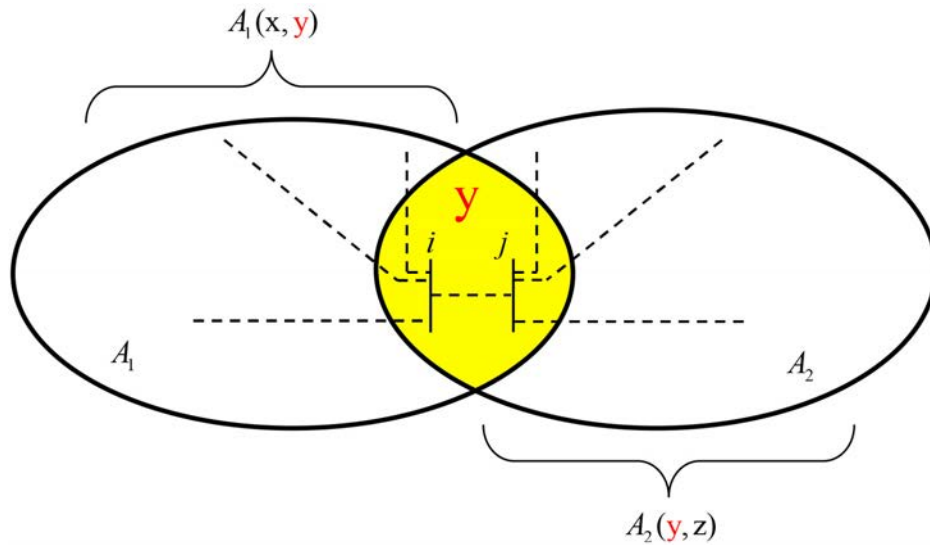
Source: The author

where x and z are the optimization variables related to the areas of A_1 and A_2, respectively, y is the border variable.

And the coupling constraint is as (132), which enforces the border variables to be equal.

$$
y_{A_1} - y_{A_2} = 0
\tag{132}
$$

4.3.2 Decomposition based on information exchange

In this decomposition technique, the coordination is attained through an iterative exchange of information between neighboring areas. This technique is based on a Lagrangian

relaxation procedure (CONEJO et al., 2002; NOGALES et al., 2003). This decomposition method is illustrated in Figure 12, in which both areas pass their exchange variables to the neighboring area, which will be specified later. Similar to section 4.3.1, there are two objective functions as $F_{A_1}(x)$ and $F_{A_2}(z)$, which are related to areas A_1 and A_2, respectively, and the overall objective function is as (133).

In Figure 12, κ_{A_1} and κ_{A_2} are the Lagrangian multipliers of equality coupling constraints; and σ_{A_1} and σ_{A_2} are the Lagrangian multipliers of inequality coupling constraints. These constraints are shown in (134).

Figure 12- Decomposition based on information exchange

$$z^*, \kappa_{A_2}, \sigma_{A_2}$$

$$x^*, \kappa_{A_1}, \sigma_{A_1}$$
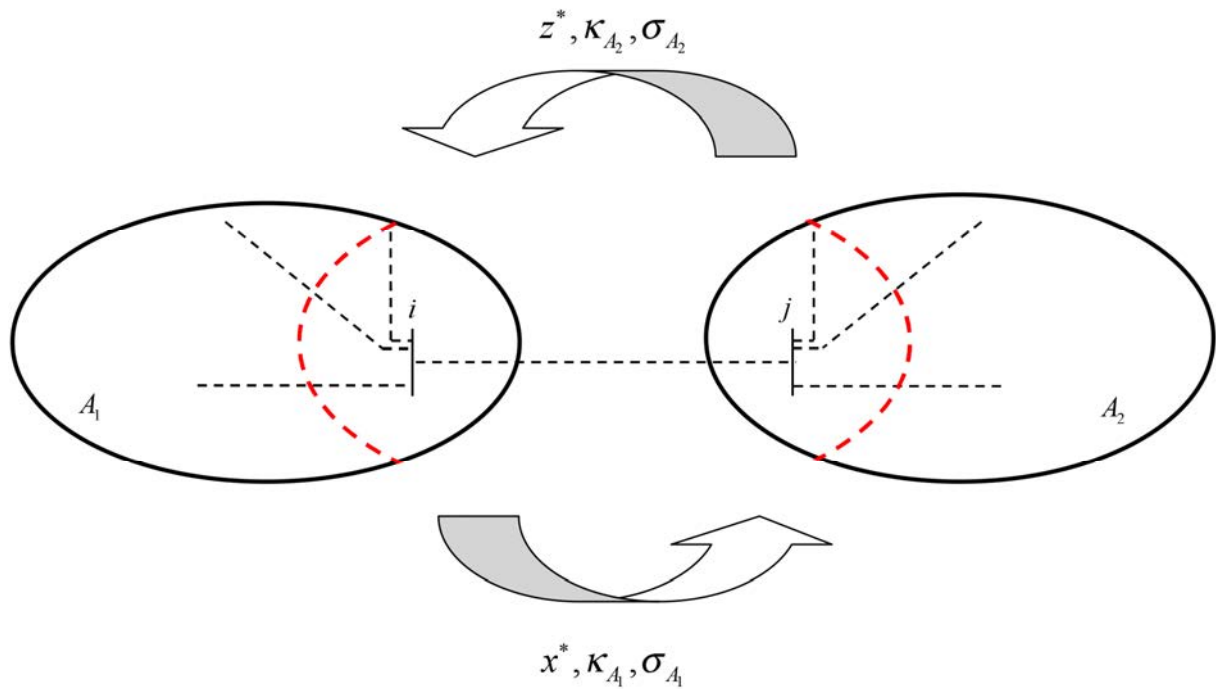
Source: The author

$$\min_{x \in A_1, z \in A_2} F_{A_1}(x) + F_{A_2}(z)$$

$$\text{subject to:}$$

$$\widetilde{G}(x, z) = 0$$

$$G_{A_1}(x) = 0$$

$$G_{A_2}(z) = 0 \tag{133}$$

$$\widetilde{H}(x, z) \leq 0$$

$$H_{A_1}(x) \leq 0$$

$$H_{A_2}(z) \leq 0$$

where $\widetilde{G}(\mathrm{x}, z)$ and $\widetilde{H}(\mathrm{x}, z)$ are the equality and inequality coupling constraints, respectively; $G_{A_1}(\mathrm{x})$ and $G_{A_2}(z)$ are the equality and inequality constraints of areas A_1 and A_2, respectively; and $H_{A_1}(x)$ and $H_{A_2}(z)$ are the inequality constraints of areas A_1 and A_2, respectively.

In order to have a decomposable form of the problem (133), the coupling constraints are split as (134).

$$
\begin{aligned}
\widetilde{G}_{A_1}(\mathrm{x}, z^*) &= 0 \\
\widetilde{G}_{A_2}(\mathrm{x}^*, z) &= 0 \\
\widetilde{H}_{A_1}(\mathrm{x}, z^*) &\leq 0 \\
\widetilde{H}_{A_2}(\mathrm{x}^*, z) &\leq 0
\end{aligned}
\tag{134}
$$

In comparison with the presented technique in section 4.3.1, instead of using one additional coupling constraint, the additional constraints in this technique are marked by tilde; x^* and z^* are the coupling or complicating variables, respectively.

4.4 MULTI-AREA ENVIRONMENTALLY-CONSTRAINED AROPF

The objective of a multi-area environmentally-constrained active-reactive optimal power flow (MA-AROPF) problem is to minimize the entire interconnected power system's costs. In both the centralized and decentralized models in sections 4.2.1 and 4.2.2, the multi-area system may face some difficulties and drawbacks.

Figure 13- The integrated model for multi-area problems
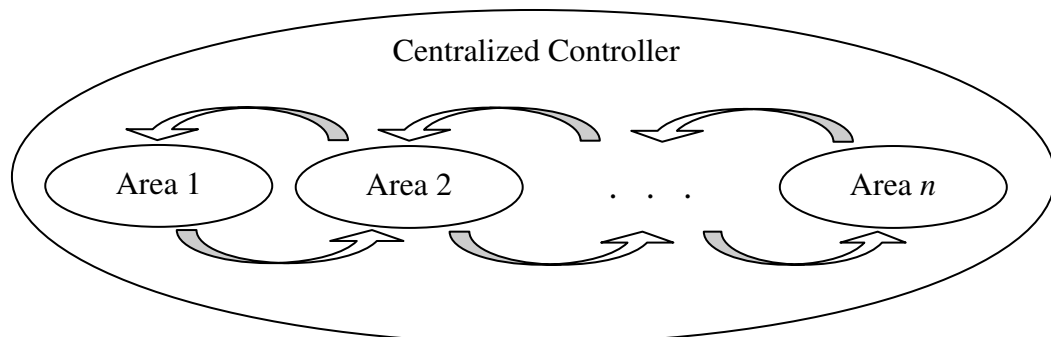
Source: The author

In this work, an integrated formulation is proposed for the multi-area OPF, which contains several concepts from the centralized and decentralized models. In the proposed

model, each area optimizes its related sub-problem and unlike the decentralized model, in which the sub-problems need to coordinate with each other, this part of coordination is performed with a centralized controller (Figure 13). Unlike the commonly used techniques presented in section 4.3, this method is straightforward and hence, it is not necessary to define extra auxiliary variables or additional constraints.

In this work, in order to obtain a multi-area formulation, which can be fast and unequivocal, several coupling constraints are defined and the resulting formulation constitutes a MA-AROPF problem that can be readily implemented and the optimal solution can be determined by using only a commercial nonlinear solver. A generalized mathematical formulation of a multi-area power system can be presented by (135)-(141).

$$\min F(\Psi, u) = \sum_{x \in \Omega_A} [\min \sum_{i \in \Omega_b^{A_x}} f_i^{A_x} (\Psi_i^{A_x}, u_i^{A_x})] =$$

$$\min \sum_{i \in \Omega_b^{A_1}} f_i^{A_1} (\Psi_i^{A_1}, u_i^{A_1}) + \min \sum_{i \in \Omega_b^{A_2}} f_i^{A_2} (\Psi_i^{A_2}, u_i^{A_2}) + \cdots$$

$$+ \min \sum_{i \in \Omega_b^{A_{(n_A-1)}}} f_i^{A_{(n_A-1)}} (\Psi_i^{A_{(n_A-1)}}, u_i^{A_{(n_A-1)}}) + \min \sum_{i \in \Omega_b^{A_{n_A}}} f_i^{A_{n_A}} (\Psi_i^{A_{n_A}}, u_i^{A_{n_A}})$$

(135)

$s.t.$

$$\mathbf{G}(\Psi_i^{A_x}, u_i^{A_x}) = 0, \qquad x \in \Omega_A \tag{136}$$

$$\mathbf{H}(\Psi_i^{A_x}, u_i^{A_x}) \le 0, \qquad x \in \Omega_A \tag{137}$$

$$\underline{u}_i^{A_x} \le u_i^{A_x} \le \overline{u}_i^{A_x}, \qquad x \in \Omega_A \tag{138}$$

$$\overset{x \ne y}{\mathbf{G}'}(\Psi_i^{A_{xy}}, u_i^{A_{xy}}) = 0, \qquad xy \in \Omega_{IA} \tag{139}$$

$$\overset{x \ne y}{\mathbf{H}'}(\Psi_i^{A_{xy}}, u_i^{A_{xy}}) \le 0, \qquad xy \in \Omega_{IA} \tag{140}$$

$$\underline{u}_i^{A_{xy}} \le u_i^{A_{xy}} \le \overline{u}_i^{A_{xy}}, \qquad xy \in \Omega_{IA} \tag{141}$$

where $\Omega_A = \{1, 2, \cdots, n_A\}$, Ω_{IA}, and $\Omega_b^{A_x}$ are the sets of areas, interconnected areas, and buses in area x, respectively, and n_A is the total number of areas; $\Psi_i^{A_x}$ and $u_i^{A_x}$ are the state and control variables of area x, respectively; $\Psi_i^{A_{xy}}$ and $u_i^{A_{xy}}$ are the state and control variables of interconnected area xy, between areas x and y, respectively; $f_i^{A_x}$ is the objective function of bus i in area x; $\mathbf{G}(\cdot)$ and $\mathbf{H}(\cdot)$, in (136) and (137), are the sets of the equality and inequality constraints of individual buses, respectively; $\mathbf{G}'(\cdot)$ and $\mathbf{H}'(\cdot)$, in (139) and (140), are the sets of the equality and inequality constraints of interconnected buses, respectively; $\underline{u}_i^{A_x}$ and $\overline{u}_i^{A_x}$, in

(138), are the lower and upper limits of control variables of individual buses, respectively; $\underline{u}_i^{A_{xy}}$ and $\overline{u}_i^{A_{xy}}$, in (141), are the lower and upper limits of control variables of interconnected buses, respectively.

$$\min F_C^{MA} = \sum_{x \in \Omega_A} [\min \sum_{i \in \Omega_g^{A_x}} C_i(P_{g_i})] = \min \sum_{i \in \Omega_g^{A_1}} C_i(P_{g_i}) + \cdots$$

$$+ \min \sum_{i \in \Omega_g^{A_x}} C_i(P_{g_i}) + \cdots + \min \sum_{i \in \Omega_g^{A_{n_A}}} C_i(P_{g_i}) \tag{142}$$

s.t.   *constraints* sets (143)-(151) and (166)-(170)

$$P_{g_i} - P_{d_i} - g_i^{sh} v_i^2 - \sum_{\substack{ij \in \Omega_L^{A_x} \\ i \neq j}} p_{ij} - \sum_{\substack{ji \in \Omega_L^{A_x} \\ i \neq j}} p_{ji} = 0, \begin{cases} i \in \Omega_b^{A_x}, & y \in \Omega_A \\ i \notin \Omega_b^{A_{xy}}, & x \neq y \end{cases} \tag{143}$$

$$Q_{g_i} - Q_{d_i} + b_i^{sh} v_i^2 - \sum_{\substack{ij \in \Omega_L^{A_x} \\ i \neq j}} q_{ij} - \sum_{\substack{ji \in \Omega_L^{A_x} \\ i \neq j}} q_{ji} = 0, \begin{cases} i \in \Omega_b^{A_x}, & y \in \Omega_A \\ i \notin \Omega_b^{A_{xy}}, & x \neq y \end{cases} \tag{144}$$

$$\left| fl_{ij/ji}(v, \theta, tp) \right| \leq \overline{fl}_{ij/ji}, \begin{cases} ij/ji \in \Omega_L^{A_x}, ij/ji \notin \Omega_{TL}^{A_{xy}} \\ y \in \Omega_A, x \neq y \end{cases} \tag{145}$$

$$\underline{P}_{g_i} \leq P_{g_i} \leq P_{g_i}^M(Q_{g_i}), \quad i \in \Omega_g^{A_x} \tag{146}$$

$$\underline{Q}_{g_i} \leq Q_{g_i} \leq \overline{Q}_{g_i}, \quad i \in \Omega_g^{A_x} \tag{147}$$

$$\underline{v}_i \leq v_i \leq \overline{v}_i, \quad i \in \Omega_b^{A_x} \tag{148}$$

$$\underline{tp}_{ij}^l \leq tp_{ij}^l \leq \overline{tp}_{ij}^l, \begin{cases} ij \in \Omega_L^{A_x}, ij \notin \Omega_{TL}^{A_{xy}} \\ y \in \Omega_A, x \neq y \end{cases} \tag{149}$$

$$EMSA_x^s = \sum_{i \in \Omega_g^{A_x^s}} Em_i \leq \overline{EMSA}_x^s, s \in \Omega_s^{A_x} \tag{150}$$

$$EMA_x = \sum_{i \in \Omega_g^{A_x}} Em_i \leq \overline{EMA}_x \tag{151}$$

where F_C^{MA} is the total cost of the multi-area system; (143)-(151) are the constraints related to individual buses; $\Omega_g^{A_x}$ is the set of generators in area x and $\Omega_s^{A_x}$ is the set of generators in the sub-area s of area x; $\Omega_L^{A_x}$ is the set of transmission lines in area x and $\Omega_{TL}^{A_{xy}}$ is the set of tie lines between areas x and y; $\Omega_s^{A_x}$ is the set of sub-areas in area x; $EMSA_x^s$ (150) is related to the emission limit of sub-area s of area x, and EMA_x, and EMA_x (151) is related to the emission limit of area x.

In this chapter, the cost function ($c_i(\cdot)$) is approximated by a quadratic function as described in (152).

$$C_i(P_{g_i}) = a_i(P_{g_i})^2 + b_i P_{g_i} + c_i \tag{152}$$

Equations (143) and (144) are the active and reactive quality constraints, respectively; in these constraints, the direct and reverse active and power injection are as (153)-(156).

$$p_{ij} = (a_{ij}^l v_i)^2 g_{ij}^l - (a_{ij}^l v_i) v_j [g_{ij}^l \cos(\theta_{ij} + \varphi_{ij}^l) + b_{ij}^l \sin(\theta_{ij} + \varphi_{ij}^l)] \tag{153}$$

$$p_{ji} = g_{ij}^l v_j^2 - (a_{ij}^l v_i) v_j [g_{ij}^l \cos(\theta_{ij} + \varphi_{ij}^l) - b_{ij}^l \sin(\theta_{ij} + \varphi_{ij}^l)] \tag{154}$$

$$q_{ij} = -(a_{ij}^l v_i)^2 (b_{ij}^l + \frac{b_{ij}^{l,ch}}{2}) - (a_{ij}^l v_i) v_j [g_{ij}^l \sin(\theta_{ij} + \varphi_{ij}^l) - b_{ij}^l \cos(\theta_{ij} + \varphi_{ij}^l)] \tag{155}$$

$$q_{ji} = -(b_{ij}^l + \frac{b_{ij}^{l,ch}}{2}) v_j^2 + (a_{ij}^l v_i) v_j [g_{ij}^l \sin(\theta_{ij} + \varphi_{ij}^l) + b_{ij}^l \cos(\theta_{ij} + \varphi_{ij}^l)] \tag{156}$$

Constraint (145) is related to the line power flow limit. This limit can be considered as active power flow, (153) and (154), or apparent power flow as (157) and (158).

$$fl_{ij} = \sqrt{p_{ij}^2 + q_{ij}^2} \tag{157}$$

$$fl_{ji} = \sqrt{p_{ji}^2 + q_{ji}^2} \tag{158}$$

Constrains (146) and (147) are the active and reactive power generation limits, respectively; more details have been provided in section 2.2.3, (70).

$$P_{g_i}^M(Q_{g_i}) = \begin{cases} \left(\dfrac{P_{g_i}'}{Q_{g_i}' - \underline{P_{g_i}}}\right)(Q_{g_i} - \underline{Q_{g_i}}), & \underline{Q_{g_i}} \le Q_{g_i} \le Q_{g_i}' \\[3mm] \sqrt{S_{g_i}^2 - Q_{g_i}^2}, & Q_{g_i}' \le Q_{g_i} \le Q_{g_i}'' \\[3mm] \dfrac{\sqrt{v_i^2(\overline{E}_i)^2 - (Q_{g_i} Xs_i + v_i^2)^2}}{Xs_i}, & Q_{g_i}'' \le Q_{g_i} \le \overline{Q}_{g_i} \end{cases} \tag{159}$$

where the maximum excitation voltage of unit i ($\overline{E}_i$) is defined as (160); the coordinates of the intersection points between the first and second portions (Q_{g_i}', P_{g_i}'), and between the second and third portions (Q_{g_i}'', P_{g_i}''), of the capability curve are calculated as (161)-(164).

$$\overline{E}_i = \sqrt{\frac{(Xs_i P_{g_i}'')^2 + (Xs_i Q_{g_i}'' + v_i^2)^2}{v_i^2}} \tag{160}$$

$$P_{g_i}' = S_{g_i} \cdot \cos(-\varphi) \tag{161}$$

$$Q'_{g_i} = S_{g_i} \cdot \sin(-\varphi) \tag{162}$$

$$P''_{g_i} = S_{g_i} \cdot \cos\varphi \tag{163}$$

$$Q''_{g_i} = S_{g_i} \cdot \sin\varphi \tag{164}$$

It should be noted that usually the bus voltage magnitude, v_i in (160), is supposed to be 1 (p.u), but in this dissertation, in order to have a more precise model, the actual voltage magnitude is considered.

Constraints (150) and (151) are the sub-area and area emission limits, respectively. In this work, the amount of emission for each generator ($Em_i(\cdot)$) is approximated by the quadratic function of (165) (VENKATESH et al., 2003).

$$Em_i(P_{g_i}) = \alpha_i(P_{g_i})^2 + \beta_i P_{g_i} + \gamma_i \tag{165}$$

Constraints of (166)-(169) are only for the buses related to interconnected areas.

$$P_{g_i} - P_{d_i} - g_i^{sh} v_i^2 - \sum_{\substack{ij \in \Omega_L^{A_x} \\ i \neq j}} p_{ij} - \sum_{\substack{ji \in \Omega_L^{A_x} \\ i \neq j}} p_{ji} - \sum_{\substack{ij \in \Omega_{TL}^{A_{xy}} \\ x \neq y}} p'_{ij} - \sum_{\substack{ji \in \Omega_{TL}^{A_{xy}} \\ x \neq y}} p'_{ji} = 0, \quad i \in \Omega_b^{A_{xy}} \tag{166}$$

$$Q_{g_i} - Q_{d_i} + b_i^{sh} v_i^2 - \sum_{\substack{ij \in \Omega_L^{A_x} \\ i \neq j}} q_{ij} - \sum_{\substack{ji \in \Omega_L^{A_x} \\ i \neq j}} q_{ji} - \sum_{\substack{ij \in \Omega_{TL}^{A_{xy}} \\ x \neq y}} q'_{ij} - \sum_{\substack{ji \in \Omega_{TL}^{A_{xy}} \\ x \neq y}} q'_{ji} = 0, \quad i \in \Omega_b^{A_{xy}} \tag{167}$$

$$\underline{tp_{ij}} \leq tp_{ij} \leq \overline{tp_{ij}}, \qquad ij \in \Omega_{TL}^{A_{xy}}, x \neq y \tag{168}$$

$$EMS \leq \overline{EMS} \tag{169}$$

$$\left| fl_{ij/ji}(v,\theta,tp) \right| \leq \overline{fl}_{ij/ji}, \qquad ij, ji \in \Omega_{TL}^{A_{xy}}, x \neq y \tag{170}$$

where p'_{ij}, p'_{ji}, q'_{ij}, and q'_{ji} are the direct and reverse active and reactive power flows of the interconnected buses. For calculating these power flows, formulations (153)-(156) are used; however, in this formulation, only the interconnected buses are considered, which means $ij \in \Omega_{TL}^{A_{xy}}$. In addition, constraint (169) presents the interconnected system's total emission limit, defined as (171).

$$EMS = \sum_{x=\Omega_A} \sum_{i \in \Omega_g^{A_x}} Em_i \tag{171}$$

The resulting formulation constitutes a MA-AROPF problem, which is readily implementable and an appropriate model for market-based problems.

Chapter 5

APPLICATION OF MULTI-AREA ENVIRONMENTALLY-CONSTRAINED ACTIVE-REACTIVE OPTIMAL POWER FLOW ON SHORT-TERM TIE LINE PLANNING

5.1 INTRODUCTION

Traditionally, tie line planning is performed by considering the location and the capacity of the tie lines, as well as the rate of return in order to obtain the optimal economic operation of the system. In the literature, the candidate buses for tie line planning are pre-defined, and therefore, the problem is mostly a transmission expansion planning, in which the stability of interconnected systems, the tie line investment costs, the multi-area security, etc. are taken into consideration. In order to determine an appropriate tie line, four types of methods can be used: metaheuristic, enumeration, sensitivity index (DA SILVA et al., 2001), and the proposed methodology based on determining the weak and strong buses. In the real world, determining appropriate transmission tie lines, which yield an improvement in the voltage stability, leads to decrease the system's total operating costs or even the system's regional or total emissions. On the other hand, enhancing the degrees of freedom is highly dependent on finding the critical buses/segments of each area in the power system. In this chapter, in order to find proper buses, the system operation is taken into account at its maximum loadability point (MLP). Although the metaheuristic and enumeration methods can determine the appropriate tie lines that result in lower cost compared to the sensitivity index method, these methods have some drawbacks; for instance, they are time consuming and inefficient in finding an appropriate tie line, which can satisfy several objectives. As an example, in enumeration methods, it is quite difficult to find a compromise between several objectives via a classic approach, while for metaheuristics, adjusting the compromise coefficients of the objectives is a complicated task (KASMAEI et al., 2013). In the sensitivity index method, if load changes, the MA-AROPF solution will change, and consequently, the Lagrangian multipliers, which determine the sensibilities, will change and an inappropriate tie line plan may then be resulted.

In this work, the optimal tie line is considered as the one that, under the MLP condition, most effectively enhances the stability of the multi-area system as well as its degree of freedom (to be easily reschedulable), while reducing the total operating costs and/or emissions. Based on the analysis of a power system at the MLP, the weak and strong buses are determined and a set of strong and weak buses are selected as candidate buses for tie line

planning and then, via a mixed integer nonlinear programming problem, the appropriate tie lines are selected. Moreover, in order to have a more appropriate plan at all the operating points, the switchable tie lines are considered.

5.2 DETERMINING THE WEAK AND STRONG BUSES

In this work, a voltage stability index is used to determine the weak and strong buses. To calculate this index, it is necessary to solve the economic operation problem (EOP) of a power system at the initial loading point and maximum loadability point (MLP). Moreover, to obtain the MLP, the maximum loadability point problem (MLPP) is taken into account. In this regard, the following optimization problems are considered.

5.2.1 Economic operation at initial loading condition

In this step, the economic operation of each area at the initial loading condition is taken into consideration. The optimization problem is defined as (172)-(181). By considering the capability curve and environmental limits, the AROPF problem becomes a more practical and highly nonlinear problem.

$$\min F_C^{A_x}(P_g) = \sum_{i \in \Omega_g^{A_x}} C_i(P_{g_i}), \qquad x \in \Omega_A = \{1,...,n_A\} \tag{172}$$

$s.t.$

$$P_{g_i} - P_{d_i} - g_i^{sh}(v_i)^2 - \sum_{\substack{ij \in \Omega_L^{A_x} \\ i \neq j}} p_{ij} - \sum_{\substack{ji \in \Omega_L^{A_x} \\ i \neq j}} p_{ji} = 0, \qquad i \in \Omega_b^{A_x} \tag{173}$$

$$Q_{g_i} - Q_{d_i} + b_i^{sh}(v_i)^2 - \sum_{\substack{ij \in \Omega_L^{A_x} \\ i \neq j}} q_{ij} - \sum_{\substack{ji \in \Omega_L^{A_x} \\ i \neq j}} q_{ji} = 0, \qquad i \in \Omega_b^{A_x} \tag{174}$$

$$\left| fl_{ij/ji}(v,\theta,tp) \right| \leq \overline{fl}_{ij/ji}, \qquad ij, ji \in \Omega_L^{A_x} \tag{175}$$

$$\underline{P_{g_i}} \leq P_{g_i} \leq P_{g_i}^M(Q_{g_i}), \qquad i \in \Omega_g^{A_x} \tag{176}$$

$$\underline{Q_{g_i}} \leq Q_{g_i} \leq \overline{Q}_{g_i}, \qquad i \in \Omega_g^{A_x} \tag{177}$$

$$\underline{v_i} \leq v_i \leq \overline{v}_i, \qquad i \in \Omega_b^{A_x} \tag{178}$$

$$\underline{tp_{ij}^l} \leq tp_{ij}^l \leq \overline{tp_{ij}^l}, \qquad ij \in \Omega_L^{A_x} \tag{179}$$

$$EMSA_x^{sa} = \sum_{i \in \Omega_g^{A_x^{sa}}} Em_i \leq \overline{EMSA_x^{sa}}, sa \in \Omega_{SA}^{A_x} = \{1,...,n_{SA}^{A_x}\} \tag{180}$$

$$EMA_x = \sum_{i \in \Omega_g^{A_x}} Em_i \leq \overline{EMA}_x \tag{181}$$

where $F_C^{A_x}(\cdot)$ is the objective function of each area. The other terms have been defined in sub-section 4.4.

5.2.2 Finding the maximum loadability point (MLP)

The maximum loadability point (MLP) of a power system is the maximum load that a power system can serve without violating the constraints related to the generation, transmission, and operation (CHANG, 2014). In this chapter, a novel mathematical formulation with respect to (DE SOUZA et al., 2004; CHANG, 2014) is proposed. Unlike the presented methodology in the aforementioned works, in which the increasing percentage of the active and reactive demands are equal, in the proposed methodology, the MLP is obtained by considering the maximum load power factor.

$$\max S_T = \sum_{i \in \Omega_D^{A_x}} S_{d_i}, \qquad x \in \Omega_A \tag{182}$$

$$s.t. \qquad Constraints\,(173)-(181)$$

$$P_{d_i}^0 \le P_{d_i}, \qquad i \in \Omega_D^{A_x} \tag{183}$$

$$\begin{cases} Q_{d_i} \ge Q_{d_i}^0 & if\ Q_{d_i}^0 \ge 0, i \in \Omega_D^{A_x} \\ Q_{d_i} \le Q_{d_i}^0 & if\ Q_{d_i}^0 \le 0, i \in \Omega_D^{A_x} \end{cases} \tag{184}$$

$$\left| Q_{d_i} \right| \le \overline{Q}_{d_i}(p.f_{d_i}, P_{d_i}), \qquad i \in \Omega_D^{A_x} \tag{185}$$

The objective of this problem (182) is to maximize the total apparent power demand, S_T. In this formulation, S_{d_i} is defined as (186).

$$S_{d_i} = \sqrt{P_{d_i}^2 + Q_{d_i}^2}, \qquad i \in \Omega_D^{A_x} \tag{186}$$

Constraint (183) is related to the active demand limit that can be greater than or equal to the initial active load. Constraints (184) and (185) stand for the lower and upper bounds of the reactive demand. In (184), if the initial load is inductive $Q_d^0 \ge 0$ or capacitive $Q_d^0 \le 0$, it can respectively become more inductive or more capacitive at the MLP. The upper bound of the reactive demand (185) has a nonlinear characteristic as it is a function of active power demand and demand power factor. This nonlinear constraint, which makes the problem an even more complicated one, is defined as (187).

$$\overline{Q}_{d_i} = \rho_i P_{d_i} \tag{187}$$

In order to define ρ_i, the following formulations are taken into account.

$$p.f_{d_i} = \frac{P_{d_i}}{S_{d_i}}, \qquad i \in \Omega_D^{A_x} \tag{188}$$

By considering (186) and (188), the following relationship (189), among active power, reactive power, and load power factor is obtained.

$$Q_{d_i} = P_{d_i} \cdot \sqrt{\left(\frac{1}{(p.f_{d_i})^2} - 1\right)}, \qquad i \in \Omega_D^{A_x} \tag{189}$$

By comparing (189) with (187), ρ_i is defined as (190).

$$\rho_i = \sqrt{\left(\frac{1}{(p.f_{d_i})^2} - 1\right)} \tag{190}$$

The minimum possible load power factor (LPF) results in the maximum possible reactive demand; in other words, in a system with LPF=0.9, $\bar{Q}_{d_i}$ is achieved by setting ρ_i at about 0.4843 ($\rho_i \simeq 0.4843$).

5.2.3 The economic operation under the MLP condition

The economic operation at the MLP is achieved via problem (172) subject to constraints (173)-(181), where the active and reactive demands are obtained from the MLP problem, (182) subject to the corresponding constraints.

5.2.4 Determining the weak and strong buses

As mentioned earlier, in order to find the weak and strong buses, from the voltage stability standpoint, a voltage stability index, is used (OBADINA; BERG, 1990). This index shows the voltage change of each bus at the MLP from its initial operating state.

$$VC_i = \frac{v_i^{ILP} - v_i^{MLP}}{v_i^{init}} \times 100, \qquad i \in \Omega_b^{A_x}, x \in \Omega_A \tag{191}$$

where v_i^{ILP} and v_i^{MLP} are the voltage obtained from the economic-oriented problems presented in subsections 5.2.1 and 5.2.3, respectively.

As the weakest bus would have the largest voltage change (voltage drop), the smallest indices identify the strongest buses, and the largest indices identify the weakest buses. Among these ranked buses, some pre-defined percentages of buses are selected as the strong and weak candidate buses. This selection process will decrease the search area toward selecting

the most effective buses in tie line planning.

5.3 TIE LINE PLANNING VIA A MA-AROPF

After solving the optimization problems in subsection 5.2 and finding the weak and strong buses, several weak and strong buses in each area are selected to find the best set of tie lines. In this planning, the economic and environmental impacts, and the voltage stability are taken into account. It then yields an improvement in the system stability, decreases the total costs, and also reduces the system emissions. It is worth mentioning that this planning is done under the critical condition of MLP.

For a multi-area system, by considering the coupling constraints, in order to determine the overall optimal point, each area optimizes its own problem while it has access to the information of other areas as well. In the literature, two commonly used methods are 1) decomposition based on the adjustment of the shared border variable (KIM; BALDICK, 1997; WANG et al., 2001), and 2) decomposition based on the information exchange (CONEJO et al., 2002; NOGALES et al., 2003). Both of the aforementioned methods are iterative and inapplicable in online-based problems such as pricing, marketing, etc.

5.3.1 Tie line planning

In this work, the objective function of tie line planning is to minimize the tie line investment costs as well as the operating costs (192), while the other aforementioned concerns, including the voltage stability and emission reduction, are considered as the constraints of this problem. This optimization problem is considered as a mixed integer nonlinear programming (MINLP) problem.

$$\min F_C^{TLP} = \min \sum_{ij \in \Omega_{TL}^{A_{xy}}} c_{ij} n_{ij} + \min F_C^{MA} \tag{192}$$

$s.t.$ $constraints$ sets (143)-(151), (166)-(170), and (193)-(199)

$$\left| fl_{ij/ji}(v,\theta,tp) \right| \le (n_{ij} + n_{ij}^o)\overline{fl}_{ij/ji}, ij/ji \in \Omega_{TL}^{A_{xy}} \tag{193}$$

$$\sum_{x \in \Omega_A} \sum_{i \in \Omega_g^{A_x}} C_i(P_{g_i}) \le Cost^{MLP} \tag{194}$$

$$EMS \le EMS^{MLP} \tag{195}$$

$$v_i \ge \underline{v}_i^{TLP} \tag{196}$$

$$0 \le n_{ij} \le \overline{n}_{ij}, \quad ij \in \Omega_{TL}^{A_{xy}}, n_{ij} \text{ is an integer} \tag{197}$$

$$\sum_{ij \in \Omega_l^{A_{xy}}} n_{ij} \ge 1, \qquad xy \in \Omega_A \tag{198}$$

$$\sum_{xy \in \Omega_{IA}} \sum_{ij \in \Omega_{TL}^{A_{xy}}} n_{ij} \le \overline{n}_{IA} \tag{199}$$

where in (166) and (167), the active and reactive power injections of tie lines between the interconnected areas x and y are calculated by (200)-(203). It is worth stating that (200)-(203) are related to tie lines, $ij \in \Omega_{TL}^{A_{xy}}$; $\overline{n}_{IA}$ is the maximum possible interconnected lines between area x and y.

$$p'_{ij} = (n_{ij} + n_{ij}^o)[(a_{ij}^l v_i)^2 g_{ij}^l - (a_{ij}^l v_i) v_j (g_{ij}^l \cos(\theta_{ij} + \varphi_{ij}^l) + b_{ij}^l \sin(\theta_{ij} + \varphi_{ij}^l))] \tag{200}$$

$$p'_{ji} = (n_{ij} + n_{ij}^o)[g_{ij}^l v_j^2 - (a_{ij}^l v_i) v_j (g_{ij}^l \cos(\theta_{ij} + \varphi_{ij}^l) - b_{ij}^l \sin(\theta_{ij} + \varphi_{ij}^l))] \tag{201}$$

$$q'_{ij} = (n_{ij} + n_{ij}^o)[-(a_{ij}^l v_i)^2 (b_{ij}^l + \frac{b_{ij}^{l,ch}}{2}) - (a_{ij}^l v_i) v_j (g_{ij}^l \sin(\theta_{ij} + \varphi_{ij}^l) - b_{ij}^l \cos(\theta_{ij} + \varphi_{ij}^l))] \tag{202}$$

$$q'_{ji} = (n_{ij} + n_{ij}^o)[-(b_{ij}^l + \frac{b_{ij}^{l,ch}}{2}) v_j^2 + (a_{ij}^l v_i) v_j (g_{ij}^l \sin(\theta_{ij} + \varphi_{ij}^l) + b_{ij}^l \cos(\theta_{ij} + \varphi_{ij}^l))] \tag{203}$$

Constraint (193) is related to the maximum allowed power flow among the candidate buses, which depends on the number of lines.

As tie lines are planned at the MLP, in order to ensure that the plan will not increase the costs and/or emissions, constraints (194) and (195) are taken into account. In these constraints, the total system costs ($Cost^{MLP}$) and the corresponding total emissions (EMS^{MLP}) are obtained by using the results of the economic operation at the MLP (subsection 5.2.3). To calculate the total emissions at the MLP, (171) is used while the total cost at the MLP is calculated by (204), respectively.

$$EMS^{MLP} = \sum_{x \in \Omega_A} \sum_{i \in \Omega_g^{A_x}} Em_i(P_{g_i}) \tag{204}$$

Another important objective of a tie line planning is to regulate the voltages at a more stable point, in comparison with the voltages prior to planning. In this regard, constraint (196) forces the planning to find a set of tie lines, in which the desired voltage limit is satisfied. Constraint (197) is related to the maximum possible candidate tie lines between two buses. Constraint (198) ensures that at least, one tie line among the candidate areas will be constructed; and constraint (199) is related to the maximum total tie lines that can be planned for all areas. It is worth mentioning that, in order to have a generalized model for tie line

planning problems, n_{ij}^0 is used, which stands for the existing tie lines.

5.4 MA-AROPF WITH SWITCHABLE TIE LINES

Fixing all the selected tie lines determined at the MLP may be inappropriate for other operating points and might result in an increase in the cost and/or emission. In this regard and in order to have a more efficient multi-area power system, tie lines are considered to be switchable. In order to obtain a mathematical formulation of MA-AROPF with switchable tie line, it is necessary to change the problem to a mixed binary programming problem. It should be expressed that in (166) and (167), p'_{ij}, p'_{ji}, q'_{ij}, and q'_{ji} are calculated by using formulations (153)-(156), but in this formulation, only the interconnected buses are considered, which means $ij \in \Omega_{TL}^{A_{xy}}$;

$$\min F_C^{MA-STL} = \min F_C^{MA}$$
$$s.t. \quad (143)\text{-}(151), \tag{205}$$
$$\quad (166)\text{-}(169), \text{ and for } p'_{ij}, p'_{ji}, q'_{ij}, and\ q'_{ji},\ ij\ /\ ji \in \Omega_{TL'}^{A_{xy}}$$

$$\left| fl_{ij/ji}(V,\theta,tp) \right| \le (n_{ij} + n_{ij}^o)\overline{fl}_{ij/ji}, \qquad ij\ /\ ji \in \Omega_{TL'}^{A_{xy}} \tag{206}$$

$$n_{ij} = \sum_{l=1}^{\overline{n}'_{ij}} n_{ij}^l, \qquad ij \in \Omega_{TL'}^{A_{xy}} \tag{207}$$

$$n_{ij}^l \quad \text{binary} \tag{208}$$

In (208), n_{ij}^l is binary, which determines the status of tie lines switches. In addition, constraint (207) ensures that the number of tie lines does not exceed the number of selected tie lines, from subsection 5.3.

Chapter 6

CASE STUDIES AND RESULTS

6.1 DYNAMIC ECONOMIC AND EMISSION AROPF

The UNBP approach is tested on three IEEE test systems. For didactic purposes, the proposed approach has been studied in detail via the small-scale IEEE 14-bus test system. This small-scale system has been selected in order to show that even in such a system, in which finding an acceptable compromise using each compromise methodology is readily at hand, the UNBP acts better in this case than the commonly used MOPCC approach. Two other case studies are the IEEE 30-bus and 118-bus test systems. In order to show the effectiveness of the UNBP, different conditions including the normal, outage (transmission line and generator), and critical conditions are considered. In this work, in order to model these methodologies, a modeling language for mathematical programming (AMPL) is applied (FOURER et al., 2002) and the nonlinear commercial solver KNITRO 9.1 is used.

6.1.1 The IEEE 14-bus test system

This system contains 11 load busses, 5 generation units, and 20 transmission lines (ONLINE). In order to have quick access, some data are available in Table 1. In this system, two emission regions have been defined. The first region contains busses 1 and 2, and the second region contains all the other busses. The EMS of the IEEE 14-bus test system is considered to be 0.36 t/h. It should be stated that in order to avoid repeating all the outputs, each of the most important outputs is reported.

Table 1- The IEEE 14-bus system quick reference data

Bus No.	Sg [p.u.]	RU (MW/h)	RD (MW/h)	EMA (t/h) Region	EMA (t/h) Limit
1	3.324	8	10	1	0.29
2	1.4	25	30		
3	1.0	4	5		
6	1.0	10	12	2	0.14
8	1.0	5	7		

6.1.1.1 Normal condition

In this case, the system is working under normal operating conditions, which means that an outage does not happen. In order to show the effect of the capability curve, the Sg of unit 2 has been changed to 0.35 p.u.

Table 2- The active power output, regional and total emission, total cost, and execution time of the economic-oriented and emission-oriented scenarios, 14-bus system

	Scenario I						Scenario II					
	h1	h2	h3	h4	h5	h6	h1	h2	h3	h4	h5	h6
P_{g_1} (MW)	175.86	175.88	183.88	191.88	191.27	181.27	47.23	51.20	59.20	67.20	62.19	52.19
P_{g_2} (MW)	32.61	27.66	13.93	34.99	34.99	9.75	35.00	29.15	15.47	35.00	35.00	11.34
P_{g_3} (MW)	35.31	39.31	43.31	47.31	44.70	39.70	68.78	72.78	76.78	80.78	78.58	73.58
P_{g_4} (MW)	0.00	10.00	20.00	30.00	18.00	6.00	48.77	56.58	66.58	76.58	69.84	57.84
P_{g_5} (MW)	22.79	27.79	32.79	37.79	36.41	29.41	60.56	65.56	70.56	75.56	72.80	65.80
Emission (t) — EMA_1	0.1876	0.1887	0.2153	0.2341	0.2321	0.2098	0.0427	0.0443	0.0501	0.0470	0.0454	0.0505
EMA_2	0.1369	0.1321	0.1284	0.1259	0.1279	0.1326	0.1259	0.1281	0.1320	0.1375	0.1339	0.1286
EMS	0.3245	0.3208	0.3437	0.36	0.36	0.3424	0.1686	0.1724	0.1821	0.1845	0.1793	0.1791
Total	2.0514						1.0660					
Cost ($)	55,915.2						62,461.5					
Time (s)	0.178						0.155					

Table 2 presents the best solution of scenarios I and II during the operating time horizon. The attained results confirm the accuracy of the aforementioned methodologies, while the ramp rate is taken into account. For example, this can be witnessed for scenarios I and bus 8. By considering hours 1 and 2, a ramp-up rate constraint satisfaction of (27.79-22.79= 5 MW/h) is seen, and considering hours 5 and 6, a ramp-down rate constraint satisfaction of (36.41-29.41= 7 MW/h) is observed. Also the regional and system emissions show that the regional emissions in scenarios I and II are less than their maximum limits, while in scenario I, the system emission limit at hours 4 and 5, has been reached.

In Figure 14, the compromise trajectories for the proposed UNBP and the MOPCC methodologies have been depicted. The starting point of these trajectories corresponds to $k \simeq 0$ (in this work, $k = \dfrac{0.01}{0.99}$), and the ending point of them corresponds to $k = big\ M$ (in this work, $M = \dfrac{0.99}{0.01}$).

Figure 14- The compromise trajectory of the UNBP and MOPCC for different values of *k*
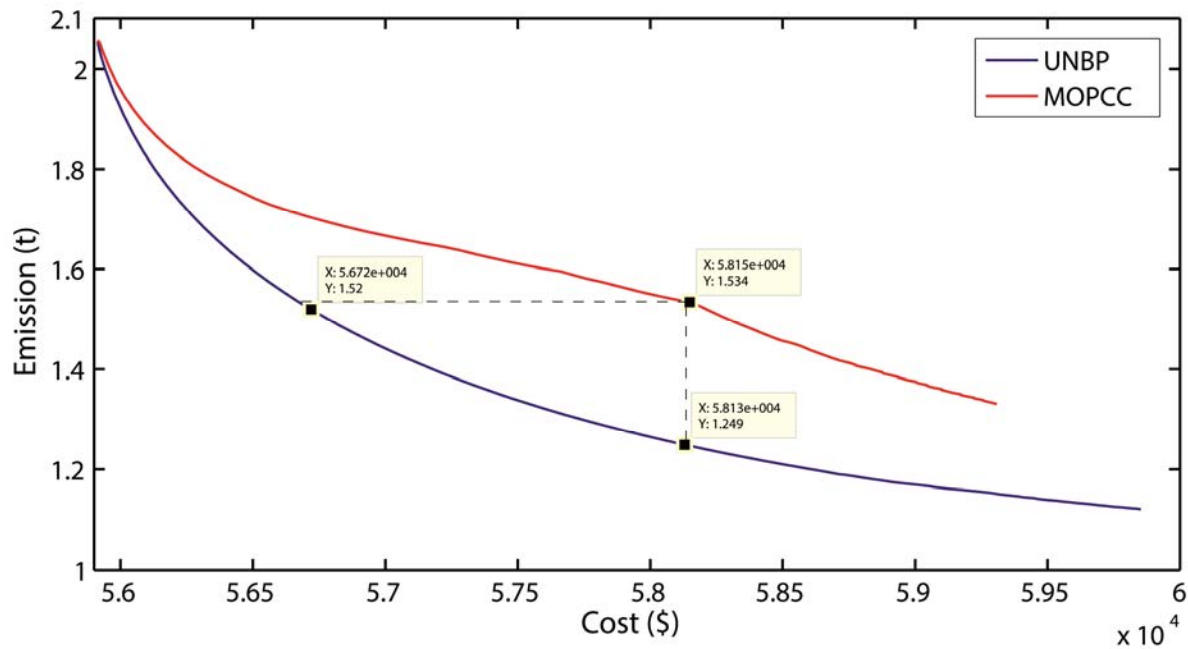
Source: The author

From an economic and emission OPF problem standpoint, a good compromise can be obtained if an insignificant increase in costs yields a significant decrease in emissions. From Figure 14, it is clear that for all the points on the compromise trajectories, a better result has been obtained via the proposed UNBP in comparison with the MOPCC, where less increase in costs yields more reduction in emissions. On the other hand, the UNBP shows a smooth compromise trend compared to the MOPCC, where in several points of the MOPCC, a jump can be spotted.

In order to compare the results with the commonly used MOPCC method, a compromise point in the MOPCC's compromise trajectory ($k = \dfrac{0.47}{0.53}$) is selected, which resulted in approximately 25% reduction in emission. In order to find the comparable point in the UNBP, two compromise points can be considered; through fixing the total emission less than or equal to the emission obtained by the MOPCC method at the selected k and finding the corresponding compromise cost and scaling factor *k* of the UNBP, or through fixing the total cost less than or equal to the MOPCC method at the selected k and finding the corresponding compromise cost and scaling factor *k* of the UNBP.

Table 3- The best compromise solution of the MOPCC and UNBP, 14-bus system

	MOPCC ($k = \dfrac{0.47}{0.53} \simeq 0.8868$)						UNBP ($k = \dfrac{0.22}{0.78} \simeq 0.2821$)					
	h1	h2	h3	h4	h5	h6	h1	h2	h3	h4	h5	h6
P_{g_1} (MW)	133.16	141.16	149.16	157.16	147.16	137.16	134.20	141.85	149.85	157.85	151.64	141.64
P_{g_2} (MW)	0	0.27	0	20.36	24.39	0	34.97	27.95	14.22	34.99	34.99	10.12
P_{g_3} (MW)	51.59	53.23	55.03	59.03	56.04	51.03	45.39	47.78	51.78	55.78	53.36	48.36
P_{g_6} (MW)	32.04	34.53	35.73	45.73	41.13	29.13	12.72	19.18	29.18	39.18	33.45	21.45
P_{g_8} (MW)	46.56	48.86	51.72	56.72	53.24	46.24	36.55	41.55	46.55	51.55	49.01	42.01
$P_{g_1}^{M}$ (MW)	332.40	332.39	332.33	332.25	332.25	332.39	332.29	332.4	332.4	332.25	332.25	332.4
$P_{g_2}^{M}$ (MW)	0	0.29	0.04	20.36	24.39	0	34.97	28.14	18.10	34.99	34.99	25.73
$P_{g_3}^{M}$ (MW)	99.98	99.97	99.97	99.66	99.63	99.99	97.04	97.89	98.05	95.96	96.32	98.18
$P_{g_6}^{M}$ (MW)	97.08	97.08	97.08	98.98	99.41	97.08	99.84	99.86	99.89	99.67	99.71	99.95
$P_{g_8}^{M}$ (MW)	99.99	99.99	99.99	99.70	99.70	99.99	99.78	99.74	99.65	99.36	99.46	99.78
Emission (t) — EMA$_1$	0.1169	0.1289	0.1426	0.1482	0.1283	0.1228	0.1053	0.1184	0.1367	0.1459	0.1339	0.1245
Emission (t) — EMA$_2$	0.1246	0.1243	0.1242	0.1245	0.1241	0.1248	0.1288	0.1267	0.1248	0.1241	0.1243	0.1262
Emission (t) — EMS	0.2415	0.2532	0.2668	0.2727	0.2524	0.2476	0.2341	0.2451	0.2615	0.27	0.2582	0.2507
Emission (t) — Total	1.5342						1.5196					
Cost ($)	58,149.1						56,719.9					
Time (s)	0.547						0.128					

Table 3 contains the best solution of the MOPCC and UNBP for the compromised-oriented scenario (scenarios III) during the operating time horizon. The solution obtained by the MOPCC shows that in several hours (h1, h2, h3, and h6), the maximum output limit of generator 2, is equal or at least close to zero, while for the UNBP method, the maximum output limit of generator 2 is at least 18.10 MW. This shows that the degree of freedom of the UNBP compared to the MOPCC is sufficiently large and this may play an important role in finding a better compromise point for large-scale systems as well as power systems under contingency condition. Moreover, it can be seen that the maximum output limit of generator 2, imposed by the capability curve, has been verified during several hours of the MOPCC (h1, h4, h5, and h6) and the UNBP (h1, h4, and h5). According to the results of this case, it can be concluded that a larger degree of freedom of the UNBP yields better compromise results than the MOPCC method, where in the MOPCC by increasing about 4% in costs ($2,233.9),

approximately 25.21% reduction in emissions (0.5172 t) is obtained, while for reducing the emissions by 25.92% (0.5318) via the UNBP, only 1.44% ($804.7) increase in costs is required, which confirms that in the UNBP, less increase in cost yields more emission reduction compared to the MOPCC. In other words, in order to decrease the total emission by nearly 26%, a saving of about $1,429.2 can be achieved by using the UNBP instead of the MOPCC. On the other hand, by fixing the total cost less than or equal to the cost obtained by the MOPCC, it can be observed that for the UNBP method with $k = \dfrac{0.51}{0.49}$, the total cost is $58,130 and the corresponding total emission is 1.2491 t. This shows that by increasing the cost by about 3.96% ($2,214.8), about 39.12% (0.8023 t) reduction in emissions is obtained.

6.1.1.2 Generator outage

In this case, the generator outage is considered as a contingency condition in order to show the effectiveness of the UNBP. In this work, the outage of unit 3 is taken into consideration. Also, in this case, EMS is changed to 0.35 t/h and EMAs are changed to 0.26 t/h and 0.10 t/h for the first and second regions, respectively.

The total fuel cost and total emission of scenario I are $56,021.74 and 1.9488 t, respectively, while in scenario II, $63,320.3 fuel costs corresponds to 0.9962 t of emission. In this case, the same as section 6.1.1.1, a compromise point in the MOPCC's compromise trajectory ($k = \dfrac{0.42}{0.58}$) has been selected, which results in about 25% reduction in emissions.

Table 4- The best compromise solution of the MOPCC and UNBP under the generator outage condition, 14-bus system

		MOPCC ($k = \dfrac{0.42}{0.58} \simeq 0.7241$)						UNBP ($k = \dfrac{0.22}{0.78} \simeq 0.2821$)					
		h1	h2	h3	h4	h5	h6	h1	h2	h3	h4	h5	h6
Emission (t)	EMA$_1$	0.1238	0.1383	0.1555	0.1736	0.1574	0.1382	0.1292	0.1362	0.1535	0.1704	0.1546	0.1363
	EMA$_2$	0.0960	0.0957	0.0957	0.0969	0.0960	0.0957	0.0963	0.0958	0.0959	0.0973	0.0961	0.0957
	EMS	0.2198	0.234	0.2512	0.2705	0.2534	0.2339	0.2255	0.2320	0.2494	0.2677	0.2507	0.232
	Total			1.4628						1.4573			
Cost ($)				56,733.8						56,625.7			
Time (s)				0.149						0.140			

Table 4 contains the best solution obtained by the MOPCC and UNBP under generators outage contingency condition. The results show that, in the MOPCC, by increasing the cost by about $712.06 (1.27%), an emission reduction of nearly 0.486 t (24.94%) is

obtained, while in the UNBP by increasing the cost by about \$603.96 (1.08%), an emission reduction of nearly 0.4915 t (25.22%) is obtained. It means that, compared to the MOPCC, less increase in cost yields more reduction in emissions via the UNBP method.

Figure 15- The voltage profile of 14-bus system at peak hour demand (hour 4), contingency condition (generator outage)
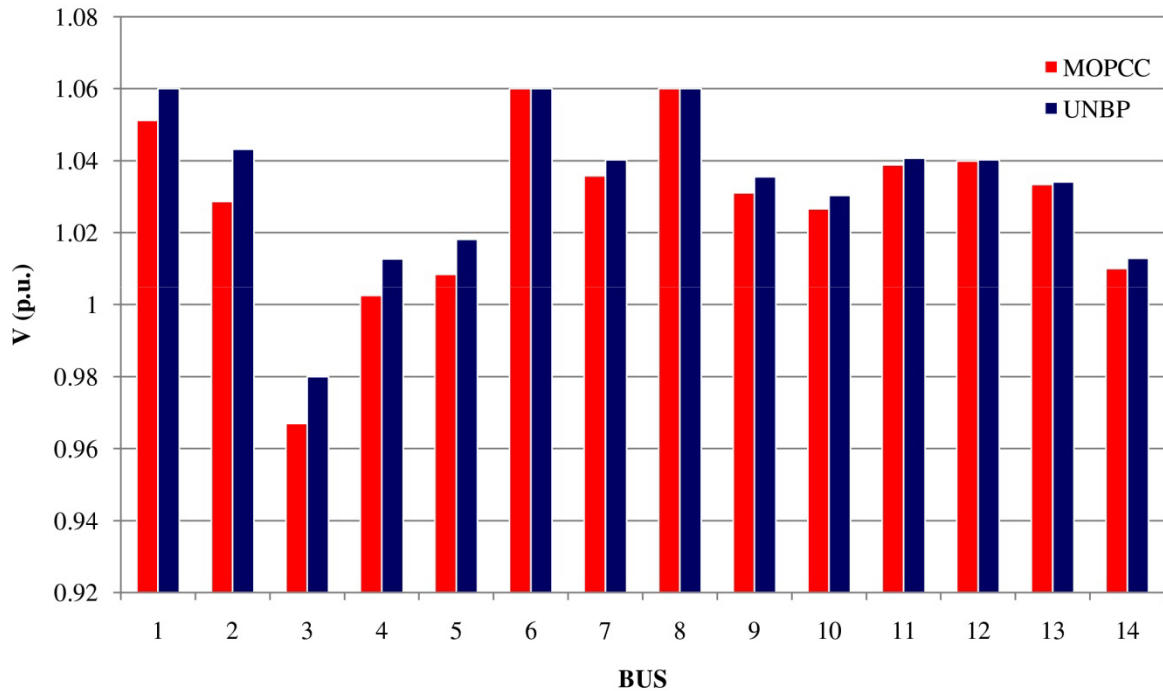
Source: The author

Figure 15 represents the voltage profile of the IEEE 14-bus test system under generators outage contingency condition at peak hour demand (hour 4). By considering this figure, it is clear that the UNBP has a better voltage profile than the MOPCC method and its superiority is much clearer at bus 3.

6.1.1.3 Line outage

Another contingency condition within the power system is related to the line outage. Here, the outage of a transmission line between bus 2 and 3 is taken into consideration. For this case, the limits of Table 1 are taken into account and the EMS is 0.36 t/h.

For this case, the total fuel cost and total emission of scenario I are \$56,385.0 and 2.0114 t, respectively, while in scenario II, \$63,166.6 of fuel cost corresponds to 1.0234 t of emissions. In this case, the same as the other cases, a compromise point in the MOPCC compromise trajectory ($k = \dfrac{0.26}{0.74}$) has been selected, which results in about 25% reduction in emissions.

Table 5- The best compromise solution of the MOPCC and UNBP under line outage
condition, 14-bus system

		MOPCC ($k = \dfrac{0.26}{0.74} \simeq 0.3514$)						UNBP ($k = \dfrac{0.19}{0.81} \simeq 0.2346$)					
		h1	h2	h3	h4	h5	h6	h1	h2	h3	h4	h5	h6
	EMA_1	0.1054	0.1141	0.1291	0.1418	0.1294	0.1158	0.1128	0.1142	0.1219	0.1341	0.1272	0.1135
Emission	EMA_2	0.1289	0.1276	0.1260	0.1245	0.1252	0.1280	0.1315	0.1291	0.1265	0.1250	0.1259	0.1289
(t)	EMS	0.2343	0.2417	0.2551	0.2663	0.2546	0.2438	0.2443	0.2433	0.2484	0.2591	0.2531	0.2424
	Total			1.4958						1.4906			
Cost ($)				57,148.6						57,083.2			
Time (s)				0.140						0.133			

Considering Table 5 and Figure 16, it has been reflected that, the same as the two previous cases, the UNBP plays a better role in the compromise scenario. By increasing by about 1.35% ($763.6) in costs, approximately 25.63% (0.5156 t) reduction in emissions is obtained via the MOPCC, while via the UNBP, a 1.24% ($698.2) increase in cost yields an emission reduction of about 25.89% (0.5208 t). Figure 16, especially bus 3, shows that the proposed UNBP is more reliable than the MOPCC method.

Figure 16- The voltage profile of 14-bus system at peak hour demand (hour 4), contingency
condition (line outage)
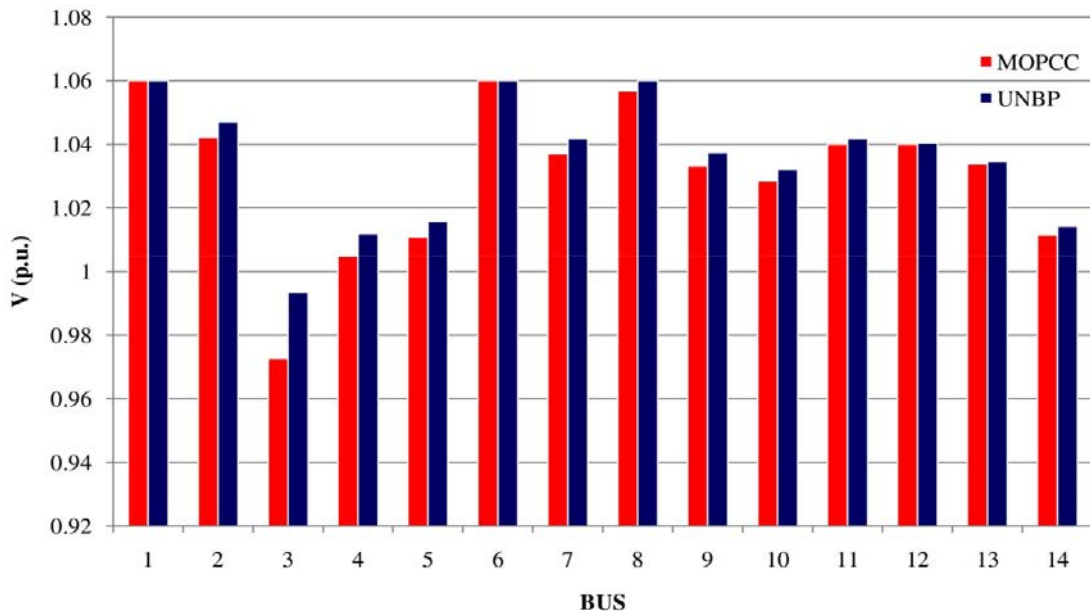
Source: The author

The data from the best solutions of the two aforementioned contingency cases verify that the system is working properly under the contingency condition. In the meantime, the system constraints have been satisfied and the voltage magnitude, obtained by the UNBP, during the scheduling time horizon is better than the voltage obtained via the MOPCC.

Conclusively, the results demonstrated that even for this small-scale system, in which finding an acceptable compromise point is not highly difficult, the proposed methodology for normal and contingency (generator outage and line outage) conditions achieved a better set of solutions in these cases (less emission corresponds with less cost).

6.1.2 The IEEE 30-bus system

This system contains 20 load busses, 6 generation units, and 41 transmission lines. For this test system, in order to compare the results of the UNBP with the results in the literature, a single-hour study has been conducted. In this benchmark system, there is no limitation on emissions and due to the lack of information from the capability curve, a pre-defined constant maximum output power has been taken into account. In this work, the same as the MSLFA approach (NIKNAM et al., 2011c), in order to ensure that the system is sufficiently far away from the point of collapse, the voltage magnitude limits of all buses are set to $0.95 \leq V_i \leq 1.05$.

Table 6- The objective function values in all scenarios, the IEEE 30-bus system

Scenarios	k	MSLFA		MOPCC		UNBP	
		Cost ($/h)	Emission (t/h)	Cost ($/h)	Emission (t/h)	Cost ($/h)	Emission (t/h)
I	-	802.287	0.3723	802.27507	0.362969	802.27507	0.362969
II	-	951.5106	0.2056	944.55486	0.204843	944.55486	0.204843
III	$\dfrac{0.1}{0.9} \simeq 0.1111$	823.27788	0.2907778	809.65769	0.293804	805.84422	0.312615
	$\dfrac{0.2}{0.8} = 0.25$	857.40576	0.2360181	823.26032	0.261487	814.24748	0.280629
	$\dfrac{0.3}{0.7} \simeq 0.4286$	877.35636	0.2260597	840.86873	0.240683	825.88479	0.258715
	$\dfrac{0.4}{0.6} \simeq 0.6667$	890.54330	0.2226469	858.68417	0.227976	841.35001	0.241384
	$\dfrac{0.5}{0.5} = 1$	891.06507	0.2197379	879.05002	0.218698	857.41759	0.229810
	$\dfrac{0.6}{0.4} = 1.5$	898.49795	0.2185756	896.01837	0.213759	877.42986	0.220305
	$\dfrac{0.7}{0.3} \simeq 2.3333$	925.51651	0.2117979	915.81676	0.209969	895.46642	0.214886
	$\dfrac{0.8}{0.2} = 4$	942.24246	0.2107835	924.97068	0.208484	918.77800	0.210417
	$\dfrac{0.9}{0.1} = 9$	948.22649	0.2092571	925.53064	0.208212	922.99976	0.209603

Table 6 presents the best solution of three scenarios for the IEEE 30-bus system via the MSLFA (NIKNAM et al., 2011c), and the proposed UNBP. For the compromise-based

scenario, different weighting factors have been considered. The results show that for the first and second scenarios, the UNBP and MOPCC have obtained better solutions (lower cost corresponds with lower emission) than the MSLFA and this may be a benefit of the commercial solvers. Therefore, this has not been considered as the superiority of our work. For scenario III, in several points, it is clear that the UNBP and MOPCC have obtained better compromise results (less increase in cost yields more emission reduction) than the MSLFA. For example, in order to reduce the emission by about 21.9% (0.082 t/h) via the MSLFA ($k \simeq 0.1111$), it is necessary to increase the fuel cost by about 2.62% (20.99 \$/h), while via the UNBP ($k = 0.25$), for achieving an emission reduction by about 22.69% (0.082 t/h), it is necessary to increase the cost by about 1.9% (11.97 \$/h). In order to consider the effectiveness of the proposed UNBP, a comparison with the critical compromise point, which was selected in (NIKNAM et al., 2011c), has been taken into account.

Table 7- A comparison between the results obtained from different approaches, the IEEE 30-bus system

Method	P_{g_1} (MW)	P_{g_2} (MW)	P_{g_3} (MW)	P_{g_4} (MW)	P_{g_5} (MW)	P_{g_6} (MW)	Cost (\$/h)	Emission (t/h)
PSO	97.8588	61.9419	31.131	34.4808	29.71	36.0884	872.8731	0.2253
GA	96.1251	68.5168	26.7031	35.0000	30.0000	34.7555	872.9601	0.2270
SFLA	98.9772	58.6832	35.0661	31.7585	29.9182	35.8174	872.8533	0.2249
MSFLA	97.55027	60.42367	31.6343	35.0000	30.0000	35.21483	867.713	0.2247
MOPCC	99.7811	51.8267	35.7891	35.0000	30.0000	35.6170	865.426	0.2246
UNBP	100.5180	49.5060	36.4135	35.0000	30.0000	36.5531	867.215	0.2246

Table 7 shows the results of different approaches including PSO (NIKNAM et al., 2011c), GA (NIKNAM et al., 2011c), SFLA (NIKNAM et al., 2011c), MSFLA (NIKNAM et al., 2011c), MOPCC, and UNBP, for the IEEE 30-bus system around a selected compromise point. Although the UNBP and MOPCC have obtained a better compromise solution than the other approaches in the literature, there is not a remarkable difference among the solutions of the MSLFA, MOPCC, and UNBP and this does not show the superiority of any of them at this point.

Figure 17- The compromise trajectory of the MSLFA, UNBP, and MOPCC for different
weighting factors
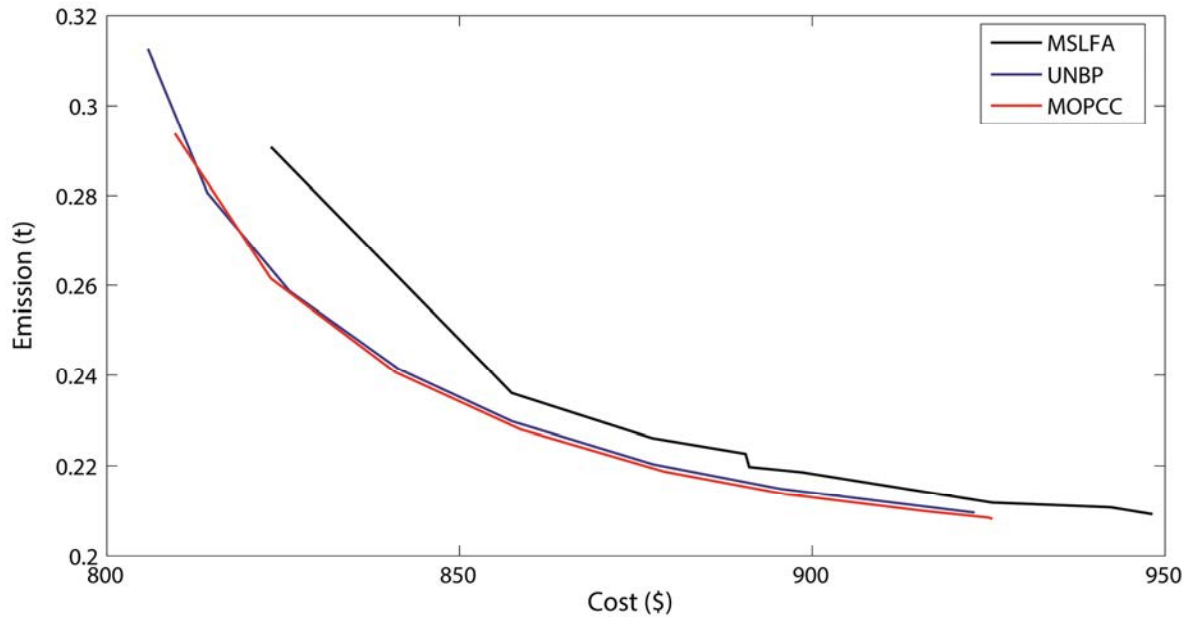
Source: The author

From Figure 17, it is clear that at some points, the UNBP has shown a better performance while at the other points, the performance of the MOPCC is better. For this system, the following points can be concluded: 1) effectiveness of the MOPCC and UNBP over the other approaches in the literature, and 2) superiority of the UNBP over the MOPCC for small-scale systems, which can be shown for a multi-period (dynamic) horizon, critical or constrained optimization conditions, like the results of the IEEE 14-bus test system in subsection 6.1.1.

6.1.3 The IEEE 118-bus system

This system has 99 load busses, 186 transmission lines, 54 generators, and 1 critical emission region (ONLINE, 2014). This emission region contains busses of 70, 73, 74, 76, 77, and 80. For this system, two case studies were conducted. In the first case, the EMA & EMS, SO_X, and NO_X limits, and the power flow limits are not considered, while for the second case, all of these limitations are taken into consideration. Emission data of this system are based on kilogram.

6.1.3.1 Without EMS and power flow limits

In this case, the regional and system emission limits and power flow limits are not considered.

Table 8- The best solution of the first and second scenarios, and the maximum emission case, the IEEE 118-bus system without limitation

Scenario		h1	h2	h3	h4	h5	h6	Total	Time (s)
I	NO_X (kg)	6.85	7.08	7.51	7.79	7.40	6.85	43.48	2.07
	SO_X (kg)	429.97	595.73	1,005.78	1,354.63	893.11	429.97	4,709.19	
	EMA (kg)	51.70	76.81	141.76	202.55	130.44	51.70	654.96	
	EMS (kg)	436.82	602.81	1,013.29	1,362.42	900.52	436.82	4,752.68	
	Cost ($)	130,477	142,484	166,913	185,098	158,249	130,477	913,698	
II	NO_X (kg)	2.25	2.39	2.75	3.07	2.61	2.25	15.32	1.73
	SO_X (kg)	0.14	0.16	0.23	0.32	0.20	0.14	1.19	
	EMA (kg)	0.25	0.28	0.33	0.38	0.31	0.25	1.80	
	EMS (kg)	2.39	2.55	2.98	3.39	2.81	2.39	16.51	
	Cost ($)	177,845	193,086	220,880	240,298	211,398	177,845	1,221,352	
Max Emission	EMS (kg)	201,178	201,178	202,856	201,185	201,182	201,178	1,208,757	31.02
	Cost ($)	148,724	159,454	181,451	199,853	173,664	148,724	1,011,870	

Table 8 contains the best solution of the cost-oriented and emission-oriented scenarios as well as the maximum emission case. In this case, in order to show the point that the system emits its maximum emission, an extra case has been considered. The results show that the fuel cost of the maximum emission case is higher than the cost of the cost-oriented scenario and less than the cost of the emission-oriented scenario. It means that, by increasing the fuel cost toward this point, the system emission may also increase and consequently, using an inappropriate compromise approach for this large-scale system might fail the finding of a proper compromise point.

Figure 18- The compromise trajectory of the MOPCC for various weighting factors
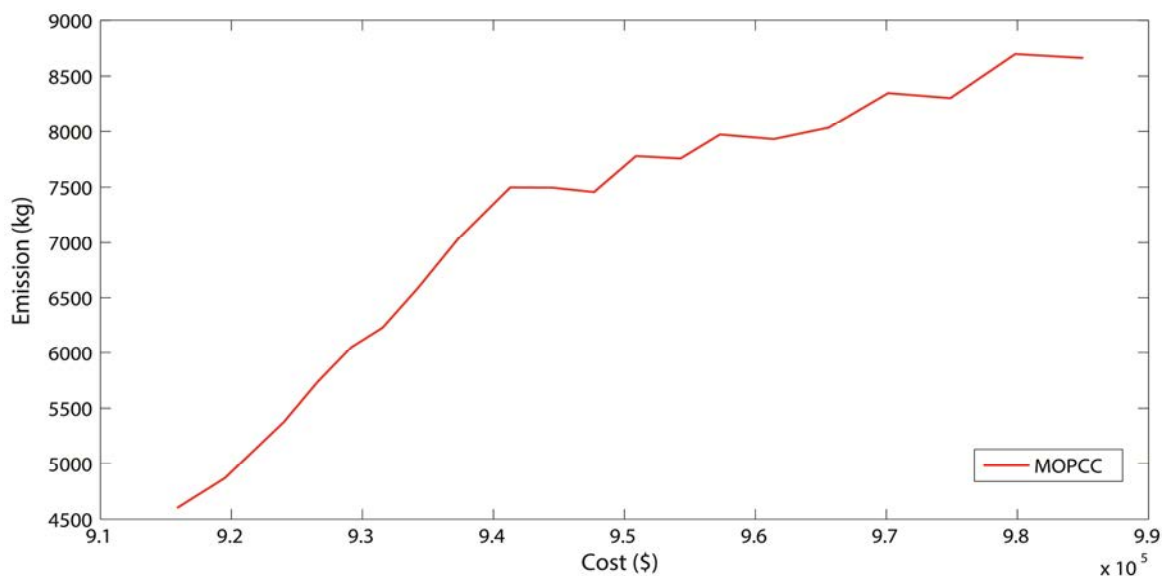
Source: The author

Figure 19- The compromise trajectory of the UNBP for various weighting factors
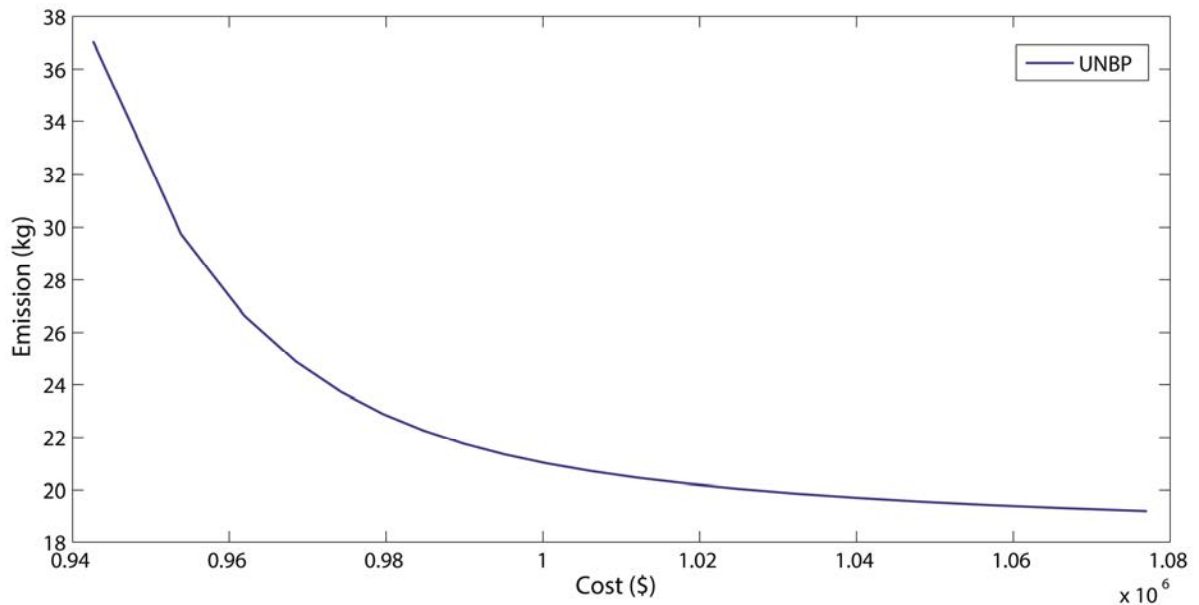
Source: The author

In Figure 18 and Figure 19, the compromise trajectories of the MOPCC and UNBP methods have been depicted, respectively. According to Figure 18, it is clear that the MOPCC cannot find an acceptable compromise point where by increasing the cost, the total emission has increased as well. As mentioned earlier, in this system, the maximum amount of emission corresponds to $1,011,870 and by moving toward this cost, the total emission may face an increase if the compromise strategy is an inappropriate one and as a result, it might be fallen into a trap. Moreover, this figure presents that the maximum increase of cost via the MOPCC cannot even reach $1,011,870. On the other hand, based on Figure 19, the UNBP shows an extraordinary role in finding a compromise point where at the first step ($k = \dfrac{0.05}{0.95} \simeq 0.053$), increasing the fuel cost by about 3.2% yields an emission reduction by about 99.2% within 9.26 (s) execution time. It is worth mentioning that for the MOPCC, this high increase in cost yields 64.97% increase in emissions within 47.60 (s). The emission increase associated with the cost increase is a major drawback of the MOPCC.

Figure 20 presents the pollution control cost of the MOPCC and UNBP for all generators at hour 3. It should be expressed that this control cost plays an important role in finding a compromise point.

Figure 20- The pollution control cost of the MOPCC and UNBP (APCC) for all generators at hour 3
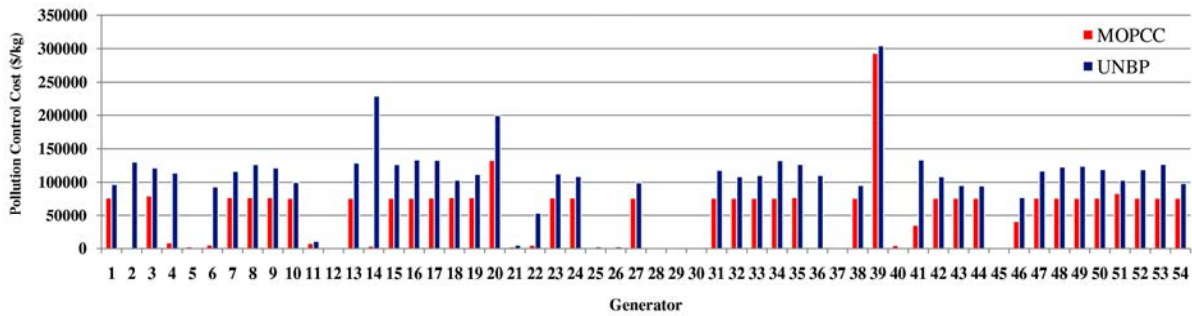
Source: The author

As stated before, generation units usually do not work at their maximum power output limit and using the MOPCC may yield an inappropriate compromise. As it is clear in Figure 20, for several generators such as 4, 6, 14, 22, and 36, the control cost difference between two methods is remarkable. The values of the APCC for the UNBP, for each generator present the cost ratio in the second scenario over the produced emission in the first scenario. For example, for generator 14, which is related to bus 31, the cost of the second scenario is $13,177.2 (corresponding to 0.06177 kg emission) and the produced emission in the first scenario is 0.0574335 kg (corresponding to $234.84). Therefore, by using (87), the APCC is 229,434.04 $/kg. By comparing the APCC with the MOPCC, which is 3,689.79 for this unit, it is revealed that the UNBP considers the reduction in the emissions of this unit more than the MOPCC method. The results of the compromise scenario prove our claim about the effectiveness of the APCC, which is a topology-based factor, and in particular, its superiority in finding a proper compromise point for large-scale systems, is evident.

6.1.3.2 With ramp rate, emissions and power flow limits

The amount of power that can be transmitted over a transmission line is limited by several constraints, including thermal limits, voltage limits, and the line capacity, and also because of security concerns. This becomes even more important when with increasing the loads, the system gets more stressed (LI; VENKATASUBRAMANIAN, 2004). In this case, the power flows over lines (4, 5) and (64, 65) are limited to 55 MW per hour and 150 MW per hour, respectively. The EMA for the critical region is 300 kg/h, EMS is 6,500 kg/h, $\overline{NO_X}$ is 40 kg/h, and $\overline{SO_X}$ is 1,650 kg/h. Also in this case, the ramp rate limits are taken into account.

Table 9 shows the best solution of the first and second scenarios of the IEEE 118-bus system, where the emission, power flow, and ramp rate limits have been considered.

Table 9- The best solution of the first and second scenarios, the IEEE 118-bus system with limitation

Scenario		h1	h2	h3	h4	h5	h6	Total	Time (s)
I	NO_X (kg)	6.82	7.06	7.45	7.72	7.30	6.85	43.20	7.79
	SO_X (kg)	376.15	477.24	898.72	1,200.51	761.26	371.94	4,085.82	
	EMA (kg)	47.52	66.44	133.73	197.32	108.22	48.18	601.41	
	EMS (kg)	382.97	484.30	906.18	1,208.23	768.56	378.78	4,129.02	
	Cost ($)	130,491	142,506	166,924	185,126	158,271	130,497	913,815	
II	NO_X (kg)	2.25	2.39	2.74	3.06	2.61	2.25	15.3	23.12
	SO_X (kg)	0.14	0.17	0.25	0.36	0.21	0.14	1.27	
	EMA (kg)	0.25	0.27	0.32	0.36	0.31	0.25	1.76	
	EMS (kg)	2.39	2.56	2.99	3.42	2.82	2.39	16.57	
	Cost ($)	177,491	192,507	220,677	240,351	210,777	177,258	1,219,061	

According to Table 9, for the first scenario, the total cost shows an increase of nearly $117 more than the similar case in subsection 6.1.3.1, which yields a decrease of nearly 623.6 kg in emissions. For the second scenario, the total emission increases by 0.06 kg, which corresponds with $2,291 decrease in the total cost.

Table 10- The best solution of the third scenario via the MOPCC and UNBP, the IEEE 118-bus system with limitation

Method		h1	h2	h3	h4	h5	h6	Total	Time (s)
MOPCC ($k=1$)	NO_X (kg)	5.14	5.62	6.18	6.70	6.01	5.44	35.09	77.94
	SO_X (kg)	257.21	514.02	1,030.2	1,650.00	781.79	371.37	4,604.59	
	EMA (kg)	16.36	32.57	65.58	124.00	55.10	24.73	318.34	
	EMS (kg)	262.35	519.63	1,036.38	1,656.70	787.8	376.82	4,639.68	
	Cost ($)	135,977	147,643	171,722	189,935	163,045	135,666	943,988	
UNBP ($k \simeq 0.053$)	NO_X (kg)	4.1	4.25	4.6	4.99	4.49	4.14	26.57	9.26
	SO_X (kg)	1.48	1.66	2.1	2.82	1.91	1.43	11.4	
	EMA (kg)	0.63	0.66	0.75	0.89	0.72	0.62	4.27	
	EMS (kg)	5.58	5.91	6.71	7.8	6.4	5.57	37.97	
	Cost ($)	135,148	147,213	171,610	189,485	163,032	135,175	941,663	

Table 10 shows the hourly and total cost and emission rates of the MOPCC and UNBP. Comparing the results of the compromise methods with the first scenario reveals that, for the MOPCC method, an increase in costs does not yield a decrease in emissions and a

3.3% increase in costs yields a 12.37% increase in emissions. On the other hand, with less than of this approximate increase in costs (3.1%) for the UNBP method ($k \simeq 0.053$), a 99.08% decrease in emissions is obtained. It shows that the MOPCC, even by spending more money, cannot decrease the emission and hence, the total emission is subjected with an increase. Also for the MOPCC at hour 4 (h4), the SO_X limit has been hit, while the UNBP shows a large degree of freedom.

Figure 21- The cost fluctuations for the MOPCC ($k=1$) and the UNBP ($k \simeq 0.053$) during the scheduling time horizon, the compromise scenario
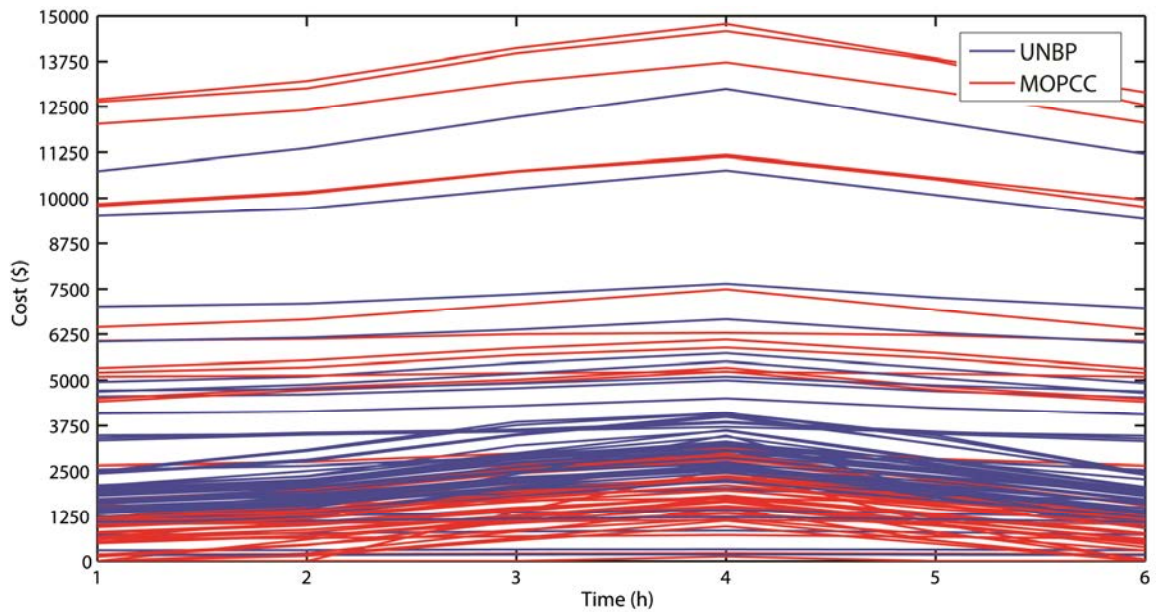
Source: The author

Figure 22- The emission fluctuations for the MOPCC ($k=1$) and the UNBP ($k \simeq 0.053$) during the scheduling time horizon, the compromise scenario
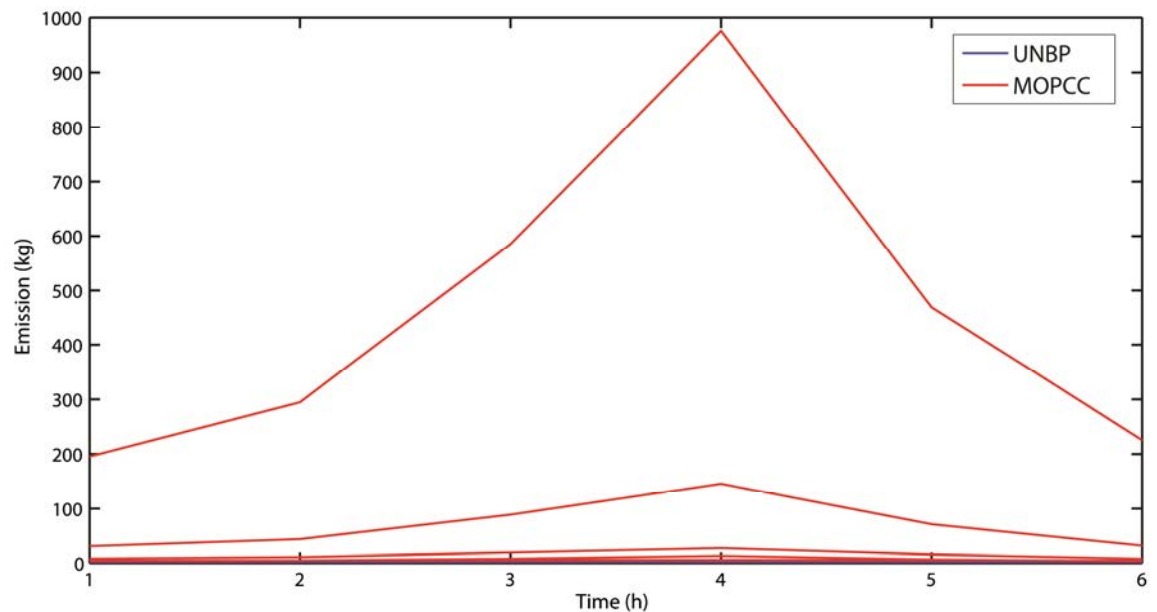
Source: The author

Figure 21 and Figure 22 exhibit the cost and emission fluctuations of all 54 generators of the IEEE 118-bus system for both the MOPCC and UNBP methods during the scheduling time horizon. In both figures, the highest values are related to the MOPCC. Figure 22 displays a big gap for the compromise values of the MOPCC, while via the UNBP, there is not any similar big gap between the lowest and highest compromise results. These figures verify the smooth manner of the UNBP approach, when it comes to finding the compromise point and is mostly the result of a normalization technique.

As a conclusion of this test system, it is completely clear that in both case studies, the UNBP obtained extraordinary results while the MOPCC cannot find an acceptable compromise point. This therefore confirms that unlike the MOPCC, which sometimes falls into a trap, the UNBP that is an adaptive method can easily escape from such traps and find acceptable compromise points.

6.1.4   Conclusion

The economic and emission compromise is and will be an important issue in power systems operation in the future. This work has proposed a straightforward compromise methodology to obtain a more effective and adaptive solution for an economic and emission AROPF problem based on an unequivocal normalization-based paradigm (UNBP). As the UNBP is a topology-based compromise methodology, the compromise parameters will be updated based on a condition that the system is faced with and consequently, a smoother compromise solution is resulted. On the other hand, the normalization procedure is a distance-based paradigm, which considers the distance of each objective from its best obtained solution and this may help the UNBP escape from a bad compromise point trap. This method has been tested on three IEEE test systems. The results of the IEEE 14-bus verifies the UNBP and shows its versatility in encountering different conditions. From the results of the IEEE 30-bus, the superiority of the UNBP method over the heuristic-based approaches used in the literature, has been demonstrated. The results of the IEEE 118-bus, as a large-scale power system, shows the effectiveness, superiority, and rapidity of the UNBP in finding a compromise point where the MOPCC fails to find an acceptable compromise.

6.2 MULTI-AREA ENVIRONMENTALLY CONSTRAINED OPF

For didactic purposes, the proposed approach has been studied in detail via a two-area test system presented in Figure 23. The other case study is a 3-area system containing the IEEE 14-bus, 30-bus, and 118-bus test systems. The values in p.u. are on 100-MVA basis, and for all test systems, the power factor is 0.9.

It should be stated that in this work, the objective of all areas is to minimize the operating costs.

Figure 23- A sample two-area power system
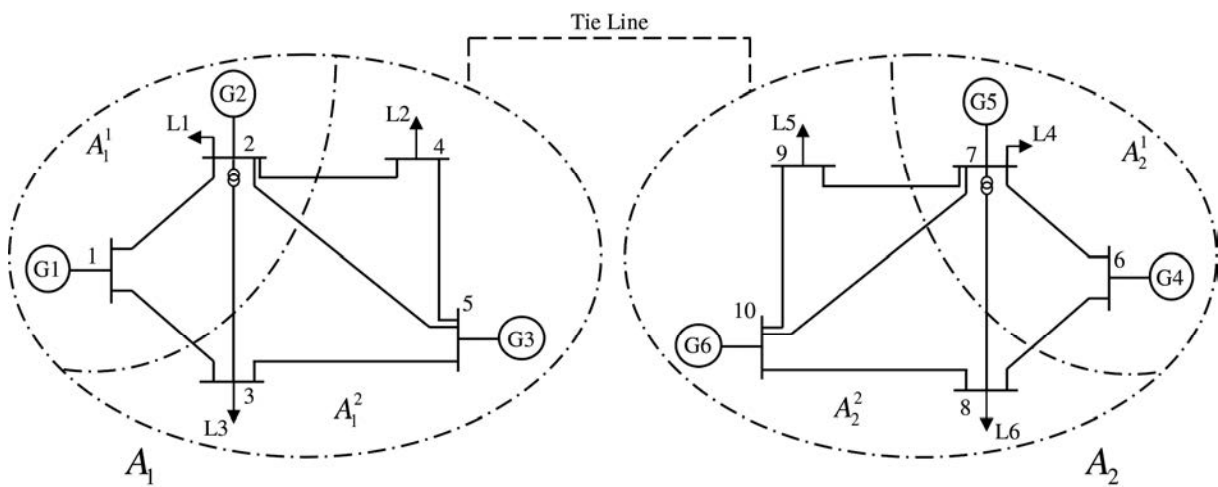
Source: The author

6.2.1 The two-area test system

The first test system has been portrayed in Figure 23, which contains two 5-bus systems connected via a tie line. The generators data, active and reactive demands, and the data of branches are available in Table 11, Table 12, and Table 13, respectively. Voltages are allowed to vary within the range of 0.95 p.u. and 1.05 p.u. Although the diagram of this system is symmetric, in order to show the effectiveness and role of the multi-area systems, the demands are not symmetric in such a way that the total demand of the second area is less than the first area.

Table 11- The generators data for the two-area system

Bus	A ($/MW^2)	b ($/MW)	c ($)	α (kg/MW^2)	β (kg/MW)	γ (kg)	Sg (p.u.)	Xs (p.u.)	Qg^{min} (MVAr)	Qg^{max} (MVAr)
1,6	0.01	40	3	0.009	-0.40	25.9	1.0	1.0	-5.0	15.0
2,7	0.08	40	3	0.007	-0.30	28.9	1.0	1.0	-13.0	50.0
5,10	0.05	20	5	0.007	-0.51	28.1	3.2	0.955	-40.0	140.0

Table 12- The demand of the two-area system

Bus	Bus type	P_d (MW)	Q_d (MVar)	Bus	Bus type	P_d (MW)	Q_d (MVar)
1	3	0	0	6	3	0	0
2	2	65.0	24.0	7	2	52.0	22.0
3	1	165.0	11.0	8	1	39.0	10.0
4	1	90.0	24.0	9	1	70.0	23.0
5	2	0	0	10	2	0	0

Table 13- The branch data for the two-area system

Line	From	to	r (p.u)	x (p.u)	c (p.u)	tp
1	1	2	0.03030	0.09990	0.02540	1.000
2	1	3	0.01290	0.04240	0.01082	1.000
3	2	3	0.00176	0.00798	0.00210	0.978
4	2	4	0.00595	0.01960	0.00502	1.000
5	2	5	0.02030	0.06820	0.01738	1.000
6	3	5	0.01290	0.04240	0.01082	1.000
7	4	5	0.00176	0.00798	0.00210	1.000
8	6	7	0.03030	0.09990	0.02540	1.000
9	6	8	0.01290	0.04240	0.01082	1.000
10	7	8	0.00176	0.00798	0.00210	0.978
11	7	9	0.00595	0.01960	0.00502	1.000
12	7	10	0.02030	0.06820	0.01738	1.000
13	8	10	0.01290	0.04240	0.01082	1.000
14	9	10	0.00176	0.00798	0.00210	1.000
Tie line	--	--	0.00176	0.00798	0.00210	1.000

Three cases are taken into consideration including the normal condition, system with emission limits, system with emission limits and power flow limits.

6.2.1.1 Case 1: Normal condition

In this case, in order to consider this two-area system under normal operating condition, no extra limitation such as emission limits or transmission line flow limits is considered.

6.2.1.2 Case 2: With emission limits (area, sub-area, and system emission limits)

For the first area, the emission limit is 285 kg/h, where the emission limit for the first and second sub-areas are 190 kg/h and 100 kg/h, respectively. For the second area, the emission limit is 255 kg/h, whereas the emission limit for the first and second sub-areas are 90 kg/h and 170 kg/h, respectively.

6.2.1.3 Case 3: With emission limits and line flow limit

For this case, not only the emission limits of the second case is taken into account, but also the tie line and transmission line limits have been taken into consideration. The power

flow limit over transmission lines (1, 2) and (7, 9) are 29 MW per hour and 30 MW per hour, respectively.

6.2.1.3.1 Before the multi-area consideration

In order to show the effectiveness of the proposed approach, at first the aforementioned three cases are analyzed as single areas and afterwards, the multi-area consideration is taken into account.

Table 14- The optimal variables of two single areas

Case No. and output variables		Bus 1	Bus 2	Bus 3	Bus 4	Bus 5	Bus 6	Bus 7	Bus 8	Bus 9	Bus 10	Time (s)
Case 1	δ	0.00	-1.25	-1.44	-0.77	-0.22	0.00	0.01	-0.01	0.37	0.80	0.020
	v	1.05	1.031	1.049	1.037	1.043	1.044	1.031	1.05	1.036	1.041	
	P_g	88.26	14.59	0.00	0.00	219.02	0.00	0.00	0.00	0.00	161.76	
	Q_g	-4.53	39.94	0.00	0.00	22.36	-2.69	33.30	0.00	0.00	19.27	
	P_g^M	99.90	91.68	0.00	0.00	319.22	99.96	94.29	0.00	0.00	319.42	
Case 2	δ	0.00	-1.36	-1.63	-1.39	-1.04	0.00	0.01	-0.01	0.37	0.80	0.040
	v	1.050	1.028	1.046	1.033	1.038	1.044	1.031	1.05	1.036	1.041	
	P_g	**100.00**	**96.91**	0.00	0.00	124.50	0.00	0.00	0.00	0.00	161.76	
	Q_g	0.16	24.66	0.00	0.00	31.26	-2.69	33.30	0.00	0.00	19.27	
	P_g^M	**100.00**	**96.91**	0.00	0.00	318.47	99.96	94.29	0.00	0.00	319.42	
Case 3	δ	0.00	-1.56	-1.89	-1.61	-1.20	0.00	-0.24	-0.25	0.07	0.52	0.020
	v	0.971	0.950	0.966	0.955	0.960	0.962	0.950	0.967	0.955	0.960	
	P_g	99.27	**97.79**	0.00	0.00	124.50	12.19	6.24	0.00	0.00	143.24	
	Q_g	1.98	20.91	0.00	0.00	34.86	-5.00	30.01	0.00	0.00	25.76	
	P_g^M	99.98	**97.79**	0.00	0.00	318.10	99.88	95.39	0.00	0.00	318.96	

Table 14 shows the optimal values of the system variables for the three aforementioned cases, when they are not connected. The boldface numbers show the generators output limit imposed by the capability curve. It is worth mentioning that, the degree of freedom in the power system operation is an important issue to schedule the units and to have an economic operation of the power system and an environmentally friendly scheduling.

Figure 24, Figure 25, and Figure 26 demonstrate a schematic of power flows of the two-area systems, prior to multi-area considerations for cases 1, 2, and 3, respectively.

Figure 24- Active and reactive power flow of case 1 before multi-area consideration

Active Power Flow (MW)   Reactive Power Flow (MVar)

Source: The author
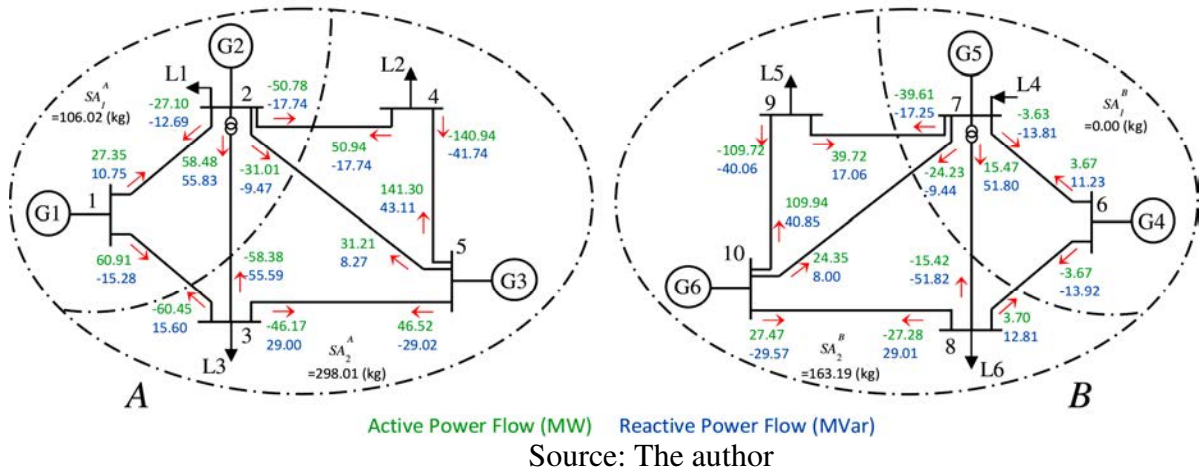
Figure 25- Active and reactive power flow of case 2 before multi-area consideration

Active Power Flow (MW)   Reactive Power Flow (MVar)

Source: The author
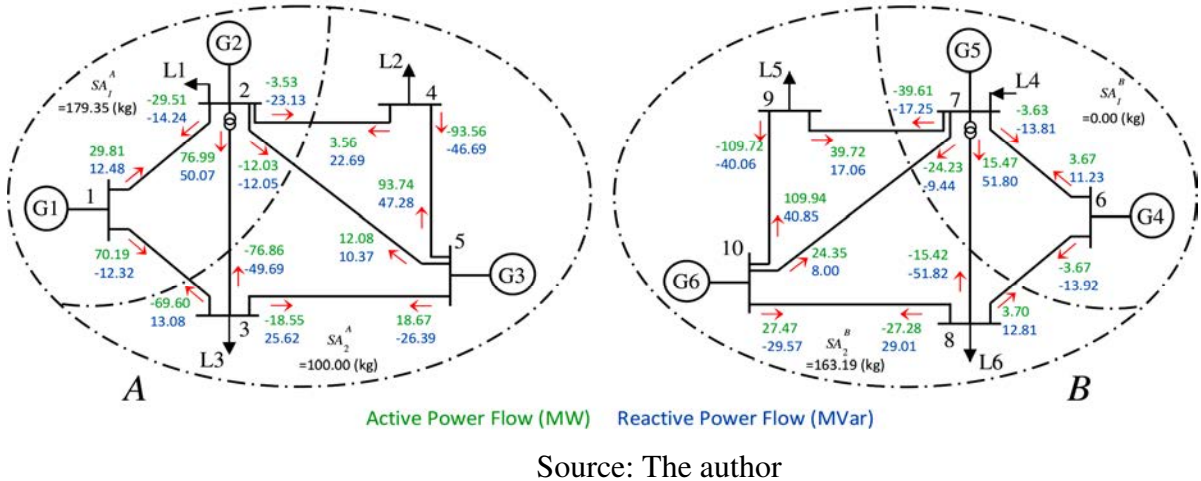
Figure 26- Active and reactive power flow of case 3 before multi-area consideration

Active Power Flow (MW)   Reactive Power Flow (MVar)

Source: The author
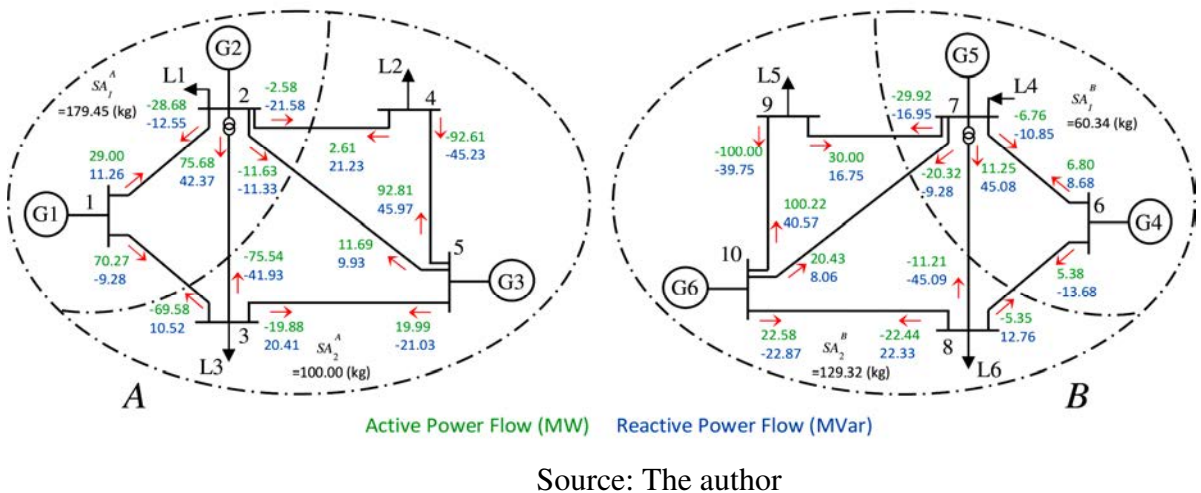
Figure 24 demonstrates that in normal condition no limit has been hit. As clear from Figure 25, which has an emission limit, in sub-area 2 of area *A*, the limitation has been reached but area 2 is working normally and its first sub-area emission is equal to zero, as

generators 4 and 5 are offline in this condition. In Figure 26, transmission lines (1,2) and (7,9) are transmitting their maximum active power flows, which yields an increase in the total amount of emissions of area *A* and *B*, whereas in comparison with Figure 25, the amount of emission in the first sub-area of area *A* has increased and in the second sub-area of area *A* is fixed, because it has reached its limit. In addition, the amount of emission in the first sub-area of area *B* has decreased, but in the second sub-area of area *B*, there is a great increase in emissions.

Figure 27- The voltage profile for three case studies of the two-area test system before multi-area consideration
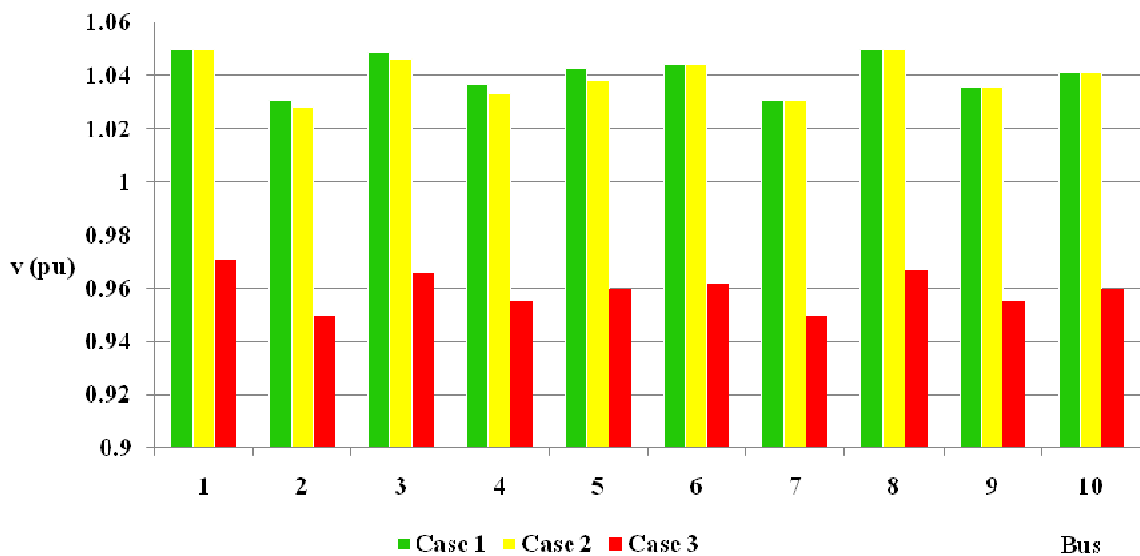
Source: The author

As obvious from Figure 27, among these three cases, case 1 has the best voltage profile and case 3 has the worst voltage profile, where the best voltage in this case corresponds to the first bus (with 0.971 (p.u)) and also all of the voltages are close to the lower bound.

6.2.1.3.2 After multi-area consideration

In this sub-section and for didactic purposes, two multi-area systems are considered where the differences between these two systems are the tie lines connections between these areas.

6.2.1.4 The first test of the two-area power system

In this system, tie line of (3-9) is taken into consideration. In the first and second cases the tie line limit is not taken into consideration and for the third case the power flow limit

over these tie lines suppose to be 60 MW/h. The results for these cases are presented in Table 15.

By comparing with Table 14, the results of Table 15 show a degree of freedom in the output active power. In other words, in Table 14, the results of case 2 show an imposed limitation on active power output by the capability curve where generation in bus 1 and 2 have been limited to 100 MW and 96.91 MW, respectively, but after considering tie line (3-9), for all three cases, there is no imposed limitation on power output by the capability curve.

Table 15- The optimal variables of the two-area system, tie line (3-9)

Case No. and output variables		Bus 1	Bus 2	Bus 3	Bus 4	Bus 5	Bus 6	Bus 7	Bus 8	Bus 9	Bus 10	Time (s)
Case 1	δ	0.00	-0.56	-0.63	-0.11	0.44	0.00	-0.41	-0.37	-0.31	0.34	0.021
	v	1.0310	1.0161	1.0341	1.0220	1.0276	1.0474	1.0306	1.0500	1.0350	1.0405	
	P_g	36.81	5.48	0.00	0.00	204.76	25.69	4.97	0.00	0.00	205.48	
	Q_g	-5.00	43.01	0.00	0.00	22.46	1.55	29.66	0.00	0.00	14.83	
	P_g^M	99.87	90.28	0.00	0.00	319.21	99.99	95.50	0.00	0.00	319.66	
Case 2	δ	0.00	-1.61	-1.59	-1.56	-1.16	0.00	-1.08	-1.00	-1.23	-0.65	0.023
	v	1.0311	1.0108	1.0293	1.0144	1.0193	1.0500	1.0287	1.0483	1.0309	1.0363	
	P_g	97.78	15.23	0.00	0.00	124.50	67.67	13.06	0.00	0.00	165.24	
	Q_g	-5.00	39.87	0.00	0.00	19.97	4.63	33.38	0.00	0.00	14.39	
	P_g^M	99.87	91.71	0.00	0.00	319.38	99.89	94.26	0.00	0.00	319.68	
Case 3	δ	0.00	-1.28	-1.34	-1.27	-0.90	0.00	-0.95	-0.87	-1.04	-0.49	0.021
	v	1.0495	1.0257	1.0422	1.0305	1.0358	1.0479	1.0300	1.0500	1.0396	1.0438	
	P_g	89.31	47.49	0.00	0.00	124.50	56.52	0.22	0.00	0.00	165.24	
	Q_g	15.00	50.00	0.00	0.00	38.01	-5.00	-13.00	0.00	0.00	21.30	
	P_g^M	98.87	78.43	0.00	0.00	317.73	99.87	99.15	0.00	0.00	319.29	

Figure 28, Figure 29, and Figure 30 demonstrate the schematic of active and reactive power flow for the two-area power system with considering tie line (3-9).

Figure 28- Active and reactive power flow of case 1, multi-area with tie line (3-9)
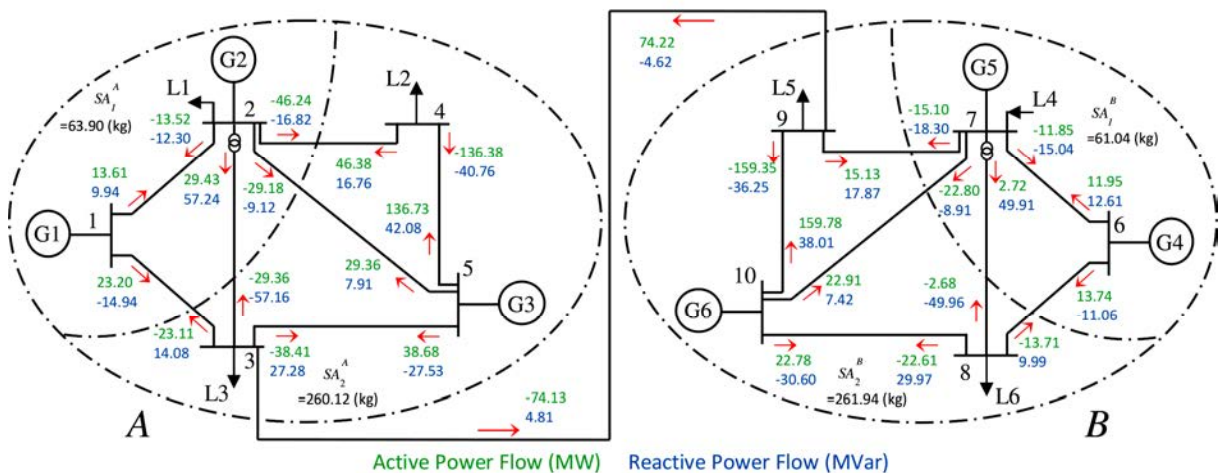
Source: The author

Figure 29- Active and reactive power flow of case 2, multi-area with tie line (3-9)
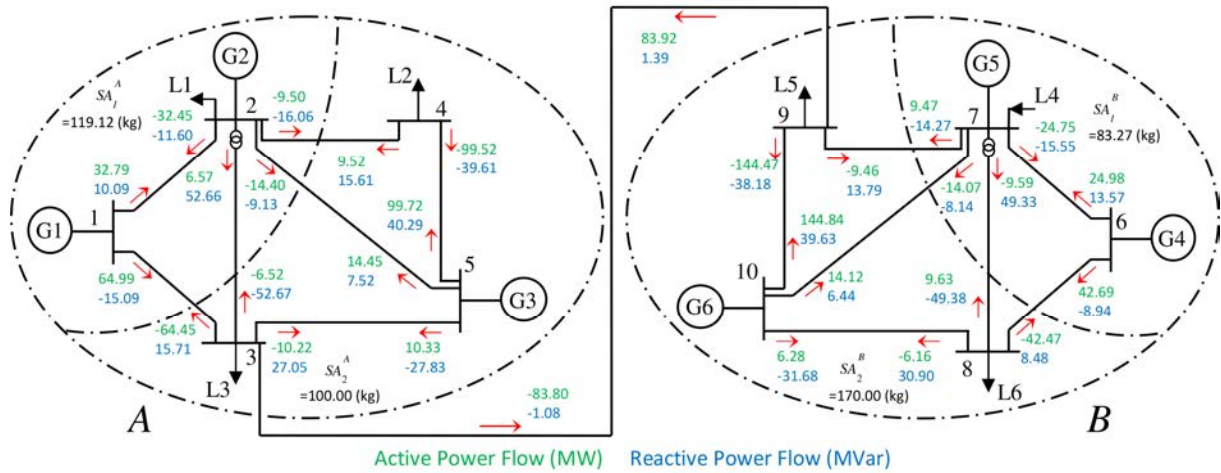
Source: The author

Figure 30- Active and reactive power flow of case 2, multi-area with tie line (3-9)
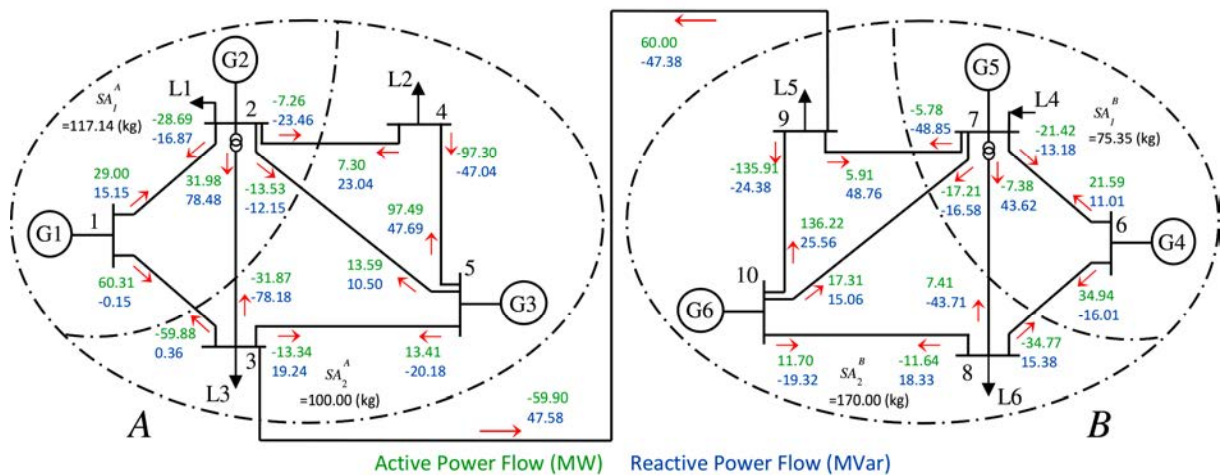
Source: The author

In order to validate the proposed approach, case 1 in Table 15 is taken into account. The results are compared with those obtained by the dummy bus method, which is a commonly used method. Since in the dummy bus method, the stopping criteria are defined based on the frontier information, it is highly dependent on the precision. In this study, as shown in Table 16, two precisions have been considered.

Table 16 contains the results of the two-area test system, in which instead of using the integrated proposed approach, a dummy between the areas, has been supposed. The results are related to case 1, while the tie line 3-9 is taken into consideration. It is worth mentioning that precision of the proposed approach is 10^{-11}.

Table 16- The optimal variables of both areas using a dummy bus information exchange with two different precisions, the two-area system, the first set of tie lines

	Optimal variables	10^{-2} Precision					10^{-4} Precision				
		Bus 1	Bus 2	Bus 3	Bus 4	Bus 5	Bus 1	Bus 2	Bus 3	Bus 4	Bus 5
First Area A_1	δ	0.00	-0.56	-0.63	-0.11	0.45	0.00	-0.56	-0.63	-0.11	0.44
	V	1.0261	1.0112	1.0291	1.0172	1.0227	1.0310	1.0161	1.0341	1.0221	1.0277
	P_g	36.86	5.48	0.00	0.00	204.72	36.82	5.48	0.00	0.00	204.76
	Q_g	-4.88	42.95	0.00	0.00	22.51	-4.99	43.00	0.00	0.00	22.46
	P_g^M	99.88	90.31	0.00	0.00	319.21	99.88	90.28	0.00	0.00	319.21
Second Area A_2	Optimal variables	Bus 6	Bus 7	Bus 8	Bus 9	Bus 10	Bus 6	Bus 7	Bus 8	Bus 9	Bus 10
	δ	0.00	-0.41	-0.38	-0.31	0.34	0.00	-0.41	-0.37	-0.31	0.34
	V	1.0436	1.0268	1.0461	1.0309	1.0364	1.0474	1.0306	1.0500	1.0350	1.0406
	P_g	25.76	4.97	0.00	0.00	205.42	25.64	4.99	0.00	0.00	205.51
	Q_g	1.87	31.44	0.00	0.00	12.80	1.53	29.10	0.00	0.00	15.41
	P_g^M	99.98	94.93	0.00	0.00	319.74	99.99	95.67	0.00	0.00	319.63

By comparing the results of Table 15 and Table 16, the proposed methodology was validated since it is more precise and does not need to pass the frontier information via an iterative approach. In addition, Table 16 shows that the results can be closer to the proposed methodology if more precision is considered.

Table 17- Comparison of the cost and emission of the proposed methodology and the dummy bus method

Bus No.	10^{-2} Precision		10^{-4} Precision		Proposed Methodology 10^{-11} Precision	
	Cost ($)	Emission (kg)	Cost ($)	Emission (kg)	Cost ($)	Emission (kg)
1	1490.87	32.07	1489.31	32.05	1489.11	32.05
2	224.51	31.84	224.46	31.85	224.54	31.84
3	0.00	0.00	0.00	0.00	0.00	0.00
4	0.00	0.00	0.00	0.00	0.00	0.00
5	6195.02	260.02	6196.48	260.11	6196.59	260.12
6	1040.06	29.14	1035.12	29.12	1037.04	29.13
7	203.68	31.90	204.43	31.90	203.91	31.90
8	0.00	0.00	0.00	0.00	0.00	0.00
9	0.00	0.00	0.00	0.00	0.00	0.00
10	6223.09	261.79	6226.94	262.03	6225.54	261.94
Total	15377.23	646.76	15376.74	647.06	15376.73	646.98

Table 17 compares the cost and emission of two methods in order to show that how precision may effect on the results. As it is clear, for the case with 10^{-4} precision, the results are very close and almost similar to the proposed methodology.

Figure 31- The output power (Pg) versus the capability curve limit (CCL) - Case 3
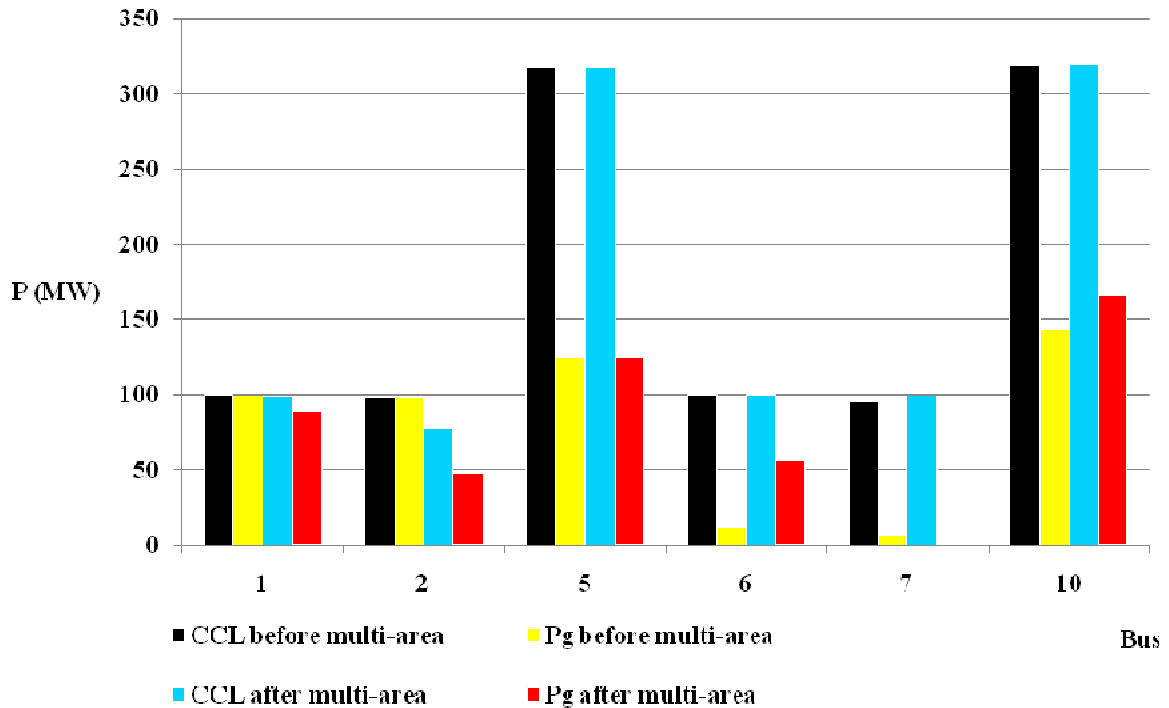
Source: The author

It is evident from Figure 31 that unlike the system before multi-area consideration, in the multi-area system, the output active powers have not been limited by the capability curve. In other words, in Figure 31, the capability curve limitations for both systems (before and after multi-area consideration) are more or less similar to each other, but the output power of the multi-area system has a degree of freedom (i.e., it does not hit the limits), which is an important issue in power systems under contingency conditions.

6.2.1.5 The second test of the two-area power system

In this system, tie line (4-10) is taken into consideration. The same as the first case, in the first and second cases, the tie line limit is not considered and for the third case, the power flow limit over these tie lines is supposed to be 60 MW per hour. The results for these cases are presented in Table 18.

For this two-area test system with tie line (4-10), the same as the first two-area test system with tie line (3-9), the results show that the degree of freedom has been increased. In case 2 and for bus 1, there is an imposed limitation on the active power generation by the capability curve but comparing the solution presented in Table 18 with the solution of the two single area in Table 14 reveals that the degree of freedom for bus 2 has been improved greatly

and thus, it can be claimed that the total degree of freedom of the system has been increased. It should be mentioned that this increment in the degree of freedom, not only does not have a bad impact on the voltage profile, but also the voltage profile is under good condition. It means that the system reliability has been increased by this multi-area model.

Table 18- The optimal variables of the two-area system considering tie line (4-10)

Optimal variables		Bus 1	Bus 2	Bus 3	Bus 4	Bus 5	Bus 6	Bus 7	Bus 8	Bus 9	Bus 10	Time (s)
Case 1	δ	0.00	-0.59	-0.85	0.20	0.63	0.00	-0.21	-0.21	0.06	0.46	0.011
	v	1.045	1.03	1.047	1.038	1.043	1.040	1.031	1.050	1.035	1.040	
	P_g	48.30	6.42	0.00	0.00	204.60	15.80	3.88	0.00	0.00	204.48	
	Q_g	-5.00	33.82	0.00	0.00	17.68	5.50	29.77	0.00	0.00	25.08	
	P_g^M	99.87	94.11	0.00	0.00	319.51	99.85	95.47	0.00	0.00	319.02	
Case 2	δ	0.00	-1.45	-1.66	-0.95	-0.70	0.00	-0.94	-0.98	-0.92	-0.63	0.017
	v	1.041	1.021	1.039	1.029	1.033	1.050	1.027	1.046	1.029	1.033	
	P_g	**99.87**	17.93	0.00	0.00	124.50	62.59	13.38	0.00	0.00	165.24	
	Q_g	-5.00	24.88	0.00	0.00	14.22	12.99	34.37	0.00	0.00	25.37	
	P_g^M	**99.87**	96.86	0.00	0.00	319.68	99.15	93.91	0.00	0.00	318.99	
Case 3	δ	0.00	-1.25	-1.49	-0.80	-0.53	0.00	-0.88	-0.84	-0.84	-0.52	0.023
	v	1.050	1.025	1.043	1.027	1.032	1.032	1.014	1.034	1.021	1.027	
	P_g	95.64	41.47	0.00	0.00	124.50	52.02	4.44	0.00	0.00	165.24	
	Q_g	15.00	48.85	0.00	0.00	11.37	-5.00	7.65	0.00	0.00	28.47	
	P_g^M	98.87	80.68	0.00	0.00	319.80	99.87	99.71	0.00	0.00	318.73	

Figure 32, Figure 33, and Figure 34 are the schematic of active and reactive power flow for the two-area system with considering tie line (4-10).

**Figure 32**- Active and reactive power flow of case 1, multi-area with tie line (4-10)
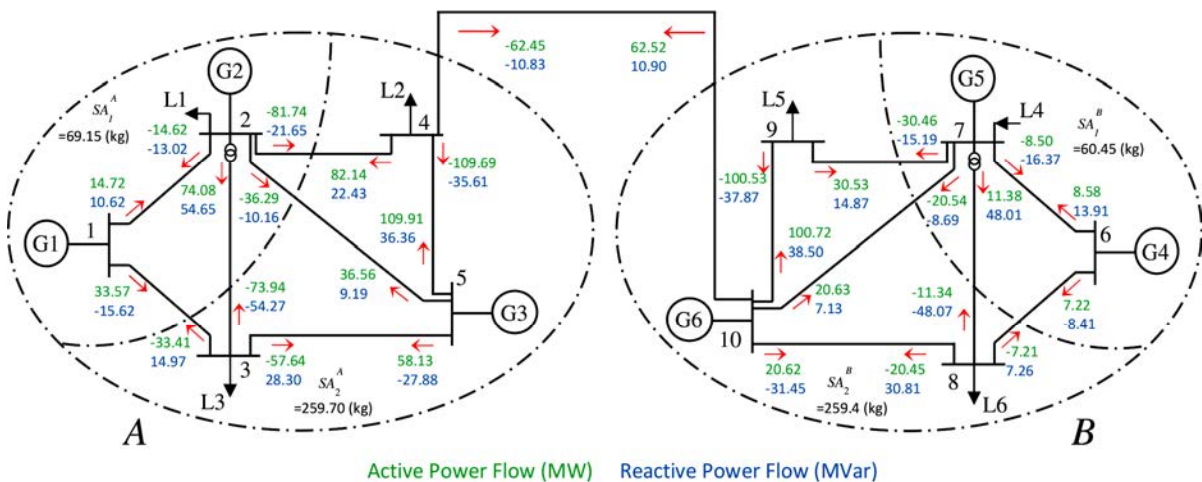
Source: The author

Figure 33- Active and reactive power flow of case 2, multi-area with tie line (4-10)

Active Power Flow (MW)   Reactive Power Flow (MVar)
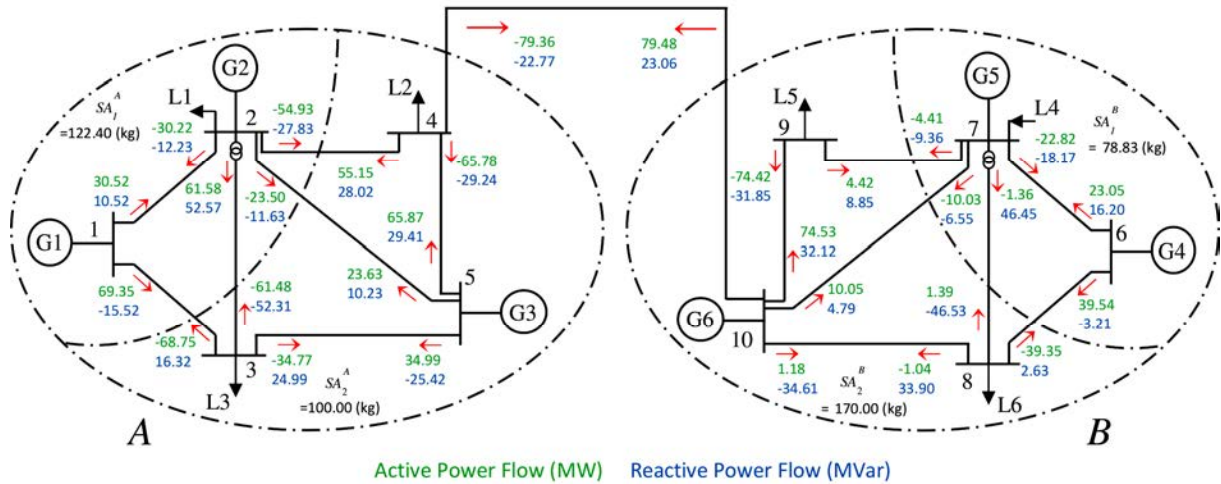
Source: The author

Figure 34- Active and reactive power flow of case 3, multi-area with tie line (4-10)

Active Power Flow (MW)   Reactive Power Flow (MVar)
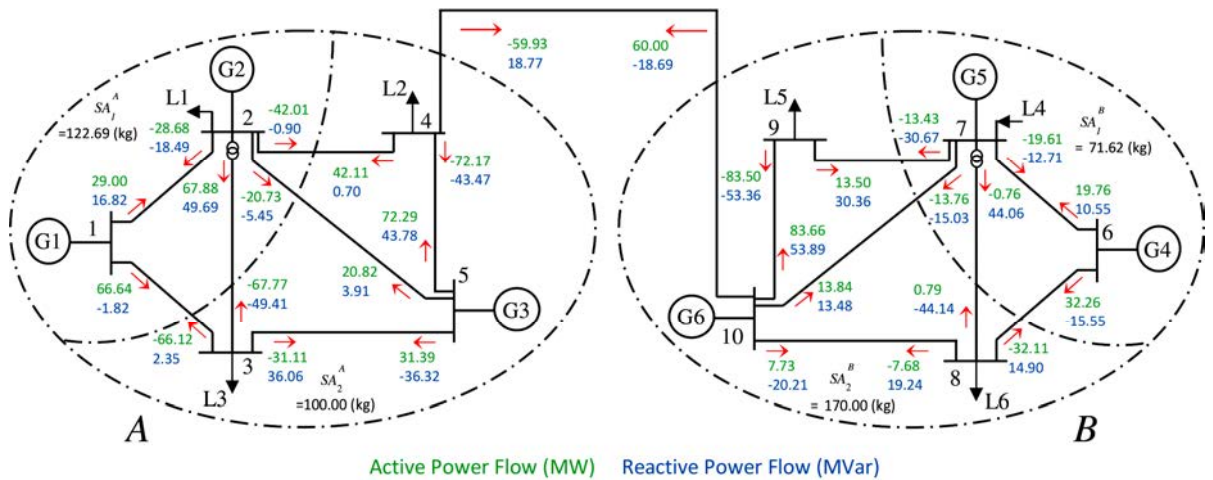
Source: The author

In the following, the cost and emission as well as the system voltage are taken into account in order to consider the effects of a multi-area system in more details.

Table 19- The system costs before multi-area consideration and via multi-area consideration (the first and second sets of tie lines), the two-area system

Case	Cost ($)		
	Before multi-area	tie lines in multi-area system	
		(3-9)	(4-10)
1	15547.52	15376.74	15393.76
2	16552.21	15879.89	15886.55
3	16665.04	15990.69	15957.08

Table 19 discloses that when several systems as multi-area systems are considered, there is a saving of between $153.76 (considering case 1 for the second test, the gray part of the table) and $707.96 (considering case 3 for the second test, the yellow part of the table).

Table 20- The system emissions before multi-area consideration and via multi-area consideration (the first and second sets of tie lines), the two-area system

Case	Area	Sub-area	Emission (kg)		
			Before tie line	multi-area system (tie lines)	
				(3-9)	(4-10)
1	1	1	106.02	63.90	69.15
		2	298.01	260.12	259.70
	2	1	0.00	61.04	60.45
		2	163.19	261.94	259.40
	1&2	1&2	567.22	647.00	648.70
2	1	1	179.35	119.12	122.40
		2	100.00	100.00	100.00
	2	1	0.00	83.27	78.83
		2	163.19	170.00	170.00
	1&2	1&2	442.54	472.39	471.23
3	1	1	179.45	117.14	122.69
		2	100.00	100.00	100.00
	2	1	60.34	75.35	71.62
		2	129.32	170.00	170.00
	1&2	1&2	469.11	462.49	464.31

Table 20 presents the emission of each area and its sub-area and also the total emission of the two-area system before and after multi-area consideration. As the emission function has an unexpected manner, there is not a common rule between the cost and emission, but usually a decrease in cost may yield an increase in emission (POURAKBARI-KASMAEI et al., 2013). The total emission by considering the first and second sets of tie lines for the two first cases has subjected an increment (for the first and second tests nearly 79.78 kg and 81.48 kg in case 1, and nearly 29.85 kg and 28.69 kg in case 2), but in case 3, after considering the multi-area system, the emission has faced a minor increase (6.62 kg and 4.80 kg for the first and second test systems, respectively), but for all cases and by considering Table 15, Table 18, and Table 19, it is clear that there is a significant decrease in costs corresponding with the increase in the degree of freedom and this slight increase in emission in these cases is negligible.

In Figure 35, Figure 36, and Figure 37, the voltage profile of the three cases is taken into consideration. Although in Figure 35, the voltage profile after multi-area consideration does not show any improvement, but this voltage profile is acceptable since all the voltages are in the upper part of the voltage limit.

Figure 35- The voltage profile of the system before multi-area consideration and via multi-area consideration, the two-area system, Case 1
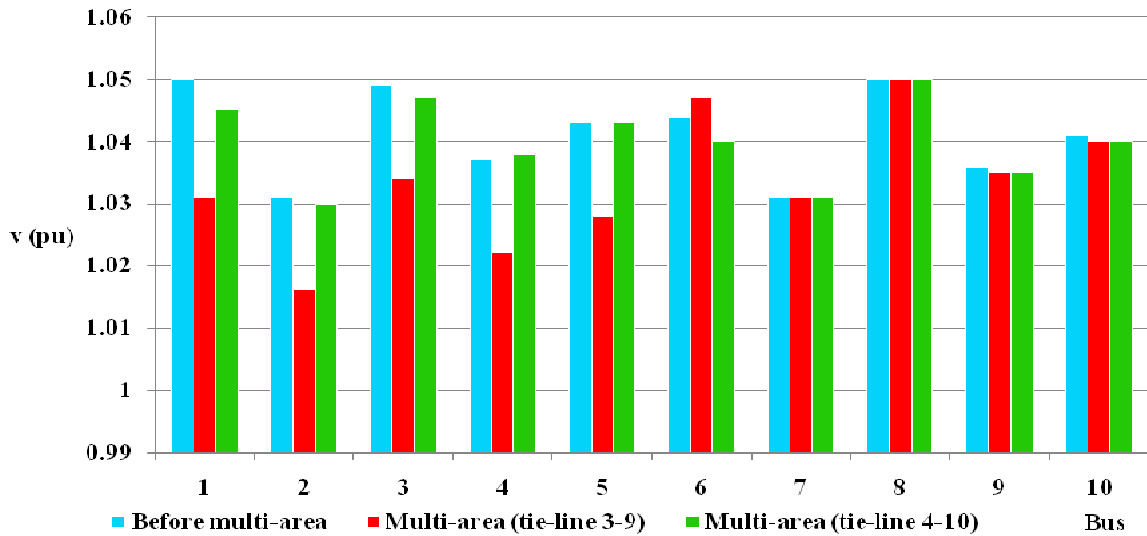
Source: The author

In Figure 36, the voltage profile relates to the second case, which is more limited by some constraints. In this figure, in some buses, there is an improvement but this improvement and also the conditions in which the system voltage is worse than the original system (i.e., before multi-area consideration), cannot show the superiority or inferiority of the multi-area system because both of the systems have good condition in their voltage profiles. In such cases, the cost, emission, and degree of freedom is taken into consideration. For the first and second cases, these considerations show the superiority of the multi-area system.

Figure 36- The voltage profile of the system before multi-area consideration and via multi-area consideration, the two-area system, Case 2
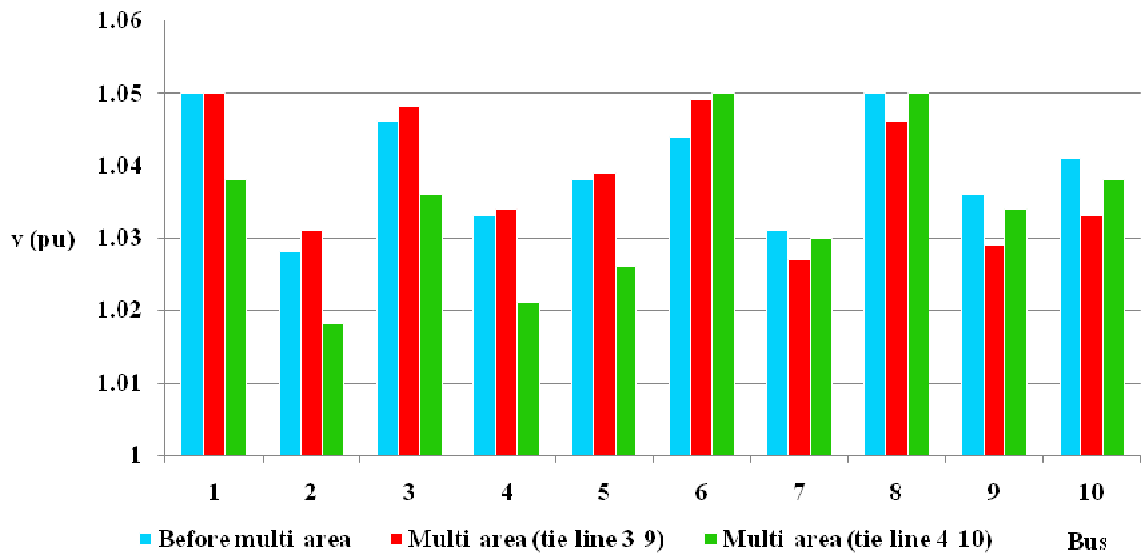
Source: The author

In Figure 37, the voltage profile of the original system for case 3 is in the critical condition where the voltages of all busses are close to the lower bound. It shows that the multi-area consideration has a dramatic effect on the voltage profile, while it shows at least 75.18% improvement (for the second test system, bus 1) and at most 91.48% improvement (for the second set of tie lines, bus 6).

Figure 37- The voltage profile of the system before multi-area consideration and via multi-area consideration, the two-area system, Case 3
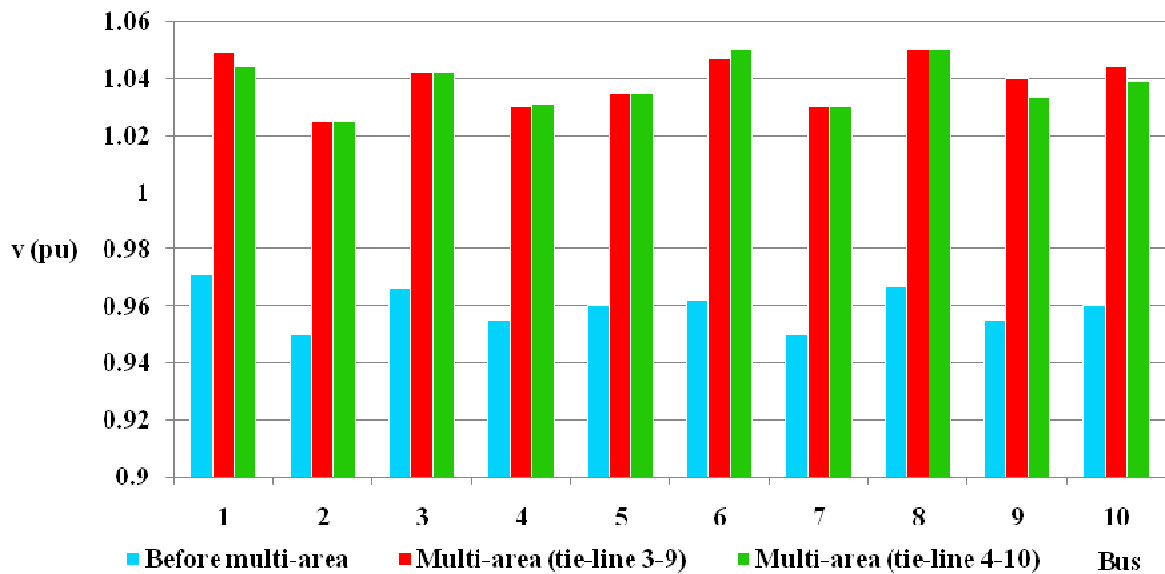
Source: The author

6.2.2 The three-area test system

This 162-bus multi-area system contains three different IEEE test systems, including 14-bus, 30-bus, and 118-bus (ONLINE). Each area has its regional emission limit, and area emission limit as exhibited in Table 21. The tie lines are as (14, 15), (41, 45), and (54, 13) and the power flow limits are 40 MW per hour, 100 MW per hour, and 50 MW per hour, respectively.

Table 21- The regional (sub-area) and area emission limits

Area	# of buses (Numbering)	Emission limit (kg/h)			
		Area	Sub-area		
			#	# of buses	Limit
1	14 (1-14)	235	1	1 and 2	200
			2	3-14	65
2	30 (15-44)	125	1	15-21 and 27	65
			2	22-26 and 28-44	65
3	118 (45-162)	5750	1	45-67, 69-76, 157-159 and 161-162	950
			2	68, 77-117, and 160	2500
			3	118-156	2500

Table 22- The cost and emission of the 3-area system, before and after tie line power flow limits

Area	Sub-area	Before multi-area consideration		After multi-area consideration			
				Before tie line flow limit		After tie line flow limit	
		Cost ($)	Emission (kg)	Cost ($)	Emission (kg)	Cost ($)	Emission (kg)
1	1	5962.98	174.22	4170.5	100.41	3965.7	92.72
	2	2134.94	60.78	1284.7	65.00	1295.1	65.00
2	1	330.514	65.00	659.8	64.75	552.6	65.00
	2	246.467	52.93	839.4	60.25	688.5	55.94
3	1	32891.8	870.37	25378.6	782.78	28570.9	854.66
	2	57261.7	2500.00	58302.8	2500.00	57944.4	2500.00
	3	41243.5	2379.63	43857.4	2467.22	42478.4	2395.34
Total		140072.0	6102.93	134493.1	6040.41	135495.6	6028.66
Time (s)		0.866		3.679		1.192	

Table 22 presents the system's regional and total emission and cost before and after the multi-area consideration. It also contains two case studies in the multi-area system such as before tie line power flow limit and after considering the tie line limits. The total cost and emission show a significant effect on reducing both cost and emission, where there is a cost reduction of about 5,578 ($) and 4,576 ($) corresponding with an emission reduction of about 62.52 (kg) and 74.27 (kg), respectively. The highlighted parts of the table show that these sub-areas have hit their limits.

6.3 APPLICATION OF MULTI-AREA ENVIRONMENTALLY-CONSTRAINED AROPF ON SHORT-TERM TIE LINE PLANNING

6.3.1 The two-area test system

The first test system, depicted in Figure 38, contains two 5-bus systems. The generators data, branch data, and demands have been listed in Table 23, Table 24, and Table 25, respectively. The voltages are allowed to vary within the range of 0.97 p.u. and 1.03 p.u., and the minimum loading power factor (LPF) is 0.8, which results in $\alpha_i = 0.75$. The area emission limit (EMA) for both areas is 2500 kg/h, where for the first and second sub-areas of the first area, the emission limits are 550 kg/h and 2000 kg/h, respectively. For the second area, the emission limits for the first and second sub-areas are 420 kg/h and 1900 kg/h, respectively. For this case, not only the emission limits of the second case are taken into account, but also the tie line and transmission line limits are taken into consideration. In this case, the maximum number of tie lines among interconnected buses ($\bar{n}_{ij}$) is 2, and the maximum tie lines between areas ($\bar{n}_{LA}$) is 5; the minimum desired voltage to be satisfied via tie line planning is 0.99; and the tie line investment cost is $1M.

Figure 38- The two-area test system
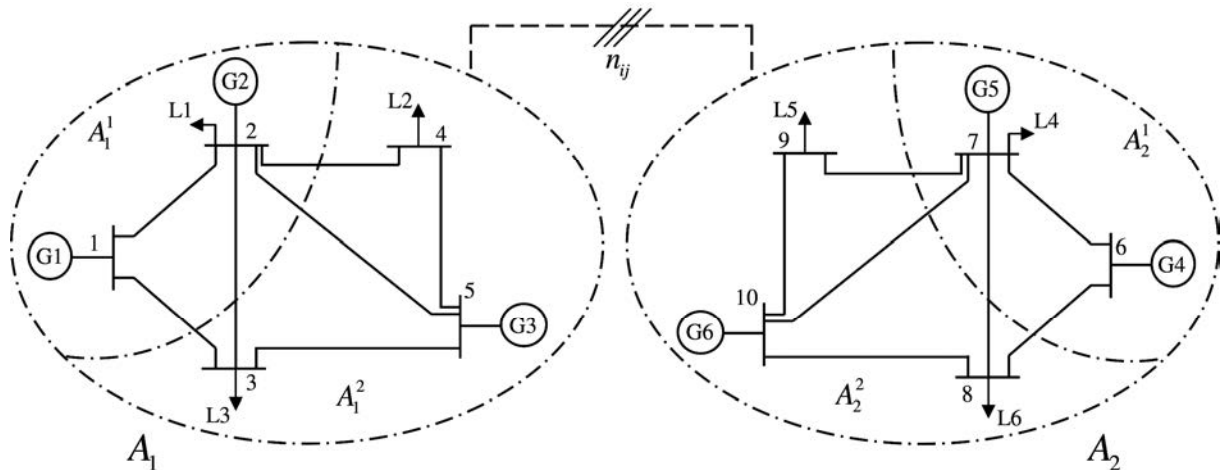
Source: The author

Table 23- The generators data for the two-area system

Bus	a ($/MW^2)	b ($/MW)	c ($)	α (Kg/MW^2)	β (Kg/MW)	γ (Kg)	Sg (p.u.)	Xs (p.u.)	Qg^{min} MVar	Qg^{max} MVar
1,6	0.12	60	6	0.027	-0.30	60.9	1.0	1.0	-5.0	15
2,7	0.19	60	6	0.026	-0.20	62.9	1.0	1.0	-13.	50
5,10	0.16	40	10	0.025	-0.31	60.1	3.2	0.955	-47	140

Table 24- The branch data for the two-area system

Line	from	To	R (p.u)	x (p.u)	c (p.u)	tp	$\overline{fl}$ (MW)
1	1	2	0.03030	0.09990	0.02540	1.000	25
2	1	3	0.01290	0.04240	0.01082	1.000	NL
3	2	3	0.00176	0.00798	0.00210	0.978	100
4	2	4	0.00595	0.01960	0.00502	1.000	NL
5	2	5	0.02030	0.06820	0.01738	1.000	NL
6	3	5	0.01290	0.04240	0.01082	1.000	NL
7	4	5	0.00176	0.00798	0.00210	1.000	180
8	6	7	0.03030	0.09990	0.02540	1.000	30
9	6	8	0.01290	0.04240	0.01082	1.000	40
10	7	8	0.00176	0.00798	0.00210	0.978	70
11	7	9	0.00595	0.01960	0.00502	1.000	70
12	7	10	0.02030	0.06820	0.01738	1.000	NL
13	8	10	0.01290	0.04240	0.01082	1.000	NL
14	9	10	0.00176	0.00798	0.00210	1.000	170
Tie line	--	--	0.00176	0.00798	0.00210	1.000	100

Table 25- The initial active and reactive demand, the two-area system

Bus	Type	P_d (MW)	Q_d (MVar)	Bus	Type	P_d (MW)	Q_d (MVar)
1	3	0	0	6	3	0	0
2	2	60.0	24.0	7	2	52.0	22.0
3	1	70.0	11.0	8	1	42.0	10.0
4	1	75.0	24.0	9	1	70	23
5	2	0	0	10	2	0	0
total	---	205.0	59.0	total	---	164.0	55.0

6.3.1.1 Determining the weak and strong buses

For determining the weak and strong buses, subsection 5.2.4, and for the economic operation of a system at the ILP and MLP, subsections 5.2.1 and 5.2.3, is taken into consideration, respectively.

Figure 39- The economic operation of the two-area test system before tie line planning, both areas at the ILP
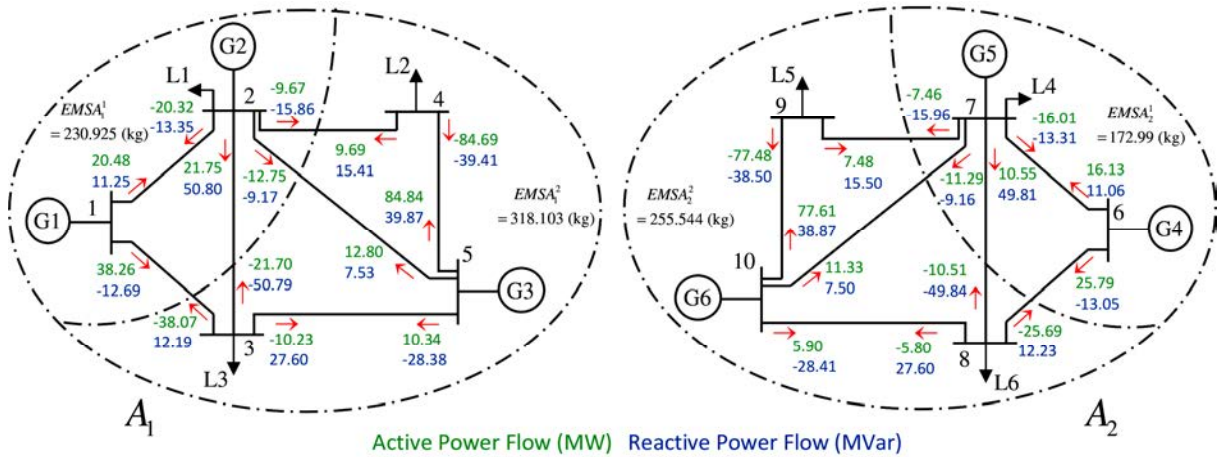
Source: The author

Figure 39 shows the power flows of the economic operation of the two-area system, where both areas are at the ILP. From Figure 39 and the aforementioned results, it is clear that none of the power flow, the area, and the sub-area emission limits have been hit and the system is working under good condition. The execution time of this case was 0.021 s.

Table 26 contains the MLP for each load bus, as a result of problem in 5.2.2. Comparing the MLP with the ILP in Table 25 reveals that, for the first area, an increase of about 55.7% in active power and 68.4% in reactive power (inductive) is obtained while for the second area, the active and reactive (inductive) increases are about 61% and 71.8%, respectively. The execution time of the MLP problem was 0.32 s.

Figure 40 represents the power flows related to the economic operation of this system before tie line planning, where both areas are at the MLP. In this case, all the power flow limits have been hit except the limit of line 8, which results in a low degree of freedom and consequently, an unexpected increase in cost and emission occurs. By comparing Figure 39 and Figure 40, it is exposed that unlike Figure 39, in Figure 40 between the sub-areas of both areas, some of the interconnected lines have hit their limits, which may create a big gap between the emitted emissions from each sub-area. The execution time of the economic operation at the MLP was 2.61 seconds.

Table 26- Active and reactive demand at the MLP, the two-area system

Bus	Type	P_d (MW)	Q_d (MVar)	Bus	Type	P_d (MW)	Q_d (MVar)
1	3	0	0	6	3	0	0
2	2	109.67	82.25	7	2	147.65	110.74
3	1	228.92	11.0	8	1	174.03	10.0
4	1	124.35	93.27	9	1	99.26	74.44
5	2	0	0	10	2	0	0
total	---	462.94	186.55	Total	---	420.94	195.18

Figure 40- The economic operation of the two-area test system before tie line planning, both areas at the MLP
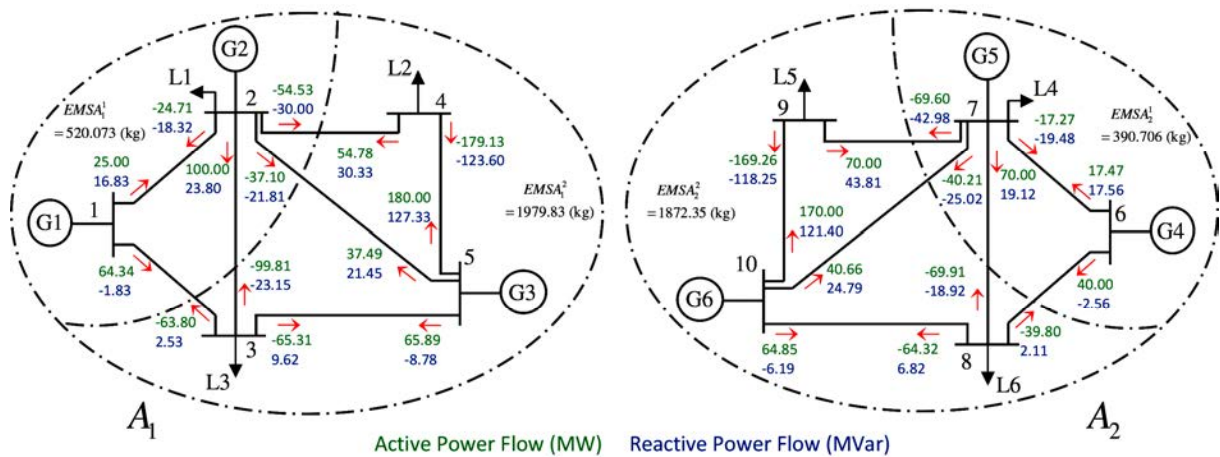
Source: The author

Table 27 shows the optimal values of the system variables, related to the EOP in which both areas are operating at the ILP, and the EOP in which both areas are operating at the MLP. The hit limits have been highlighted by boldface and underlined numbers, which are with generators output, imposed by the capability curve, and the reactive power generation.

Table 27- The optimal values of the EOP at the ILP and the EOP for the MLP before tie line planning, the two-area system

	Bus	1	2	3	4	5	6	7	8	9	10
EOP- Both Areas at ILP	δ	0.00	-0.92	-0.96	-0.86	-0.53	0.00	-0.68	-0.68	-0.65	-0.35
	v	1.0297	1.011	1.03	1.015	1.0197	1.028	1.011	1.03	1.015	1.019
	P_g	58.76	39.01	0.00	0.00	107.98	41.91	27.80	0.00	0.00	94.84
	Q_g	-1.44	36.42	0.00	0.00	19.02	-1.99	33.38	0.00	0.00	17.96
	P_g^M	99.99	93.13	0.00	0.00	319.43	99.98	94.26	0.00	0.00	319.50
EOP- Both Areas at MLP	δ	0.00	-1.16	-1.60	-0.62	0.10	0.00	-0.67	-0.96	-0.03	0.61
	v	0.996	0.970	0.988	0.979	0.993	1.016	0.992	1.012	1.005	1.017
	P_g	89.34	**93.32**	0.00	0.00	283.38	57.47	**90.57**	0.00	0.00	275.51
	Q_g	<u>15.00</u>	35.93	0.00	0.00	<u>140.00</u>	<u>15.00</u>	42.38	0.00	0.00	<u>140.00</u>
	P_g^M	98.87	**93.32**	0.00	0.00	287.57	98.87	**90.57**	0.00	0.00	287.56

The voltages obtained through solving the EOP at two operating conditions as presented in Table 27 (where for the first and second conditions, both areas are at the ILP and MLP, respectively), are used to calculate the voltage change index (VCI) (191), as shown in Table 28. The buses are ranked from the strongest to the weakest in ascending order. For this test system, 40 percent of the first and last ranked buses are selected as the strong and weak buses, respectively.

Table 28- The voltage change and rank, and the status of buses, the two-area system

Area	Bus	VC	Rank	Status	Area	Bus	VC	Rank	Status
A_1	1	3.30373	2	strong	A_2	6	1.20675	3	Null
	2	4.0984	5	weak		7	1.91587	5	weak
	3	4.05439	4	weak		8	1.79539	4	weak
	4	3.51163	3	Null		9	1.00286	2	strong
	5	2.63466	1	strong		10	0.210037	1	strong

6.3.1.2 Tie Line Planning

At this step, all the combinations of the selected buses of the first area (5, 1, 3, 2) and the second area (10, 9, 6, 7) are taken into account. The reason that we do not consider only the combination among the weak and strong buses but also, the weak and weak buses as well as the strong and strong buses, is based on this fact that the planning problem may find a tie line from the strong bus of the first area to the strong bus of the second area and make it stronger and may plan another tie line from that bus to a weak bus of the first area, and vice versa.

Figure 41- The economic operation of the two-area test system after tie line planning, both areas at the MLP
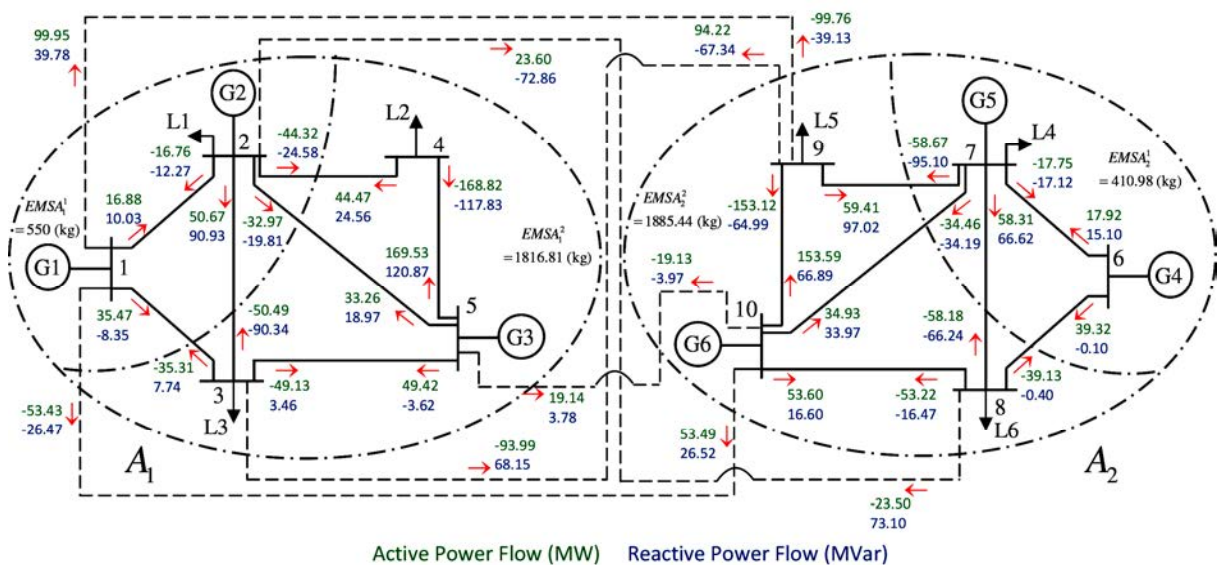
Source: The author

Figure 41 represents the power flow of the economic operation at the MLP and after tie line planning. As can be grasped from this figure, the selected tie lines for critical operation condition at the MLP are as 1-9, 1-10, 2-8, 3-9, and 5-10. Considering transmission lines power flow in this figure, it is revealed that unlike Figure 40, in which several limitations have been hit, after constructing the mentioned tie lines, no line hits its limit.

6.3.1.3 The MA-AROPF with switchable tie lines

As mentioned before, a tie line planning at the maximum loadability point, guarantees the system performance at that point, but it may have a negative effect on the other operating points. For example, if for the economic operation at the ILP, we switched on all the selected tie lines, it results in a total cost and a total emission of about \$22,642.1 and 1,007.06 kg, respectively, which would reflect an increase in both cost and emission by nearly \$72.1 and 29.5 kg, respectively, and this would confirm the necessity of using switchable tie lines.

Table 29 presents the costs and emissions of the system, each area, and sub-areas before and after tie line planning under different conditions, where the last column contains the switched-on tie lines. In the first case, both areas are operating at their ILP, while in the second case, both areas are operating at the MLP and in the third case, the first area is operating at the MLP and the second area is operating at the ILP. The power flow for this case has been presented in Figure 42.

Figure 42- The economic operation of the two-area test system after tie line planning, the first area at the MLP

Source: The author

As the cost and emission have conflicting objectives, a decrease in cost usually may yield an increase in emissions (POURAKBARI-KASMAEI et al., 2013). Table 29 reveals that the higher the load increase is, the more number of tie lines will be switched on. In addition, the results showed that, in all cases, the total costs and the corresponding amount of emissions have been decreased. I.e., in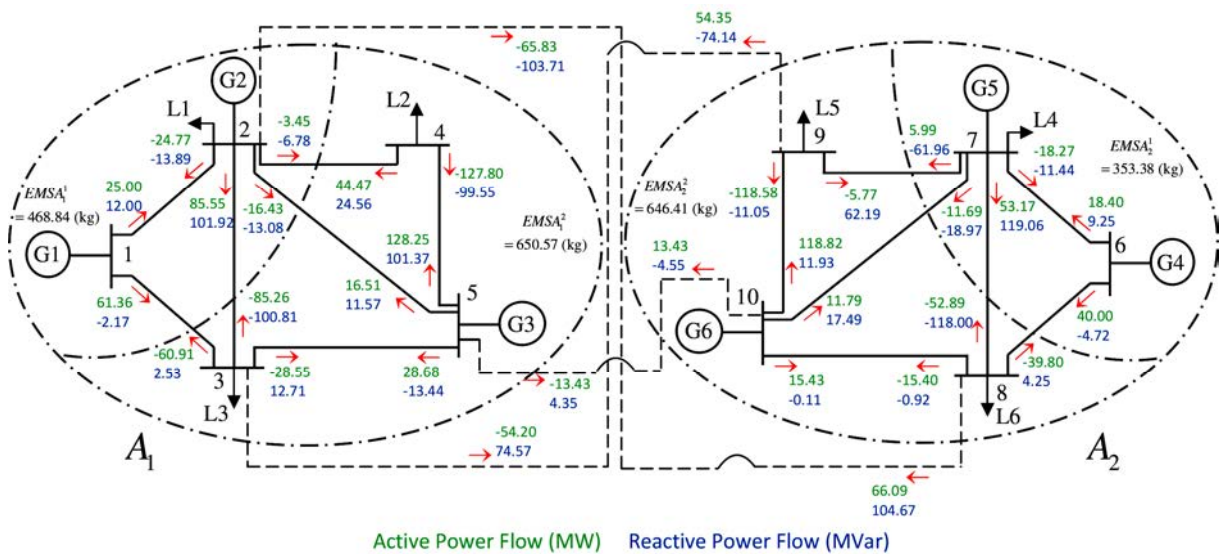 the first case, by decreasing $39.4 in costs, 5.45 kg reduction in emissions will be resulted. In the second case, a decrease of nearly $547.8 in costs results in a reduction of about 99.73 kg in emissions; Also, in the third case, the tie line planning shows a great advance, in such a way that it results in a dramatic reduction in cost and emission by about $4,019.9 and 809.23 kg, respectively.

Table 29- The costs and emissions of the system, each area, and sub-areas before and after tie line planning under different conditions

Case	Area	Sub-area	Emission (kg)		Cost ($)		Tie Lines
			Before TL	After TL	Before TL	After TL	
EOP- ILP	1	1	230.93	207.68	6580.8	5815.8	3-9
		2	318.10	289.29	6194.5	5765.4	
	2	1	172.99	189.91	4552.3	5245.7	
		2	255.54	285.23	5242.4	5703.7	
	1&2	1&2	977.56	972.11	22570	22530.6	
EOP- MLP	1	1	520.073	550.00	13584.3	14046.3	1-9
		2	1979.83	1816.81	24193.7	22645.5	1-10
	2	1	390.706	410.98	10849.4	11263.2	2-8
		2	1872.35	1885.44	23175.4	23300.0	3-9
	1&2	1&2	4762.96	4663.23	71802.8	71255.0	5-10
EOP- First Area at MLP	1	1	520.07	468.84	13584.3	12537.7	
		2	1979.83	650.57	24193.7	10506.9	2-8
	2	1	172.99	353.38	4552.3	10050.6	3-9
		2	255.54	646.41	5242.4	10457.5	5-10
	1&2	1&2	2928.43	2119.20	47572.6	43552.7	

A question that may haunt is: how this tie line planning helps to decrease both cost and emission? Having compared Figure 39-Figure 42, it is realized that via the proposed tie line planning, the switched on tie lines make a positive effect on increasing the transmission lines' degree of freedom by making a uniform cost and emission dispatch among demands. To prove this claim, a corrected standard deviation (CSD) is employed as (209).

$$\sigma = \sqrt{\frac{1}{N-1} \sum_{i=1}^{N} (x_i - \overline{x})} \qquad (209)$$

Table 30 shows the CSDs of each area and the related multi-areas for the three aforementioned cases. The results indicate that, after the presented tie line planning, the CSDs of all three cases are less than their CSDs before implementing the tie line plan, which confirms the uniform dispatch of cost and emission for all areas and the related sub-areas.

Table 30- The corrected standard deviation before and after adding a tie line

Case	Division	σ			
		Emission		Cost	
		before	after	before	after
EOP- ILP	Sub-Areas	34.7	29.8	530.6	151.2
	Areas	85.2	15.4	2107.6	446.6
EOP- MLP	Sub-Areas	491.8	458.3	3883.9	3504.7
	Areas	167.5	49.8	2653.8	1505.1
EOP- First Area at MLP	Sub-Areas	487.8	83.7	5294.5	645.8
	Areas	1464.7	84.6	19787.2	1793.6

The optimal variables for the three aforementioned cases, after switching on the appropriate tie lines, have been presented in Table 31. By comparing this table with Table 27 it can be comprehended that for the case of both areas at the MLP, after tie line planning, three generators have hit their limits, imposed by the capability curve, and it seems that this tie line planning decreases the system's degree of freedom. In order to answer this question, the new MLP for the multi-area system considering all tie lines is obtained, and the voltages drop at this operating point are taken into consideration. It is worth mentioning that for a power system with a low degree of freedom, at the MLP, a considerable voltage drop happens. At the new MLP of multi-area, the total active and reactive demand of the first area are 453.89 MW and 171.8 MVar (inductive) and of the second area are 442.23 MW and 212.12 MVar (inductive), respectively.

Table 31- The optimal variables of the two-area system, after the tie line planning

	Bus	1	2	3	4	5	6	7	8	9	10
EOP- Both Areas at ILP	δ	0.00	-0.91	-0.90	-0.89	-0.56	0.00	-0.73	-0.73	-0.81	-0.45
	v	1.015	1.000	1.0171	1.004	1.009	1.030	1.011	1.030	1.016	1.019
	P_g	53.29	34.08	0.00	0.00	102.15	46.80	32.67	0.00	0.00	101.30
	Q_g	-5.00	50.00	0.00	0.00	29.59	3.85	16.08	0.00	0.00	8.85
	P_g^M	99.87	78.86	0.00	0.00	318.63	99.93	98.70	0.00	0.00	319.88
EOP- Both Areas at MLP	δ	0.00	-0.74	-0.87	-0.34	0.28	0.00	-0.73	-0.92	-0.40	0.21
	v	1.026	1.010	1.025	1.018	1.030	1.021	0.9995	1.015	1.022	1.029
	P_g	**98.87**	**89.90**	0.00	0.00	271.35	57.25	**95.09**	0.00	0.00	276.48
	Q_g	<u>15.00</u>	43.65	0.00	0.00	<u>140.00</u>	<u>15.00</u>	30.95	0.00	0.00	<u>140.00</u>
	P_g^M	**98.87**	**89.90**	0.00	0.00	287.55	98.87	**95.09**	0.00	0.00	287.55
EOP- First Area at MLP	δ	0.00	-1.15	-1.43	-1.14	-0.67	0.00	-0.84	-0.96	-1.12	-0.61
	v	1.030	1.010	1.023	1.011	1.021	1.022	1.007	1.019	1.018	1.021
	P_g	86.36	**84.74**	0.00	0.00	160.01	58.40	**81.21**	0.00	0.00	159.47
	Q_g	9.83	46.71	0.00	0.00	103.85	4.53	48.69	0.00	0.00	24.76
	P_g^M	99.52	**84.74**	0.00	0.00	302.68	99.90	**81.21**	0.00	0.00	319.04

The voltage profile of the two-area system at different conditions, such as the economic operation at the ILP, the MLP before and after tie line planning, and at the new

MLP of the constructed multi-area, defined as the new MLP of multi-area, have been depicted in Figure 43. This figure shows a high voltage drop at the MLP before tie line planning, where three buses have a voltage less than 0.99 p.u. and in bus 2, the lower limit has been hit. After tie line planning, the voltage profile exhibited a significant enhancement where the voltages of all buses are more than 1.01 p.u., except for bus 7, which is close to 1 p.u. The other effectiveness of this tie line planning is that if the constructed multi-area reaches its maximum loadability point, the voltage fluctuation and especially its drop will be insignificant, which means that this tie line planning strategy enhances the system's degree of freedom.

Figure 43- The voltage profile of the economic operation at the ILP, the MLP before and after tie line, and at the new MLP after tie lines, the two-area test system
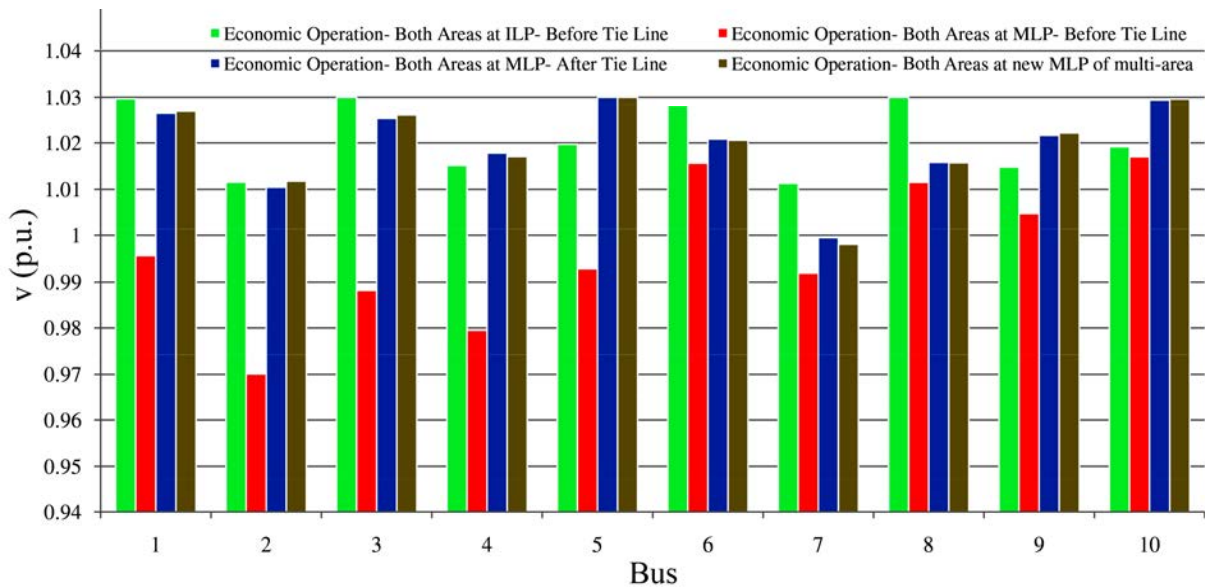
Source: The author

Considering the voltage profiles, costs, as well as emissions, it can be understood that via a uniform dispatch of cost and emission, not only the costs and emissions have been decreased, but also the stability of the system has been adjusted to a good condition. Meanwhile, the degree of freedom of the system has been enhanced.

6.3.2 The three-area test system

This 162-bus multi-area system contains three different IEEE test systems: 14-bus, 30-bus, and 118-bus (ONLINE,). Each area has its own area and sub-area emission limits that are presented in Table 32. In this case, the maximum number of tie lines among interconnected buses $(\bar{n}_{ij})$ is 2, and the maximum number of tie lines between areas $(\bar{n}_{LA})$ is 8.

Each area has its voltage limit, and the minimum desired voltage to be satisfied via tie line planning is 0.98 (p.u.), and the tie line investment cost is $1M.

Table 33 presents the ILP of three areas and the MLP of three areas before tie line planning. The results show that a total increase of about 59.21% in active power demand and a total increase of about 122.82% in reactive power demand (117.87% in inductive and 1984.36% in capacitive demand) has been obtained.

Table 32- The regional (sub-area) and area emissions limit

Area	# of buses (Numbering)	Emission limit (kg/h)			
		Area	Sub-area		
			#	# of buses	Limit
1	14 (1-14)	235	1	1 and 2	200
			2	3-14	65
2	30 (15-44)	125	1	15-21 and 27	65
			2	22-26 and 28-44	65
3	118 (45-162)	5750	1	45-67, 69-76, 157-159 and 161-162	950
			2	68, 77-117, and 160	2500
			3	118-156	2500

For this three-area system, after finding the optimal solution of the economic operation at the ILP and MLP and consequently, the weak and strong buses, the candidate buses to be considered in the tie line planning, are selected. The number of selected buses, in ascending order from the weakest to the strongest, are as follow: for the 14-bus system, three weak buses (3, 2, and 14) and three strong buses (6, 5, and 4); for the 30-bus system, five weak buses (37, 16, 33, 32, and 15) and five strong buses (35, 39, 36, 41, and 27); for the 118-bus system, ten weak buses (156, 154, 153, 152, 151, 148, 150, 149, 147, and 116) and ten strong buses (48, 161, 49, 56, 47, 51, 46, 50, 45, and 52). For the tie line planning, all the possible combinations among the aforementioned buses are taken into account. After tie line planning at the MLP, 6 tie lines such as: 2-33, 2-46, 16-156, 27-147, 39-116, and 41-150 are selected. The execution time of the EOP at the ILP and MLP are 0.624 s and 4.96 s, respectively; and for the MLP problem is 1.306 s.

Table 33- The ILP and MLP of the three area test system

Status	Area	Active (MW)	Reactive (MVar)	
			Inductive	Capacitive
All areas at ILP	1	259	77.4	3.9
	2	189.2	107.2	---
	3	4242	1438	---
	Total	4690.2	1622.6	3.9
All areas at MLP	1	451.74	137.48	81.29
	2	366.11	177.3	---
	3	6649.6	3220.38	---
	Total	7467.45	3535.16	81.29

Table 34 presents the emissions, costs, and the switched on tie lines at three different conditions such as all areas at the ILP, the first and second areas at the ILP and the third area at the MLP, and all areas at the MLP. The execution time for the aforementioned cases are 68.77 s, 21.63 s, and 471.63 s, respectively.

Table 34- The costs and emissions of the three-area system, before and after the tie line power flow limit

Case	Area	Sub-area	Emission (kg)		Cost ($)		Tie Lines
			Before TL	After TL	Before TL	After TL	
EOP- All Areas at ILP	1	1	135.93	180.93	5187.48	6079.49	2-46 16-156 27-147 39-116 41-150
		2	56.95	49.06	2988.79	4495.09	
	2	1	65.00	65.00	330.51	666.17	
		2	52.93	60.00	246.47	846.46	
	3	1	870.37	853.82	32891.8	29944	
		2	2500.00	2500.00	57261.6	56316.6	
		3	2379.63	2291.19	41243.5	35695.7	
	Total		6060.81	6000.00	140150.2	134043.51	
EOP- Areas 1 and 2 at ILP, Area 3 at MLP	1	1	135.93	34.15	5187.48	2145.7	2-46 16-156 27-147 39-116 41-150
		2	56.95	65.00	2988.79	8951.43	
	2	1	65.00	63.05	330.51	651.683	
		2	52.93	61.95	246.47	864.018	
	3	1	950.00	950.00	68361.4	53454.3	
		2	2500.00	2500.00	102636	99913.7	
		3	2300.00	2300.00	106726	83808.6	
	Total		6060.81	5974.15	286476.65	249789.43	
EOP- All Areas at MLP	1	1	138.38	148.65	5306.21	5505.43	2-33 2-46 16-156 27-147 39-116 41-150
		2	65.00	65.00	10812.3	10815.6	
	2	1	65.00	65.00	674.64	677.36	
		2	60.00	60.00	856.70	850.95	
	3	1	950.00	950.00	68361.4	61742	
		2	2500.00	2500.00	102636	102423	
		3	2300.00	2289.73	106726	105004	
	Total		6078.38	6078.38	295373.25	287018.34	

From Table 34, for the first case, the maximum emission has been restricted to 6,000 kg, which results in switching on five switchable tie lines. From this table, it can be deduced that for all cases, a considerable reduction in cost is obtained. For the first case, after switching on the appropriate tie lines, the total cost will decrease to $134,043.51, i.e., a decrease of approximately 4.36% in the total cost ($6,106.69) is attained, where on the other side, a reduction of about 60.81 kg in emission has been obtained. For the second case, in which the third area is under the critical condition of MLP, a total decrease of $36,687.22 (about 12.8%) is at hand, where this corresponds to a reduction of about 86.67 kg (about 1.4%) in emission. For this case, the same as the first case, five out of six tie lines are switched on to obtain the minimum cost. In the last case, the total emissions, before and after tie line switching, are the same, but a total decrease of $8,354.91 (about 2.83%) has been obtained by switching on all six tie lines. Figure 44 presents the voltage profiles of the three-

area system at four different operating conditions. In this figure, only the critical buses are taken into consideration. A bus will be in critical condition if the voltage drops under 0.98 (p.u). The last bar is to test the system stability at the new MLP of multi-area, where all the tie lines have been switched on. For this three-area system, the total active and reactive (inductive and capacitive) demand at the new MLP of multi-area are 7,480.51 MW and 3,622.80 MVar (3,550.19 MVar and 72.61 MVar), respectively.

Figure 44- The voltage profile of the economic operation at the ILP, the MLP before and after tie line, and at the new MLP after tie lines, the three-area test system
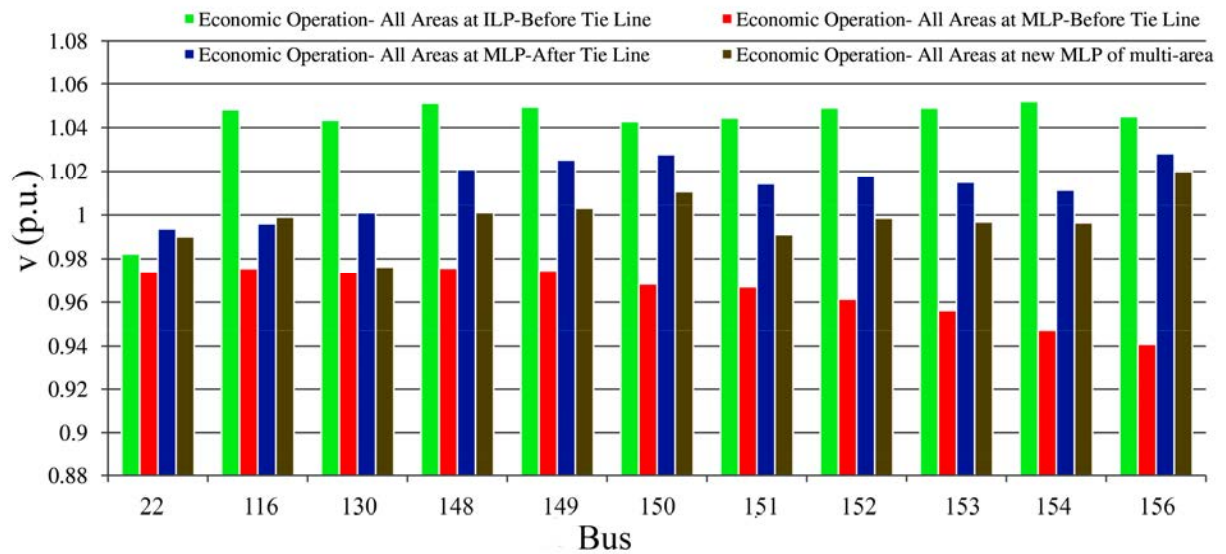
The voltage profile of Figure 44 indicates that for the three-area system, most buses with critical voltages are located in the third area and the minimum bus voltage, before switching on the appropriate tie lines, is 0.9471 (p.u.), which corresponds to bus 156 located in the third area. This bus, after switching on the tie lines, shows an increase of approximately 6.79% in its voltage. As it is clear, via this tie line planning, the voltage stability has been improved and even at the new MLP condition, there is not any considerable voltage drop.

Chapter 7

CONCLUSIONS AND FUTURE WORKS

7.1 CONCLUDING REMARKS

In this work, two novel mathematical models for two challenging problems in electric power system have been proposed.

The objective of the first problem is to find a compromise between cost and emission via active-reactive optimal power flow. In this work, in order to find an acceptable compromise, a novel unequivocal normalization-based paradigm (UNBP) for solving the dynamic economic and emission active-reactive OPF has been presented. Until now, for solving such problems, two main groups of studies such as heuristic-based models that are time consuming, and convex combination models that use the maximum output-based pollution control cost (MOPCC), which may not find an acceptable compromise, have been presented. Unlike the heuristic-based models, the proposed UNBP approach is fast, and unlike the convex combination models, it uses the adaptive pollution control cost (APCC), which is a topology-based control and this feature makes the proposed approach a real-time compromise approach. Another drawback of the compromise approaches becomes apparent when the objectives' values are not close enough, and hence, the optimization process will focus on the objective with a higher weight. The UNBP approach uses a normalization procedure and consequently, by diminishing the gap between objectives' values, a smooth compromise is obtained. The other advantage of the UNBP is its application to complicated problems such as OPF, while the other compromise approaches may not find a high-quality compromise solution even for less complicated problems such as the economic dispatch problem.

For the second problem, which is a multi-area optimal power flow, a novel integrated formulation has been proposed. In the literature and after introducing the decentralized model of power systems, most of researchers focused on solving such problems via decomposition techniques, which are useful for market-based applications, and in this area of research, many progresses have been made. These progresses are related to the precision, convergence, easy implementation, etc. Even with such advancements, the auxiliary variable, which increases the complexity, and the iterative manner of decomposition methodologies, which needs defining a stopping criterion, are some of the drawbacks of such methodologies. In this work, an integrated environmentally constrained multi-area active-reactive OPF (MA-AROPF) has been presented. As the proposed integrated formulation is not an iterative method, it is not

necessary to define a stopping criterion, which sometimes yields major problems and, on the other hand, there is no need to use auxiliary variables, because this model does not need to be decomposed. This model is easily implementable in modeling languages such as AMPL, GAMS, SAMPL, etc. and can be solved via commercial solvers. The proposed model is very fast and as the solution is achieved via a commercial solver, its precision is about E-10. With such real-time characteristics of the proposed model, it is useful for nonlinear multi-area management-based problems. Since in market-based problems, it is supposed that areas do not have any information about their adjacent areas and only their contracts are taken into account, therefore, a decomposed approach must be used for this model, which may be obtained by a Master-Slave model. This is one of the drawbacks of the proposed formulation.

Moreover, an application of MA-AROPF for finding the optimal tie line has been considered as the one that, under the maximum loading point (MLP) condition, most effectively enhances the stability of the multi-area system as well as its degree of freedom (to be easily reschedulable), while reducing the total operating costs and/or emissions. Based on the analysis of a power system at the MLP, the weak and strong buses have been determined and a set of strong and weak buses have been selected as candidate buses for tie line planning and then, via a mixed integer nonlinear programming problem, the appropriate tie lines have been selected. Moreover, in order to have a more appropriate plan at all the operating points, the switchable tie lines have been considered.

7.2   FUTURE WORKS

7.2.1   Market based multi-area OPF

In order to consider the proposed multi-area OPF model in the market-based application, it is necessary to decompose the problem to several sub-problems. In the literature, many decomposition methodologies such as Lagrangian relaxation, augmented Lagrangian decomposition, optimality condition decomposition, complicating variables, Dantzig-Wolfe decomposition, etc. have been used. For a novel work in this area, a Master-Slave approach may be considered to decompose such a problem.

7.2.2   OPF with considering the disjoint operating zone

In order to consider the OPF problems in a more practical way, the prohibited operating zone will be considered. This consideration for an OPF problem, which is a hardly

nonlinear problem, makes it even a more complicated problem. In the literature, for solving these kinds of problems, the metaheuristic-based methodologies were used where for the simple model of OPF, which is called the economic dispatch (ED) and is not a nonlinear but a quadratic problem, a mixed integer quadratic programming was proposed in (PAPAGEORGIOU; FRAGA, 2007) and in 2014, further progress has been made in (DING et al., 2014a). These methodologies are good for the models, which are not very complicated and time consuming such as quadratic-based models, but for OPF problems with nonlinear nature, it may yield an inefficient solution. In order to solve this problem, a distance-based approach may be helpful to strive toward an efficient model.

REFERENCES

ALMEIDA, K. C.; SALGADO, R. Optimal power flow solutions under variable load conditions. **Power Systems, IEEE Transactions on**, United States of America, v. 15, n. 4, p. 1204–1211, 2000.

ALMEIDA, K. C.; SENNA, F. S. Optimal active-reactive power dispatch under competition via bilevel programming. **Power Systems, IEEE Transactions on**, United States of America, v. 26, n. 4, p. 2345–2354, 2011.

AL-MUHAWESH, T. A.; QAMBER, I. S. The established mega watt linear programming-based optimal power flow model applied to the real power 56-bus system in eastern province of Saudi Arabia. **Energy**, England, v. 33, n. 1, p. 12–21, 2008.

ALRASHIDI, M. R.; EL-HAWARY, M. E. Hybrid particle swarm optimization approach for solving the discrete OPF problem considering the valve loading effects. **Power Systems, IEEE Transactions on**, United States of America, v. 22, n. 4, p. 2030–2038, 2007.

BAKIRTZIS, A. G.; BISKAS, P. N. A decentralized solution to the DC-OPF of interconnected power systems. **Power Systems, IEEE Transactions on**, United States of America, v. 18, n. 3, p. 1007–1013, 2003.

BALDICK, R.; CHATTERJEE, D. Coordinated dispatch of regional transmission organizations: Theory and example. **Computers & Operations Research**, England, 2013.

BASU, M.; CHATTOPADHYAY, P. K.; R. N. CHAKRABARTI; GHOSHAL, T. K. Economic emission load dispatch with non-smooth fuel cost and emission level functions through an interactive fuzzy satisfying method and evolutionary programming technique. **Journal of the Institution of Engineers (india). Electrical Engineering Division**, India, v. 87, p. 41–46, 2006.

BERIZZI, A.; DELFANTI, M.; MARANNINO, P.; PASQUADIBISCEGLIE, M. S.; SILVESTRI, A. Enhanced security-constrained OPF with FACTS devices. **Power Systems, IEEE Transactions on**, United States of America, v. 20, n. 3, p. 1597–1605, 2005.

BHATTACHARYA, B.; MANDAL, K. K.; CHAKRABORTY, N. A hybrid cultural approach for combined economic and emission dispatch. In: INDIA CONFERENCE-INDICON, 3., 2011, Hyderabad. **Annual…** IEEE, 2011. p. 1-4.

BISKAS, P. N.; BAKIRTZIS, A. G.; MACHERAS, N. I.; PASIALIS, N. K. A decentralized implementation of DC optimal power flow on a network of computers. **Power Systems, IEEE Transactions on**, United States of America, v. 20, n. 1, p. 25–33, 2005.

BOUCHEKARA, H. R. E. H.; ABIDO, M. A.; BOUCHERMA, M. Optimal power flow using Teaching-Learning-Based Optimization technique. **Electric Power Systems Research**, Netherland, v. 114, p. 49–59, 2014.

BOYD, S.; XIAO, L.; MUTAPCIC, A.; MATTINGLEY, J. **Notes on decomposition methods.** United states of America: [s.n.], 2008. Available:

<http://see.stanford.edu/materials/lsocoee364b/08-decomposition_notes.pdf>. Access: 13 Apr. 2008.

CAI, L. J.; ERLICH, I.; STAMTSIS, G. Optimal choice and allocation of FACTS devices in deregulated electricity market using genetic algorithms. In: POWER SYSTEMS CONFERENCE AND EXPOSITION, 3., 2004, United States of America. 2004. **Annual**... United States of America: IEEE PES, 2004. p. 201-207.

CAIN, M. B; ONEILL, R. P.; CASTILLO, A. **History of optimal power flow and Formulations.** United states of America: [s.n.], 2012. Available: < http://www.ferc.gov/industries/electric/indus-act/market-planning/opf-papers/acopf-1-history-formulation-testing.pdf >. Access: Dec. 2012.

CARO, E.; CONEJO, A. J.; MINGUEZ, R. Decentralized state estimation and bad measurement identification: An efficient Lagrangian relaxation approach. **Power Systems, IEEE Transactions on**, United States of America, v. 26, n. 4, p. 2500–2508, 2011.

CHANG, Y.-C. Multi-objective optimal thyristor controlled series compensator installation strategy for transmission system loadability enhancement. **Generation, Transmission Distribution, IET**, England, v. 8, n. 3, p. 552–562, mar. 2014.

CHEN, H.; BO, M. L.; ZHU, Y. Multi-hive bee foraging algorithm for multi-objective optimal power flow considering the cost, loss, and emission. **International Journal of Electrical Power & Energy Systems**, England, v. 60, p. 203–220, 2014.

CHEN, H.; CHEN, J.; DUAN, X. Multi-stage dynamic optimal power flow in wind power integrated system. In: TRANSMISSION AND DISTRIBUTION CONFERENCE AND EXHIBITION: ASIA AND PACIFIC, 3., 2005, Dalian. **Annual**... [S.l.]: IEEE/PES, 2005.

CHUNG, C. Y.; YAN, W.; LIU, F. Decomposed predictor-corrector interior point method for dynamic optimal power flow. **Power Systems, IEEE Transactions on**, United States of America, v. 26, n. 3, p. 1030–1039, 2011.

CONEJO, A. J.; AGUADO, J. A. Multi-area coordinated decentralized DC optimal power flow. **Power Systems, IEEE Transactions on**, United States of America, v. 13, n. 4, p. 1272–1278, 1998.

CONEJO, A. J.; DE LA TORRE, S.; CANAS, M. An optimization approach to multiarea state estimation. **Power Systems, IEEE Transactions on**, United States of America, v. 22, n. 1, p. 213–221, 2007.

CONEJO, A. J.; NOGALES, F. J.; PRIETO, F. J. A decomposition procedure based on approximate Newton directions. **Mathematical Programming**, Germany, v. 93, n. 3, p. 495–515, 2002.

DA SILVA, E. L.; ORTIZ, J. M. A.; DE OLIVEIRA, G. C.; BINATO, S. Transmission network expansion planning under a Tabu Search approach. **Power Systems, IEEE Transactions on**, United States of America, v. 16, n. 1, p. 62–68, 2001.

DE SOUZA, A. C. Z.; HONORIO, L. M.; TORRES, G. L.; LAMBERT-TORRES, G. Increasing the loadability of power systems through optimal-local-control actions. **Power Systems, IEEE Transactions on**, United States of America, v. 19, n. 1, p. 188–194, fev. 2004.

DING, T.; BO, R.; GU, W.; SUN, H. Big-M based MIQP method for economic dispatch with disjoint prohibited zones. **Power Systems, IEEE Transactions on**, United States of America, v. 29, n. 2, p. 976–977, 2014a.

DING, T.; BO, R.; LI, F.; GU, Y.; GUO, Q.; SUN, H. Exact penalty function based constraint relaxation method for optimal power flow considering wind generation uncertainty. **Power Systems, IEEE Transactions on**, United States of America, v. PP, n. 99, p. 1–3, 2014b.

DIXIT, G. P.; DUBEY, H. M.; PANDIT, M.; PANIGRAHI, B. K. Artificial bee colony optimization for combined economic load and emission dispatch. In: INTERNATIONAL CONFERENCE ON SUSTAINABLE ENERGY AND INTELLIGENT SYSTEMS- SEISCON, 1., 2011, Chennai. **Annual...** Chennai: IET, 2011.

FOURER, R.; GAY, D. M.; KERNIGHAN, B. W. **Ampl:** a modeling language for mathematical programming. [S.l.]: Duxbury Press, 2002.

GABASH, A.; LI, P. Active-reactive optimal power flow in distribution networks with embedded generation and battery storage. **Power Systems, IEEE Transactions on**, United States of America, v. 27, n. 4, p. 2026–2035, 2012.

GEETHA, R.; BHUVANESWARI, R.; SUBRAMANIAN, S. Artificial immune system based combined economic and emission dispatch. In: CONFERENCE TENCON, 8., 2008, Hyderabad. **Annual...** Hyderabad: IEEE, 2008.

GONG, D.; ZHANG, Y.; QI, C. Environmental/economic power dispatch using a hybrid multi-objective optimization algorithm. **International Journal of Electrical Power & Energy Systems**, England, v. 32, n. 6, p. 607–614, 2010.

GRANADA, M. E.; RIDER, M. J.; MANTOVANI, J. R. S.; SHAHIDEHPOUR, M. Multi-areas optimal reactive power flow. In: TRANSMISSION AND DISTRIBUTION CONFERENCE AND EXPOSITION: LATIN AMERICA, 3., 2008, Bogota. **Annual...** Bogota: IEEE/PES, 2008.

GUNDA, J.; ACHARJEE, P.; BISWAS, S. Incremental cost based combined economic and emission dispatch using hybrid differential evolution. In: INTERNATIONAL CONFERENCE ON RECENT ADVANCEMENTS IN ELECTRICAL, ELECTRONICS AND CONTROL ENGINEERING- ICONRAEeCE, 5., 2011, Sivakasi. **Annual**... Sivakasi: IEEE, 2011. p. 13-18.

HAPP, H. H. Optimal power dispatch--A comprehensive survey. **Power Apparatus and Systems, IEEE Transactions on**, United States of America, v. 96, n. 3, p. 841–854, 1977.

HESLIN, J. S.; HOBBS, B. F. A multiobjective production costing model for analyzing emissions dispatching and fuel switching [of power stations]. **Power Systems, IEEE Transactions on**, United States of America, v. 4, n. 3, p. 836–842, ago. 1989.

JIANG, S.; JI, Z.; SHEN, Y. A novel hybrid particle swarm optimization and gravitational search algorithm for solving economic emission load dispatch problems with various practical constraints. **International Journal of Electrical Power & Energy Systems**, England, v. 55, p. 628–644, 2014.

KASMAEI, M. P.; RIDER, M. J.; MANTOVANI, J. R. S. A novel straightforward compromising method for dynamic economic and emission dispatch considering valve-point effect. In: INTERNATIONAL CONFERENCE ON ENVIRONMENT AND ELECTRICAL ENGINEERING- EEEIC, 12., 2013. **Annual...** [S.l.]: IEEE, 2013.

KHODAEI, A.; SHAHIDEHPOUR, M.; WU, L.; LI, Z. Coordination of short-term operation constraints in multi-area expansion planning. **Power Systems, IEEE Transactions on**, United States of America, v. 27, n. 4, p. 2242–2250, 2012.

KIM, B. H.; BALDICK, R. Coarse-grained distributed optimal power flow. **Power Systems, IEEE Transactions on**, United States of America, v. 12, n. 2, p. 932–939, 1997.

KUMARAPPAN, N.; MOHAN, M. R. Hybrid genetic algorithm based combined economic and emission dispatch for utility system. In: INTERNATIONAL CONFERENCE ON INTELLIGENT SENSING AND INFORMATION, 1. , 2004, Chennai. **Proceedings…** Chennai: [s.n.], 2004.

LAMONT, J. W.; OBESSIS, E. V. Emission dispatch models and algorithms for the 1990s. **Power Systems, IEEE Transactions on**, United States of America, v. 10, n. 2, p. 941–947, maio 1995.

LI, Y.; VENKATASUBRAMANIAN, V. Coordination of transmission path transfers. **Power Systems, IEEE Transactions on**, United States of America, v. 19, n. 3, p. 1607–1615, 2004.

LIMA, F. G. M.; GALIANA, F. D.; KOCKAR, I.; MUNOZ, J. Phase shifter placement in large-scale systems via mixed integer linear programming. **Power Systems, IEEE Transactions on**, United States of America, v. 18, n. 3, p. 1029–1034, 2003.

LO, K. L.; MENG, Z. J. Newton-like method for line outage simulation. **Generation, Transmission and Distribution, IEE Proceedings**, England, v. 151, n. 2, p. 225–231, mar. 2004.

MADANI, R.; SOJOUDI, S.; LAVAEI, J. Convex relaxation for optimal power flow problem: Mesh Networks. **Power Systems, IEEE Transactions on**, United States of America, v. PP, n. 99, p. 1–13, 2014.

MITTAL, C. **Fuel cost function estimation for economic load dispatch using evoevolution programming**. Patiala: Electrical and Instrumentation Engineering Department, 2011.

MOMOH, J. A. **Electric power system applications of optimization**. [S.l.]: CRC Press, 2000.

MONTICELLI, A. J. **Fluxo de carga em redes de energia elétrica**. São Paulo: Edgard Blucher, 1983.

MORI, H.; GOTO, Y. A parallel tabu search based method for determining optimal allocation of FACTS in power systems. In: INTERNATIONAL CONFERENCE ON POWER SYSTEM TECHNOLOGY, 1., 2000, Perth. **Proceedings…** Perth: IEEE, 2000.

NAGALAKSHMI, P.; HARISH, Y.; KUMAR, R. K.; JADA, C. Combined economic and emission dispatch using intelligent water drops-continuous optimization algorithm. In: INTERNATIONAL CONFERENCE ON RECENT ADVANCEMENTS IN ELECTRICAL, ELECTRONICS AND CONTROL ENGINEERING-ICONRAEeCE, 3., 2011, Sivakasi. **Annual...** Sivakasi: IEEE, 2011.

NIKNAM, T.; AZIZIPANAH-ABARGHOOEE, R.; NARIMANI, M. R. Reserve constrained dynamic optimal power flow subject to valve-point effects, prohibited zones and multi-fuel constraints. **Energy**, England, v. 47, n. 1, p. 451–464, 2012.

NIKNAM, T.; DOAGOU-MOJARRAD, H. Multiobjective economic/emission dispatch by multiobjective teta-particle swarm optimisation. **Generation, Transmission Distribution, IET**, England, v. 6, n. 5, p. 363–377, 2012a.

NIKNAM, T.; DOAGOU-MOJARRAD, H. Multiobjective economic/emission dispatch by multiobjective ?-particle swarm optimisation. **Generation, Transmission Distribution, IET**, England, v. 6, n. 5, p. 363–377, 2012b.

NIKNAM, T.; MOJARRAD, H. D.; MEYMAND, H. Z.; FIROUZI, B. B. A new honey bee mating optimization algorithm for non-smooth economic dispatch. **Energy**, England, v. 36, n. 2, p. 896–908, 2011a.

NIKNAM, T.; NARIMANI, M. R.; AGHAEI, J.; TABATABAEI, S.; NAYERIPOUR, M. Modified honey bee mating optimisation to solve dynamic optimal power flow considering generator constraints. **Generation, Transmission Distribution, IET**, England, v. 5, n. 10, p. 989–1002, 2011b.

NIKNAM, T.; RASOUL NARIMANI, M.; JABBARI, M.; MALEKPOUR, A. R. A modified shuffle frog leaping algorithm for multi-objective optimal power flow. **Energy**, England, v. 36, n. 11, p. 6420–6432, 2011c.

NOGALES, F.; PRIETO, F.; CONEJO, A. A decomposition methodology applied to the multi-area optimal power flow problem. **Annals of Operations Research**, Netherland, v. 120, n. 1-4, p. 99–116, 2003.

OBADINA, O. O.; BERG, G. J. Identifying electrically weak and strong segments of a power system from a voltage stability viewpoint. **Generation, Transmission and Distribution, IEE Proceedings C**, England, v. 137, n. 3, p. 205–212, maio 1990.

ONGSAKUL, W.; JIRAPONG, P. Optimal allocation of FACTS devices to enhance total transfer capability using evolutionary programming. In: IEEE INTERNATIONAL SYMPOSIUM ON CIRCUITS AND SYSTEMS- ISCAS, 4., 2005, Kobe. **Annual**... Kobe: IEEE, 2005.

PADHY, N. P. Congestion management under deregulated fuzzy environment. In: IEEE INTERNATIONAL CONFERENCE ON ELECTRIC UTILITY DEREGULATION, RESTRUCTURING AND POWER TECHNOLOGIES- DRPT, 7., 2004, Idnow. **Proceedings…** Idnow: [s.n.], 2004.

PALANICHAMY, C.; BABU, N. S. Analytical solution for combined economic and emissions dispatch. **Electric Power Systems Research**, Switzerland, v. 78, n. 7, p. 1129–1137, 2008.

PAPAGEORGIOU, L. G.; FRAGA, E. S. A mixed integer quadratic programming formulation for the economic dispatch of generators with prohibited operating zones. **Electric Power Systems Research**, Switzerland, v. 77, n. 10, p. 1292–1296, 2007.

POURAKBARI-KASMAEI, M.; RASHIDI-NEJAD, M. An effortless hybrid method to solve economic load dispatch problem in power systems. **Energy Conversion and Management**, England, v. 52, n. 8-9, p. 2854–2860, 2011.

POURAKBARI-KASMAEI, M.; RIDER, M. J.; MANTOVANI, J. R. S. Congestion effect on consumers allocated cost and system emission via environmental active-reactive OPF. In: INTERNATIONAL CONFERENCE ON ELECTRIC POWER AND ENERGY CONVERSION SYSTEMS- EPECS, 13., 2013, Polska. **Annual**... Polska: IEEE, 2013.

POURAKBAR-KASMAEI, M.; RIDER, M. J.; MANTOVANI, J. R. S. A novel straightforward compromising method for dynamic economic and emission dispatch considering valve-point effect. In: INTERNATIONAL CONFERENCE ON ENVIRONMENT AND ELECTRICAL ENGINEERING- EEEIC, 12., 2013, Polska. **Annual**... Polska: IEEE, 2013.

PRASANNA, T. S.; SOMASUNDARAM, P. Fuzzy mutated evolutionary programming based algorithm for combined economic and emission dispatch. In: CONFERENCE TENCON, 10., 2008, Hyderabad. **Annual**... Hyderabad: IEEE, 2008.

PUDJIANTO, D.; AHMED, S.; STRBAC, G. Allocation of VAr support using LP and NLP based optimal power flows. **Generation, Transmission and Distribution, IEE Proceedings,** England, v. 149, n. 4, p. 377–383, jul. 2002.

REGIONAL TRANSMISSION ORGANIZATIONS. **Federal energy regulatory Commission**. Idnow: [s.n.], 2000. Available: <http://www.ferc.gov/legal/maj-ord-reg/land-docs/2000A.pdf>. Access: Sept. 2000.

RUEDA, S. M. V; ALMEIDA, K. C. Optimal power flow solutions under variable load conditions: reactive power cost modeling. In: POWER INDUSTRY COMPUTER APPLICATIONS- PICA; INNOVATIVE COMPUTING FOR POWER - ELECTRIC ENERGY MEETS THE MARKET, 22., 2001, Sydney. **Annual**... Sydney: IEEE, 2001.

SHAHIDEHPOUR, M.; YAMIN, H.; LI, Z. **Market operations in electric power systems:** forecasting, scheduling, and risk management. [S.l.]: IEEE-Wiley-Interscience, 2002.

SHI, L.; HAO, J.; ZHOU, J.; XU, G. Ant colony optimization algorithm with random perturbation behavior to the problem of optimal unit commitment with probabilistic spinning

reserve determination. **Electric Power Systems Research**, Switzerland, v. 69, n. 2-3, p. 295–303, 2004.

SILVA, I. DE J.; RIDER, M. J.; ROMERO, R.; GARCIA, A. V; MURARI, C. A. Transmission network expansion planning with security constraints. **Generation, Transmission and Distribution, IEE Proceedings-**, England, v. 152, n. 6, p. 828–836, 2005.

SINHA, N.; PURKAYASTHA, B. S.; PURKAYASTHA, B. Optimal combined non-convex economic and emission load dispatch using NSDE. In: INTERNATIONAL CONFERENCE ON OMPUTATIONAL INTELLIGENCE AND MULTIMEDIA APPLICATIONS, 1., 2007, Sivakasi. **Annual**... Sivakasi: IEEE, 2007.

SIVASUBRAMANI, S.; SWARUP, K. S. Sequential quadratic programming based differential evolution algorithm for optimal power flow problem. **Generation, Transmission Distribution, IET**, England, v. 5, n. 11, p. 1149–1154, 2011.

SONI, S. K.; BHURIA, V. Multi-objective emission constrained economic power dispatch using differential evolution algorithm. **International Journal of Engineering and Innovative Technology (IJEIT)**, India, v. 2, n. 1, p. 120–125, 2012.

SUDHAKARAN M. S; M. R. SLOCHANAL; R SREERAM; CHANDRASEKHAR, N. Application of refined genetic algorithm to combined economic and emission dispatch. **Journal of the Institution of Engineers (india). Electrical Engineering Division**, India, v. 85, p. 115–119, 2004.

SYSTEM data. [S.l.: s.n.], 2014. Available: <www.mahdipk.com/data.html>. Access: Sept. 2014.

SWARNKAR, K. K.; WADHWANI, S.; WADHWANI, A. K. Optimal power flow of large distribution system solution for combined economic emission dispatch problem using partical swarm optimization. In: INTERNATIONAL CONFERENCE ON POWER SYSTEMS-ICPS, 9., 2009, Kharagpur. **Annual**... Kharagpur: IEEE, 2009.

TONG, X.; LIN, M. Semismooth Newton-type algorithms for solving optimal power flow problems. In: TRANSMISSION AND DISTRIBUTION CONFERENCE AND EXHIBITION: ASIA AND PACIFIC, 5., 2005, Dalian. **Annual**... Dalian; IEEE/PES, 2005.

TONG, X.; ZHANG, Y.; WU, F. F. A decoupled semismooth Newton method for optimal power flow. In: POWER ENGINEERING SOCIETY GENERAL MEETING, 9., 2006, Montreal. **Annual**... Montreal: IEEE, 2006.

VAHIDINASAB, V.; JADID, S. Joint economic and emission dispatch in energy markets: A multiobjective mathematical programming approach. **Energy**, England, v. 35, n. 3, p. 1497–1504, 2010.

VAISAKH, K.; SRINIVAS, L. R. A genetic evolving ant direction DE for OPF with non-smooth cost functions and statistical analysis. **Energy**, England, v. 35, n. 8, p. 3155–3171, 2010.

VENKATESH, P.; GNANADASS, R.; PADHY, N. P. Comparison and application of evolutionary programming techniques to combined economic emission dispatch with line flow constraints. **Power Systems, IEEE Transactions on**, United States of America, v. 18, n. 2, p. 688–697, 2003.

VLACHOGIANNIS, J. G.; LEE, K. Y. Determining generator contributions to transmission system using parallel vector evaluated particle swarm optimization. **Power Systems, IEEE Transactions on**, United States of America, v. 20, n. 4, p. 1765–1774, 2005.

WANG, X.; SONG, Y.-H.; LU, Q. Lagrangian decomposition approach to active power congestion management across interconnected regions. **Generation, Transmission and Distribution, IEE Proceedings-**, England, v. 148, n. 5, p. 497–503, 2001.

XIA, Y.; CHAN, K. W. Dynamic constrained optimal power flow using semi-infinite programming. **Power Systems, IEEE Transactions on**, United States of America, v. 21, n. 3, p. 1455–1457, 2006.

XU, Y.; DONG, Z.-Y.; MENG, K.; ZHAO, J. H.; WONG, K. P. A hybrid method for transient stability-constrained optimal power flow computation. **Power Systems, IEEE Transactions on**, United States of America, v. 27, n. 4, p. 1769–1777, 2012.

YAMIN, H. Y.; AL-TALLAQ, K.; SHAHIDEHPOUR, S. M. New approach for dynamic optimal power flow using Benders decomposition in a deregulated power market. **Electric Power Systems Research**, Switzerland, v. 65, n. 2, p. 101–107, 2003.

YAN, W.; YU, J.; YU, D. C.; BHATTARAI, K. A new optimal reactive power flow model in rectangular form and its solution by predictor corrector primal dual interior point method. **Power Systems, IEEE Transactions on**, United States of America, v. 21, n. 1, p. 61–67, 2006.

ZARCO, P.; GOMEZ-EXPOSITO, A. Power system parameter estimation: a survey. **Power Systems, IEEE Transactions on**, United States of America, v. 15, n. 1, p. 216–222, 2000.

ZEHAR, K.; SAYAH, S. Optimal power flow with environmental constraint using a fast successive linear programming algorithm: Application to the algerian power system. **Energy Conversion and Management**, England, v. 49, n. 11, p. 3362–3366, 2008.

ZHU, J. **Optimization of power system operation**. [S.l.]: Wiley-IEEE, 2009.

PUBLICATIONS

A. I.   JOURNAL PAPERS:

1. **M. Pourakbari-Kasmaei,** M. J. Rider , and J. R. S. Mantovani. "Multi-Area Environmental-Constrained Active-Reactive Optimal Power Flow- A Short-Term Tie Line Planning Study", Under Review**.**

2. **M. Pourakbari-Kasmaei,** M. J. Rider , and J. R. S. Mantovani. "An Unambiguous Distance Based MIQP Model to Solve Economic Dispatch Problem with Disjoint Operating Zone", Accepted, IEEE Trans. On Power Syst. 2015.

3. **M. Pourakbari-Kasmaei,** M. J. Rider , and J. R. S. Mantovani. "An Unequivocal Normalization-Based Paradigm to Solve the Dynamic Economic and Emission Active-Reactive OPF", Energy, V. 73, pp. 554-566. August 2014.

A. II.   CONFERENCE PAPERS:

1. **M. Pourakbari-Kasmaei,** M. J. Rider , and J. R. S. Mantovani "An Environmental Constrained Active-Reactive OPF to Consider The Congestion Effect on Consumers Allocated Cost and System Emission". IEPEM. 2013.

2. **M. Pourakbari-Kasmaei,** M. J. Rider , and J. R. S. Mantovani "Congestion Effects on Regional & System Emission and Consumers Allocated Cost" The 3rd International Conference on Electric Power and Energy Conversion Systems (EPECS), **IEEE Indexed.** 2013.

3. **M. Pourakbari-Kasmaei,** M. J. Rider , and J. R. S. Mantovani. "A Novel Straightforward Compromising Method for Dynamic Economic and Emission Dispatch Considering Valve-Point Effect". The 12th International Conference on Environmental and Electrical Engineering (EEEIC). **IEEE Indexed**. 2013.

4. H. khorasani, **M. Pourakbari-Kasmaei,** R. Romero**.** "Transmission Expansion Planning Via a Constructive Heuristic Algorithm in Restructured Electricity Industry. The 3rd International Conference on Electric Power and Energy Conversion Systems (EPECS), **IEEE Indexed.** 2013.

5. H. khorasani**,** **M. Pourakbari-Kasmaei,** R. Romer**o.** "A Heuristic Method for Transmission Network Expansion Planning under Security Constraints" IEPEM. 2013.

6. M. A. J. Delgado, **M. Pourakbari-Kasmaei,** M. J. Rider. "A Modified Branch and Bound Algorithm to Solve the Transmission Expansion Planning Problem". The 13th International Conference on Environmental and Electrical Engineering (EEEIC). **IEEE Indexed**. 2013.